Development of zeolite stabilized precious metal nanoclusters
Synthesis, characterization and application of a new catalytic material

D i s s e r t a t i o n

zur Erlangung des Doktorgrades
der Ingenieurwissenschaften

vorgelegt von
Dipl.- Chem. Univ. Markus Hutt
aus München

genehmigt von der Fakultät für Mathematik/Informatik und Maschinenbau

der Technischen Universität Clausthal,

Tag der mündlichen Prüfung
12.04.2013

Vorsitzende/Vorsitzender der Promotionskommission

Prof. Dr.-Ing. Alfons Esderts

Hauptberichterstatterin/Hauptberichterstatter

Prof. Dr.-Ing. Thomas Turek

Berichterstatterin/Berichterstatter

Priv.-Doz. Dr. habil. Frank Klose

To my Family,
Friends
and Tamara

Mein Dank gilt all jenen die zu dem gelingen dieser Arbeit beigetragen haben.
Besonderer Dank gilt meinem geschätzten akademischen Lehrer

Prof. Dr.-Ing. Thomas Turek

für die Betretung Unterstützung bei der Anfertigung dieser Arbeit sowie

Dr. Arno Tißler

für das interessante Projekt sowie seinen besonderen Einsatz.
Außerdem danke ich

Priv.-Doz. Dr. habil. Frank Klose

für seien Unterstützung, seinen guten Rat, Einsatz, die anregenden akademischen Diskussionen, Diskurse, Ideen und Anregungen sowie für die gemeinsam Zeit auch außerhalb des Labors.

Weiterhin danke ich allen Kollegen am Standort Heufeld für das gute kollegiale und angenehme Arbeitsklima. Besonderer Dank gilt Dr. Olga Manoylova für spannende und lehrreiche Einführung in die IR Spektroskopie, Dr. Klaus Wanninger und Dr. Martin Schneider für die Bereitstellung ihrer Testanlagen, Unterstützung und fruchtbare Diskussionen. Zusätzlich danke ich dem ganzen BEE-Team für die Aufnahme in das Team, Einführung und Unterstützung im Labor und der Durchführungen und Auswertung der zahlreichen Tests, im besonderen Margit Schuschke, Gregory Reznikov und Andane Stein, Sebastian von Moltke und Gabi Lindinger. Spezieller Dank gebührt Sascha Podehl für die Planung und Durchführung Ofentests das „Bierpatent“ und seine Unterstützung in allen Lebenslagen.

Mein Dank gilt auch dem Team der Analytik Abteilung um Andreas Trautwein und Helmut Hartsberger für die gute und verlässliche Zusammenarbeit sowie den Mitarbeiten der Elektro- und Mechanischen Werkstatt für ihre tatkräftige Unterstützung auch wenn ich nicht immer ein einfacher Kunde war. Zusätzlich danke ich der Patentabteilung für die Unterstützung bei zahlreichen Anmeldungen und der interessanten und spannenden Einführung in das Patentrecht.

Der größte Dank gilt meiner Familie für ihre Unterstützung, Geduld und Zuspruch in allen Lebenslagen. Insbesondere möchte ich mich bei meinen Eltern Ingeborg und Rainer Hutt sowie meiner Schwester Katharina Marx für ihre Unterstützung bedanken. Und natürlich der kleinen Lea.

Table of Contents

1. General Introduction

Pollutants are emitted continuously form both stationary and mobile sources. The growing industrial activities and the increasing mobility require continuous improvement of environmental technologies to limit the uncontrolled pollution of the common environment. The stationary sources for gaseous emissions range from private households over small industries to large coal fired power plants [1]. Until nowadays, vehicles are equipped with internal combustion engines, which use fossil fuel to perform the mayor part of on-road transportation. These vehicles range from small two-wheelers to huge heavy duty trucks, and are either equipped with spark-ignition engines (Otto engine) or compressed ignition engines (Diesel engine).

Typical pollutants produced by these incineration processes are nitrogen oxides (NO_x) and sulphur dioxide (SO_2), which lead to acidification of the environment and Greenhouse gases for example carbon dioxide (CO_2) and nitrous oxide (N_2O) which contribute to the global warming. Other products of the combustion such as volatile organic compounds (VOC), carbon monoxide (CO) and NO_x cause the photochemical summer smog. Additionally other emissions like dioxins, volatile organic compounds (VOC) and heavy metals such as Hg are directly harmful to human beings.

One strategy, amongst others, is to convert these pollutants to less harmful substances. This goal can be achieved either with non-catalytic converters or in catalytic processes. Catalytic processes have the advantage that the activation energy is lowered, and therefore less energy is required for this transformation.

1.1. Legal requirements

Legislation is the one key driver for the development and implementation of off-gas cleaning technology. Both, the emission from stationary and from mobile sources, were limited by the governments in the last decades. In Germany, the emission of pollutants is regulated by *"Bundes-Immissionsschutzgesetz"* and the *"TA Luft"*. The latest program of the European Union is the so called *"Clean Air For Europe" (CAFE)* program [2]. Contrary to earlier programs, this directive is not only limited to certain pollutants but focuses on all relevant factors influencing the maintenance and improvement of the air quality. This directive lays down national emission ceilings for the air pollutants sulphur dioxide (SO_2), nitrogen oxides (NO_x), ammonia (NH_3) and non-methane hydrocarbon (NMHC) which may not be exceeded

after 2010. In Table 1 the maximum emissions of the different pollutants according this directive are listed.

Table 1: Maximum emission according to national emission ceiling (NEC) for Germany [3]

	SO_2 [kt/a]	NO_x [kt/a]	NH_3 [kt/a]	NMHC [kt/a]
Max. emission (NEC)	520	1051	550	995
Forecast	459	1112	610	987
Difference	-61	+61	+60	-8

To achieve these ambitious goals, all sources, such as mobile sources (cars and small motor), stationary sources such as all kinds of industry as well as agriculture, have to contribute to the reduction of these emissions. The highest NO_x and NMHC reduction can be achieved in the fields of mobile and stationary emission sources, whereas agriculture is the major source of ammonia pollution.

1.1.1. Mobile sources

Since the introduction of the first regulation for spark ignition engines in the middle of the 1960's in California, all industrial nations have regulations and limitations for the release of pollutants which are produced in vehicle engines or in industries. The European Union and California are the driving forces for ongoing intensification of these limitations. The European Union limits the emission of carbon monoxide, hydrocarbons, nitrogen oxides and particulate matter (PM). The actual limitations for spark ignition engine and diesel engine passenger cars are summarized in Table 2.

In December 2006 the European Union decided a further intensification of the Euro 4 limitation and installed the Euro 5 and Euro 6 limitations. A further reduction of emission from mobile sources is considered to lead to an additional improvement of the air quality and therefore life quality. For spark-ignition engines the amount of unburned HC, CO and NO_x are limited in these regulations. For Diesel engines the regulations are focused on the reduction of PM and of nitrogen oxides. For PM, these regulations can only be met by the implementation of Diesel particulate filter (DPF). The requested reduction in NO_x emissions requires the introduction of new catalytic systems, which convert NO_x to nitrogen and water by selective catalytic reduction (SCR).

Table 2: Limitations for passenger cars [1]

Commencement		Euro 4 01.01.2005	Euro 5 01.09.2009	Euro 6 01.09.2014
Spark ignition				
CO	[g/km]	1.0	1.0	1.0
HC	[g/km]	0.1	0.1	0.1
NO_x	[g/km]	0.08	0.06	0.06
Diesel				
CO	[g/km]	0.5	0.5	0.5
NO_x	[g/km]	0.25	0.18	0.08
HC + NO_x	[g/km]	0.3	0.23	0.17
PM	[g/km]	0.025	0.005	0.005

1.1.2. Stationary sources

Industrial activities play an important role in the economic well-being of Europe contributing to its sustainable growth. However, industrial activities also have a significant impact on the environment. The largest industrial installations account for a considerable share of total emissions of key atmospheric pollutants (83 % for sulphur dioxide (SO_2), 34 % for oxides of nitrogen (NO_x), 43 % for dust and 55 % for volatile organic compounds (VOC)) [4]. Emissions from industrial installations have therefore been subject to EU-wide legislations. Since the 1970's various directives have been drawn up which have led to the adoption of the following main parts of legislation:

- The Integrated Pollution Prevention and Control Directive (IPPC): The EU had adopted in 1996 a set of common rules for permitting and controlling industrial installations in the IPPC Directive (Directive 96/61/EC), which had been modified in 2008 (Directive 2008/1/EC). In essence, the IPPC Directive is about minimising pollutions from various industrial sources throughout the European Union. The IPPC Directive is based on several principles, namely an integrated approach, best available techniques, flexibility and public participation [4].
- The so-called sectoral directives lay down specific minimum requirements, including emission limit values for certain industrial activities (large combustion plants, waste incineration, activities using organic solvents and titanium dioxide production).

- The European Pollutant Release and Transfer Register (E-PRTR) publishes detailed information on the emissions and the off-site transfers of pollutants and waste from approximately 24 000 industrial facilities [5].

1.1.3. Special challenges in environmental catalysis

In chemical and petrochemical industries, the reaction conditions have to be aligned to the reaction and the catalyst. Therefore, systems operate in a very narrow window of reaction condition, which guarantees optimal feedstock conversion, high selectivity towards the desired product at minimum catalyst deactivation. Also in stationary environmental applications, the changes in temperature and feed composition are commonly moderate, slow and relatively marginal during the operation. Therefore, catalysts can be designed for the particular conditions available in the plant and process.

In contrast to catalysts applied stationary or industrial applications, catalysts used in vehicles, are subjected to changing temperatures and concentrations, due to the fast changes in the operation condition of the engine. Especially, the temperature, the gas velocity and the concentration of the pollutant are closely related to the state of the engine, which is correlated to the driving conditions. For this reason, the temperature can vary from around 300 °C when the engine is idling up to 1000 °C, when the engine is fully loaded. Because of that, modern catalysts for mobile applications have to be active at relatively low temperature on one hand but on the other hand have to withstand high temperatures without serious deactivation.

1.2. Emission of combustion engines

Today's combustion engines, are mainly fired with fossil fuels or biomass with mainly consist of hydrocarbons. To burn these fuels, a mixture of fuel and air is required. The main components of air are nitrogen (78.1 vol%) and oxygen (20.95 vol%). Additionally, small amounts of other gases such as argon (0.94 vol%) and CO_2 (0.04 vol%) are present [6].

For the complete combustion of 1 kg of fuel (under ideal conditions in a spark-ignition engines) 14.7 kg of air are required, which corresponds to stoichiometric ratio of HC to O_2. The ratio of air to fuel is the so called λ-value.

$$\lambda = \frac{actual\ engine\ {}^{A}/_{F}}{stoichiometric\ engine\ {}^{A}/_{F}} \qquad \textbf{eq. 1}$$

Where A/F is:

$$\frac{A}{F} = \frac{Mass\ of\ air\ consumed\ by\ the\ engine}{Mass\ of\ fuel\ consumed\ by\ the\ engine} \qquad \textbf{eq. 2}$$

In case of a stoichiometric mixture the λ-value is one. In excess of air (λ > 1) the engine runs under lean condition, in lack of air (λ < 1) the engine runs under rich conditions.
Under ideal conditions and complete combustion, the only exhaust-gasses are water and CO_2. Due to the non-ideal combustion conditions, e.g. too short residence time, non-evaporated fuel or thermodynamically hindered conversion especially at high temperatures, the real off-gas contains of a variety of undesired components such as carbon monoxide and unburned hydrocarbons. Furthermore, nitrogen oxides are formed in undesired side reactions of nitrogen and oxygen. In Table 3 typical raw off-gas compositions of spark ignition and diesel engines are listed.

Table 3: Typical off-gas composition of passenger cars [1]

		Spark ignition	Diesel
N_2	[vol%]	72.1	73.8
O_2	[vol%]	0.7	9
CO_2	[vol%]	12.3	8
H_2O	[vol%]	13.8	9
NO_x	[vol%]	0.13	0.17
CO	ppm	9000	80
HC	ppm	900	80

The pollutant concentration in a spark ignition engine is only ~1 %, whereas it is even less (0.2 %) in a Diesel engine. However, the NO_x emission is at the same level, and additionally, the Diesel engines emit particulate matters, which is not listed in the table above. The different pollutants are produced in various processes which are described briefly:

Hydrocarbons (HC): In dependency on the reaction temperature, the fuel used, the oxygen concentration and the engine itself, a huge variety of hydrocarbons such as aliphatic, aromatic, olefinic and aldehydic hydrocarbons can be formed.

Carbon monoxide (CO): Under ideal conditions the fuel is completely oxidized to CO_2. Under real condition, the oxidation might be incomplete and CO is formed as undesired side product of the reaction of hydrocarbons and oxygen. This partial oxidation is primarily caused by too low combustion temperature, too short residue time or by a lack of oxygen.

Nitrogen oxide (NO_x):

Nitrogen oxides are formed during combustion process either by the oxidation of atmospheric nitrogen or by the oxidation of nitrogen containing hydrocarbons. Since NO_2 is thermodynamically unstable at elevated temperatures NO is the main pollutant emitted.

According to their sources and mechanism of formation, nitrogen oxides can by classified in three groups [7]:

- Fuel related NO_x, which has its origin in the fuel itself. This source plays a minor role, since the modern fuel is more or less free of such nitrogen containing hydrocarbons.
- Prompt NO_x, which is formed by the Fenimore mechanism. During the oxidation of HC, HC-radicals are formed, which can react with the N_2 forming cynic acid and nitrogen radicals. The nitrogen radical can react with an oxygen molecule resulting in NO and an oxygen radical. The formed oxygen radical is able to convert the cyanic acid and NO radicals to NO. This process requires rich conditions, and therefore plays a minor role. Additionally, cyanides can occur as side products at low temperatures.
- Thermal NO_x is the major source of NO_x. Thermal NO_x is formed by the reaction of N_2 and O_2 at temperatures above 1300 °C. This mechanism is called Zeldovich mechanism. The NO_x is formed in three steps. This process is initiated by the reaction of N_2 and atomic oxygen, forming nitrogen radicals which can react with oxygen or hydroxyl radical resulting in NO.

Soot/Particles:

Noteworthy amounts of particulate matter are only formed in Diesel engines, whereas the emission of PM is negligible in spark ignition engines. If the fuel is not burned completely soot and ash particles are formed in the cylinder. Mainly, they consist of agglomerated carbon-particles with a huge specific surface. On this surface, other unburned or partially burned hydrocarbons can accumulate. The typical size of these particulate matters is between 5 and 100 nm. Due to their size these particles can penetrate into the lung and are under suspicions to cause cancer.

Different approaches to reduce the pollutants emitted had been implemented. One approach focuses on the optimization of the engine (engine management) to reduce the amount of off-gases produced in the motor. One famous example for engine management is the so called "Exhaust gas recirculation" (EGR) focusing on the reduction of NO_x in Otto and Diesel engines. In this technique, exhaust gas is added to the fuel/oxygen mixture, leading to an increase of the specific heat capacity of the cylinder content and reduces the adiabatic flame temperature. NO_x is formed at higher temperatures, therefore lower temperatures in the cylinder caused by the EGR reduces the amount of NO_x the combustions generates.

Another approach is the combustion of the pollutants in an afterburner or post-combustor. The combustion might either be thermally or catalytically induced. The thermal combustion of VOC proceeds at temperatures of 800 °C and more [8]. The drawback of this approach is the high temperature, resulting in high costs. Moreover, at the temperatures required, other harmful by-products, such as CO, NO_x and dioxins are formed and must be taken care of. Catalysts applied in catalytic combustions lower the required temperature and increase the selectivity towards the total oxidation products CO_2 and H_2O. The advantages of catalysts currently applied in the catalytic combustion and the challenges in their development will be discussed in the following chapters.

1.3. Precious metal based catalysts for exhaust gas purification

Many different catalytic systems had been used for oxidation reactions and this reflects the diversity of catalysts used for the combustion of volatile organic components (VOC). The types of catalysts used might be categorized in two groups [9]: noble metal containing catalysts and transition metal oxide based catalysts.

It is generally accepted that metal oxide catalysts are more resistance against poisoning and are cheaper compared to noble metal catalysts, but on the other hand they are less active for the oxidation reaction and therefore require a lower space velocity or higher temperatures to give comparable performance [9]. Since noble metal catalysts have a high catalytic activity and selectivity towards carbon dioxide and water at relatively low temperatures, supported precious metals are most commonly used for the catalytic combustion of VOC. Approximately 75 % of VOC oxidation catalyst currently employed in commercial applications are based on precious metals [9].

1.3.1. Reactivity of precious metal based catalysts

The catalytic performance of a noble metal based VOC oxidation catalyst depends on the noble metal, the precursor, the synthesis and the support used. The influence of these different factors will be discussed here. For the combustion of unburned hydrocarbons and the decomposition of nitrogen oxides the most commonly used noble metals are platinum, palladium, rhodium and ruthenium.

The choice, which precious metal is used, depends on the pollutants in the off-gas and the gas atmosphere. Commonly, the combustion of hydrocarbons proceeds in excess of oxygen. The most prominent exception is the off-gas after treatment of spark-ignition-engines, in which the amount of oxygen is limited and hydrogen is present as well. For the oxidation of VOC in excess of oxygen, platinum, palladium or bimetallic mixtures are most commonly used. Besides these metals, rhodium, ruthenium and iridium are used as well but their application is limited by their availability and high costs.

The general mechanism for the total oxidation of VOC over noble metal based catalysts is thought to involve the dissociative adsorption of oxygen

$$O_2 + [\ ] \rightarrow [O_2] \rightarrow 2\,[O] \qquad \textbf{eq. 3}$$

where [ ] represents a “surface site” [10]. Deep oxidation over noble metal based catalysts may either follow a Langmuir-Hinshelwood type mechanism or an Eley-Rideal mechanism. In case of nucleophilic reactant (e.g. olefins or carbon monoxide), both, the oxygen and the pollutant molecule are adsorbed and activated on the catalyst surface prior the reaction (Langmuir-Hinshelwood mechanism). If the adsorption and activation of the oxygen on the surface is followed by the direct reaction of the gaseous organic reactant the reaction follows the Eley-Rideal mechanism.

The differences in the activity of the different precious metals are attributed to their ability to activate at least one of the involved educts. Palladium and platinum are the most reactive noble metal in oxygen rich atmosphere. On the other hand ruthenium and rhodium are more suitable for reactions in which hydrogen is one of the reactants as for example in three-way catalysts. The preferred reactivity to either hydrogen or oxygen is ascribed to the “percentage of d-character” of the noble metal [11]. The “percentage of d-character” increases from platinum (44 %) to rhodium (50 %) [12]. This parameter refers to participation of the metal atom d-orbitals in metal bonding as described by Pauling [13]. The d-character follows the order Pt > Pd > Ir > Ru ≥ Rh which is in line with the reactivity towards oxygen. In reactions

in which hydrogen is involved, such as the hydrogenolysis of ethane, the reactivity follows nearly the inverse order: Ru > Rh > Ir >> Pd = Pt. The activation of hydrogen is not only influenced by the electronic structure of the metal but also by its radius, therefore the order is not exactly inverse to the order given for the oxygen activation.

If the reaction follows a Langmuir-Hinshelwood mechanism, both reactants are adsorbed on the catalysts. Since the Langmuir-Hinshelwood mechanism is supposed to be dominant, the overall activity of the catalyst depends not only in the activation of the oxygen but also on the interactions of the catalyst with the pollutant. Cant and Hall [11] investigated the deep oxidation of ethylene and propylene over different precious metals and found the order given above. This order is also true for the oxidation of aliphatic and aromatic hydrocarbons.

The deep oxidation of short-chain alkanes is the exception. In case of the catalytic conversion of methane, palladium is the most reactive noble metal. Muto et al. [14] reported that the turnover frequency (TOF) for oxidation of methane over palladium based catalysts is 50 times higher than over platinum based catalysts. Contrary to this, Burch and Loader [15] found that platinum has a higher activity than palladium under methane rich conditions. This difference can be explained by the different oxidation states of platinum and palladium, different activity of these states and by the activation mechanisms that depends on the metal used. In case of the palladium, it is generally agreed, that under oxygen-rich atmosphere at temperatures between 300-400 °C, palladium oxide is formed which is stable up to 800 °C. At temperatures above 800 °C metallic Pd is the thermodynamically favoured species. The active PdO species is formed by reversible temperature depending $PdO \leftrightarrow Pd^0$ transformation in the presence of oxygen under reaction conditions, which is well known [16]. It is generally agreed, that PdO represents the main active species for the oxidation of methane [15, 17]. This fully oxidized PdO exposes $Pd^{2+}O^{2-}$ ion pairs on the surface, which activate the almost non-polar C-H bonds by a heterolytic mechanism [18], similar to what is proposed by Choudhary and Rane [19]. In this mechanism, the C-H bond of adsorbed methane is polarized by the acid/base properties of the $Pd^{2+}O^{2-}$ ion pair. The polarization is followed by the heterolytic rupture of this bond forming CH_3^- adsorbed on Pd^{2+} and the protonation of the O^{2-}. The reactivity of platinum towards oxygen and the stability of the platinum oxide species strongly differ from the reactivity of palladium. By contrast, PtO_2 is highly unstable and decomposes to Pt^0 at much lower temperatures, around 400 °C. Additionally, PtO_2 is exceedingly volatile. This property is often considered to explain the reconstruction of platinum surfaces under oxidizing atmosphere [20]. It is also established, that Pt^0 even after calcination in air is the thermodynamically favoured oxidation state. Hwang and Yeh studied the formation of

platinum oxide species formed by the oxidation of reduced Pt deposited on γ-Al_2O_3 [21, 22] and on SiO_2 [15]. For the Pt/Al_2O_3 catalyst, essentially four different forms of oxidized platinum species were found, depending on the temperature applied for the oxidation: at room temperature, oxygen is adsorbed on the platinum surface Pt_s-O, at 100 °C Pt is oxidized to PtO, which is further oxidised to PtO_2 at 300 °C. At higher temperature (600 °C) Pt start to react with the alumina carrier and $PtAl_2O_4$ is formed. On SiO_2 no reaction between the precious metal and the carrier is observed. Additionally the O/Pt stoichiometry for Pt/SiO_2 is decreased, which is attributed to the decomposition of PtO and PtO_2. According to Burch and Loader [15], the extent of oxidation of the platinum would be the key-factor for the catalytic behaviour. A less oxidised platinum surface is reported to be more active compared to a more oxidized one. Contrary to the mechanism over Pd, a homolytic mechanism for the activation of methane on platinum is proposed. This mechanism is inhibited by oxygen. This inhibition by an excess of oxygen can be explained by the fact, that the surfaces of the platinum clusters are fully covered with oxygen because in the competitive adsorption of oxygen and saturated hydrocarbons the adsorption of oxygen is strongly favoured [23]. The dependency of the reaction rate on the oxygen concentration is called self-poisoning. Therefore, the optimum surface for the oxidation of methane over a platinum catalyst is only partially covered with oxygen and exhibits free sites for the adsorption of saturated hydrocarbons. This situation is given in methane rich atmosphere. The different reactivity of palladium and platinum towards oxygen can explain the different order of activity for rich/lean condition as mentioned above. The reactivity is not only dependent on the metal used but also on the shape of the PM clusters [12]. Catalytic combustion over Pt and Pd is known to be sensitive to the precious metal cluster size (structure sensitive reactions). Hicks et al. [24, 25] studied the influence of palladium and platinum cluster sizes on the oxidation of methane. They found the following order of reactivity:

Dispersed phase of Pt < small particles of Pd < crystalline phase of Pt < large particles of Pd. In their experiments, they varied the platinum dispersion from 100 % down to 6 %. The palladium dispersion was varied from 84 % to 12 %. For platinum the highest reaction rates were found over Pt catalyst with medium dispersions between 40-20 %. For samples with higher dispersions (90 % and 67 %) the reaction rate was 100 times slower and over bigger clusters (6 % dispersion), the reaction was 10 times slower compared to the medium size clusters. In case of the palladium catalysts, the reaction rate increases with decreasing dispersion. The catalyst with the highest dispersion (84 %) has a turnover frequency of 0.02 s^{-1}. If the dispersion is decreased to 12 % the turnover frequency is increased to 5.6 s^{-1}. As

mentioned in the previous paragraph, the metal surface is covered with oxygen and therefore it is concluded that the structure sensitivity of the oxidation reaction is related to the different activity of the adsorbed oxygen. When the platinum is completely dispersed, it is oxidized to PtO_2 at around 300 °C [16, 26]. However, if the platinum is present in form of crystallites, only the surface is oxidized during the heating up to 600 °C. Consequently, small platinum crystallites consist of a Pt^0 core, with is covered by an "oxygen containing" platinum layer. The stability of this layer is independent on the size of the crystallites [27]. As mentioned above, the PtO_2 is inactive for the oxidation of hydrocarbons whereas the chemisorbed oxygen on the crystallites is highly active. Accordingly, the cluster size has to exceed a certain size to become active but should not become too big, since the reactivity is correlated to the surface area of the metal as well. This is not only true for the oxidation of methane. Radic et al. [28] investigated the deep oxidation of n-hexane and toluene over Pt/Al_2O_3. In their experiments, they found that the turnover frequencies for both hydrocarbons were ten times higher over a catalyst with a Pt particle size of 15.5 nm than over a catalyst with particle of size only 1 nm.

The oxidation of saturated and unsaturated hydrocarbons is not the only reaction that is sensitive to the noble metal cluster size. Yao [29] studied influence of the precious metal cluster size on the oxidation of CO over Pt, Pd and Rh deposited on Al_2O_3 in excess of oxygen. For this the reaction, the formation of CO_2 clearly correlates to the dispersion. The rate of the CO_2 formation is increased with increasing metal dispersion. Another important reaction is the conversion of NO into NO_2. The oxidation of NO to NO_2 over Pt/silica favours platinum clusters with an average cluster size between 4-6 nm as described by Jayta [30].

1.3.2. Influence of the support on the catalytic activity

Niwa and co-workers [31] where the first, who reported the influence of the support material on the catalytic combustion of methane. For supported platinum catalysts, they found that the activity is increased in the following order: Pt/SiO_2-Al_2O_3 > Pt/Al_2O_3 > Pt/SiO_2. Ishikawa et al. [32] extended this study to other metal oxide carriers and mixtures of them, commonly used in catalysis, for instance SiO_2, Al_2O_3, TiO_2, CeO_2, ZrO_2 and La_2O_3. Additionally, they studied the influence of sulphated carriers such as ZrO_2-SO_4 and Al_2O_3-SO_4. The propane conversion was 60 % and 100 % at 623 K and 773 K, respectively over the Pt/SiO_2 catalyst which is the most active platinum catalyst supported on single oxides, whilst Pt/La_2O_3 gave only ca. 1 and 15 % conversion under the same reaction conditions. They found that the activities are in the order of Pt/SiO_2 > Pt/Al_2O_3 = Pt/TiO_2 = Pt/CeO_2 > Pt/ZrO_2 > Pt/La_2O_3.

This activity pattern is similar to the order of acid strength of the support oxide: $TiO_2 > SiO_2 > ZrO_2 > La_2O_3$, though Pt/SiO_2 seems to be the exception. It is also reported, that the platinum dispersion correlates to the surface area of the support used. The dispersion is poor on low surface area carriers such as La_2O_3 and increases with the surface area of the support [9]. For this reason, the dispersion was found to vary from 9 % on La_2O_3 and 67 % on Al_2O_3. Nevertheless, it is concluded, that mayor effect on activity is induced by the acid properties of the support and that the dispersion plays only a minor role. The same order of reactivity was found by Yazawa [33, 34] for the oxidation of propane and by Pliangos [35] for the combustion of ethylene. Both studies conclude that the differences in the activity arise from the interactions between the carrier and the precious metal and not to the structure sensitivity of the reaction. Additionally, Yazawa [33, 34] studied the influence of the support acidity on the electronic properties of platinum clusters supported on various metal oxide carriers by IR measurement of adsorbed CO. A strong CO stretching band was observed on the IR spectra of every catalyst in the range of 2050-2080 cm^{-1}. The position of this band depends on the support, and is shifted to higher wavenumbers with increasing acidity of the support. It is widely recognized, that the wavenumber of CO stretching reflects the variation in the electronic state of the noble metal and increases with the increasing electron-deficiency of the noble metal [36, 37]. Thus, it is confirmed, that platinum on acidic supports is more electron deficient than on basic supports such as MgO. As mentioned above, the catalytic activity is linked with the oxidation state of the metal. Yazawa et al. [38] demonstrated that the electron-deficient metal clusters are more resistant toward oxidation and that the higher dispersion can be better maintained. They also proved that the same is true for palladium based catalyst. The self-inhibiting by oxygen is much more pronounced over basic metal oxide. In line with the effect of the carrier, it is reported, that the self-inhibition by oxygen can be influenced by the addition of different metals. Yoshida [39] investigated the influence of potassium, magnesium, aluminium, vanadium, tungsten and molybdenum on the activity of a Pt/Al_2O_3 catalyst. The addition of strongly electropositive metals such as potassium depresses the activity, whereas the addition of less electropositive metals such as vanadium, tungsten and molybdenum had a positive effect of the reaction rate. Thus, the reactivity increases with increasing electronegativity. From what said above Yoshida [39] summarized:

"The total electrophilic property of support materials and additives improves the oxidation-resistance of noble metal, which results in high activity".

This knowledge provides the possibility to develop noble metal based catalyst by the choice of the support and promoters by adjusting the electron density in the precious metal valence orbitals.

Another well documented method to improve the activity of platinum based VOC oxidation catalysts is the application of sulphated carriers as for example ZrO_2-SO_4 and Al_2O_3-SO_4 [40-42]. The increased reactivity by sulphatization of the alumina carrier is explained in different ways by different researchers. Lee et al. [41] and Burch et al. [43] assigned this effect to the formation of stable sulphate species at the platinum/support interface. They conclude, that the dissociative adsorption of propane and thereby the intrinsic activity of platinum is enhanced. Hinz et al. [44] suggest, that new acid sites are formed at the Pt/Al_2O_3-SO_4 interface, which generate a new reaction pathway consisting of the initial cracking of propane. Another explanation was recently given by Corro et al. [45]. They propose that the promoting effect of the sulphate is due to interactions of surface sulphate species with highly oxidized Pt atoms at the edges of platinum particles.

1.3.3. Deactivation mechanism of noble metal based catalysts

Besides the intrinsic activity of a catalyst, its resistance against thermal deactivation and chemical poisoning is a mayor issue for developing new attractive catalysts for environmental applications. One of the major sources of catalyst deactivation is the exposure to high temperatures, especially in automotive applications. Another source of deactivation origins from poisons in the fuel such as sulphur containing compounds or from the precursor used for the synthesis of the catalyst. The influence of these deactivation mechanisms will be discussed here.

Thermally induced deactivation:

Thermally induced deactivation may influence the catalytic performance in three different ways. First, sintering of the metal species, resulting in a cluster growth and a reduced number of surface atoms exposed to the reactants. Second, the thermal stress may induce structural changes in the support and third the precious metal and the support might react, forming an inactive species.

Thermally induced changes of the precious metal:

Thermally induced agglomeration of small precious metal clusters supported on carriers leads to a reduction of the active noble metal surface since the surface-to-volume ratio is decreased [46]. Due to this coalescence, fewer active metal atoms can participate in the reaction. This sintering leads to a “loss of sites” which is accompanied by a shift in the conversion as a function of the temperature plot towards higher temperatures but has no effect on the activation energy of the reaction as far as there are no phase transformations. Sintering processes generally occur at high temperatures and are favoured by the presence of water vapour. Exceeding the Tamman temperature (half of the melting point of the metal $T_{Tamman} = 0.5 * T_{melting}$), the metal atoms and clusters become mobile and can randomly move over the support [47]. Three principal mechanisms of metal crystallite growth have been reported: (1) crystallite migration, (2) atomic migration, and (3) vapour transport at very high temperatures [48]. Crystallite migration involves the migration of entire crystallites over the support surface followed by collision and coalescence [48]. Atomic migration occurs via escape of metal atoms from a crystallite, transport of these atoms across the surface of the support, and subsequent capture of the migrating atoms by collision with other metal crystallites. Since larger crystallites are more stable (the metal-metal bond energies are often greater than the metal-support interaction), small crystallites diminish in size and the larger ones increase [49]. In this case, the decrease in mass-based activity is proportional to the decrease in metal surface area [48].

Besides the reduction of active surface species, structure sensitive reactions are influenced by the morphology of the noble metal clusters. Therefore, the specific activity can either increase or decrease with increasing metal crystallite size during sintering if the reaction is structure-sensitive, or it can be independent of changes in metal crystallite size if the reaction is structure-insensitive. Thus, for a structure-sensitive reaction, the impact of sintering may be either magnified or moderated; while for a structure insensitive-reaction, sintering has in principle no effect on specific activity (per unit surface area), but will decrease the overall performance due to the loss of active surface area.

In addition, bigger clusters expose cluster planes to the reactants on with the reactants can absorb more strongly. Therefore, the reaction rate might be influenced by self-inhibition by the educts such as oxygen, ethylene or CO, as mentioned above. Moreover, the thermal treatment in excess of air might change the oxidation state of the precious metals. For Pt this can result in the formation of a less active species such as Pt^{4+} [50].

Thermally induced changes of the carrier:

Thermal stress can also influence the crystal structure of the support. For example, γ-Al_2O_3 is dehydrated at elevated temperatures. This loss of water is associated with the a gradual loss of the internal pore structure network [46] and a fundamental loss of porosity. As a result of this sintering phenomenon, the pore opening is progressively getting smaller, resulting in an increased pore diffusion limitation and finally in a loss of active sites. Additionally, the catalytic active species is encapsulated in the collapsed pores and as a result no more accessible for the educt molecules. This phenomenon can be determined by a gradual decrease of the activation energy, which can easily be recognized by a decrease of the slope in the conversion as a function of the temperature plot. An additional mechanism for the deactivation due to thermally induced changes of the support is the conversion of the support material into another crystal structure which is mostly accompanied by a reduction of the surface area. For example, the surface area of alumina is reduced from approximately 150 m^2/g to < 50 m^2/g if the crystal structure is converted from γ-Al_2O_3 to δ-Al_2O_3. The same is true for other carriers such as TiO_2 if the anatase structure is converted into rutile structure. The phase transfer temperatures are 1200 °C [6] and 610 °C [51] for Al_2O_3 and TiO_2, respectively.

Catalytic species-carrier interactions:

Phase transformation by reaction of the catalytic active component with the support can be another source of deactivation if the reaction product is less reactive than the initial dispersed metal species. One well-known example is the deactivation of tree-way catalyst (TWC). In state of the art TWC catalysts, rhodium is deposited as Rh_2O_3 on oxide carriers such as alumina or zirconia. At temperatures of about 800-900 °C and under an oxidizing atmosphere, Rh starts to react with the alumina carrier, forming inactive Rh-aluminate [52]. One approach to overcome this problem is the use of less reactive carriers such zirconium or ceria/zirconium. These carriers have a rather randomized pore structure and therefore, the PM on the surface has a high tendency to sinter at evaporated temperatures and to form bigger and less reactive clusters. Besides the cluster grown, the Rh can react with the CeO_2 during the high-temperature lean conditions, reducing the catalytic activity of both components. The formation of precious metal aluminates at elevated temperatures is also reported for palladium [16] and platinum [53].

Poisoning:

Poisoning is the strong chemical interaction of a catalytically active site with products or impurities instead of interacting with the educts of the reaction of interest transforming active species into less active or non active ones. Maxted [54] reported that for metal catalysts containing metal of the groups VIIIB (Fe, Ru, Os, Co, Rh, Ir, Ni, Pd, Pt) and IB (Cu, Ag, Au), typical poisons are molecules containing elements of the groups VA (N, P, As, Sb), VIA (O, S, Se, Te) and VIIA (Cl, Br, I). The poisoning by the elements mentioned above can be either reversible or irreversible.

The strength of the interaction between the active metal and the poison depends of the electronic structure of both elements and the steric accessibility of the valence orbital of the poison. The strength of the interaction follows the Lewis Hard-Soft-Acid-Base model (HSAB). The poisoning activity of a given poisoning element depends also on the accessibility of the valence orbital of the corresponding element. For example the lone electron pairs of sulphur in H_2S are less shielded than in SO_2. Thus H_2S is a more effective poison than SO_2. However, catalysts used in environmental catalysis are mainly oxidation catalysts, operating in excess of oxygen. As a result H_2S is oxidised to SO_2 or SO_3 and therefore has the same impact towards the catalyst activity as SO_2 or SO_3.

The poisoning effect of chloride and sulphur containing components is of special interest. Poisoning by chloride is of importance since supported palladium and platinum catalyst are partly prepared by impregnation of the support materials with Cl-containing precursors. Additionally, it turned out that commercial supports might also contain significant amounts of chloride [20]. The impact of sulphur containing components is of interest since most off-gas feeds contain these components.

The inhibiting effect of halogenated compounds in the feed on the deep oxidation of methane was first reported by Cullis and Williatt [55]. They found, that palladium is more sensitive to poisoning by chloride containing pollutants than platinum. Moreover the activity of Pt/Al_2O_3 can fully be restored. Contrary to this, the chlorine poisoning of Pd/Al_2O_3 is only partly reversible. It was proven by XPS, that the deactivation of the Pd catalyst was caused by the reduction of PdO to Pd^0 and that used catalysts can be partly reactivated by oxidative treatments.

The situation for catalysts prepared by chloride containing precursors or carrier in the oxidation of hydrocarbons is different to the oxidation of chlorinated VOCs. Simone et al. [56] were the first who reported this phenomena. They compared two catalysts, one prepared by $Pd(NO_3)_2$ and one prepared by $PdCl_2$. The catalyst prepared with the nitrate

precursor was more active in the oxidation of methane but had a lower dispersion. Moreover, the first catalyst was deactivated by thermal treatment whereas the latter became more active after the same thermal treatment. This activation of the catalyst prepared with the chloride containing precursor was attributed to desorption of residual chloride from the metal cluster due to the high temperature treatment. The mechanism which causes the strong inhibition of the catalytic activity by chloride is not yet established. Roth et al. [57] proposed for Pd based catalysts, that chloride is mainly is located on the support, regardless how it was introduced and desorbs in the form HCl under reaction condition. It is proposed, that HCl competitively adsorbs on the metal site, block these sites and as a result suppresses the activity.

In case of Pt/Al_2O_3 a second chloride species is proposed by Marceau et al. [58]. They suggest, that beside the chloride adsorbed on the carrier, an additional chloride species exists, which is supposed to be located at the interface of the platinum cluster and the support, eventually bridging between Pt and Al and therefore having direct positive influence to the adsorption and catalytic properties of noble metal.

Sulphur dioxide can act as poison but also as a promoter. It is known, that it acts as a poison in the oxidation of alkenes [18] and in the oxidation of methane over palladium and rhodium catalysts [59]. However, alkane oxidation over platinum on alumina catalyst is promoted by SO_2.

It is known that PdO is the active species for the oxidation of methane. It is proposed by Meeyoo et al. [59] that the deactivation is due to the reaction of the noble metal oxide with SO_2 forming the inactive $PdSO_4$. They gave the same explanation for the deactivation for rhodium based catalysts. Limited amounts of rhodium oxide are formed on the rhodium cluster surface under oxidizing atmosphere [60]. For that reason, it is again concluded, that the formation of sulphate species is the reason for the deactivation. The rate of the deactivation of Pd is dependent on the support properties. Some of the adsorbed SO_2 is oxidized to SO_3 over the noble metal, followed by a spill over to the carrier. In case of alumina this reaction leads to the formation of $Al_2(SO_4)_3$. This reaction is not possible if the precious metal is deposited on non-sulphatable carriers such as SiO_2. The formation of $Al_2(SO_4)_3$ is a reservoir for SO_2 and hence, the deactivation is slower over aluminium compared to the non-sulphating supports as reported by Hoyes et al. [61].

Contrary to the deactivation of palladium and rhodium, the oxidation of methane over platinum on alumina is promoted by SO_2. Since PtO is not the favoured oxidation state of platinum under reaction condition, the formation of platinum sulphate is less likely. Hence, the change of the reactivity is not assigned to interaction of SO_2 with the precious metal but to

interaction with the support. It is commonly established, that the alumina carrier reacts with the sulphur dioxide forming $Al_2(SO_4)_3$. The sulphating of the carrier enhances the oxidation rate of alkanes on platinum catalysts [33-35]. Since the promoting effect is due to the interaction between the support and SO_2, this effect can only occur on carriers that form sulphates, but not on non-sulphatable carriers. Besides the positive effects of sulphating the alumina carrier, this reaction slowly causes pore blocking, resulting in pore diffusion limitations and a loss of active sites affecting the activity of the catalyst [33-35].

Additionally to the poisoning by chemical interactions as mentioned above, the catalysts activity is affected by the presence of water and soot. Both substances can reduce the accessibility of the active species by pore blocking. This kind of poisoning is at least partially reversible e.g. water and soot can be removed at increased temperature by vaporisation of water or total oxidation of the soot.

Washcoat loss:

The loss of catalytically active washcoat due to attrition or erosion is a serious source of irreversible deactivation. This kind of deactivation is of special importance for monolithic catalysts, since the gases are flowing with high velocities through the honeycomb channels and active component is exposed to sudden changes in the process and temperature. Differences in the thermal expansion of the honeycomb and the washcoat lead to the loss of the binding between these two components that result in irreversible loss of the active material.

1.4. Zeolites in catalysis

Zeolites represent a well known class of catalysts. They are either used “as synthesised” or they are metal exchanged resulting in bifunctional catalysts. Pure large pore zeolite such as BEA and FAU zeolites are catalyst for various acid/base catalyzed reactions e.g. FCC [62], alkylation [63, 64] or acylation [65] of hydrocarbons. Besides the pure zeolites, metal oxide and precious metal containing zeolites are used in catalysis. Copper [66-68] and iron [69-71] containing zeolites for the SCR of NO_x are the most widely studied metal containing zeolites in environmental catalysis. Precious metal containing zeolites are widely used in petroleum and petrochemical industries. Among the most important applications of bifunctional zeolites are the hydroisomerisation of paraffins over acidic Pt/H-MOR and the selective reforming of naphtha to aromatics over non-acidic Pt/LTL. Additionally, noble metal containing zeolites are used in the deep oxidation of hydrocarbons and HC-SCR. The synthesis and advantages of

precious metal containing zeolites for environmental catalysis will be discussed in the following chapter.

1.4.1. Structure and catalysis of zeolites

Zeolites are crystalline aluminosilicates with precisely defined microporous structures. Their pores and cages have molecular dimensions, which make it possible to discriminate between molecules of different sizes; hence, zeolites are also known as molecular sieves featuring shape selective properties. The channel like structure allows fast intracrystalline transport proceeding. Aluminium and silicon atoms (denoted as T-atoms) are tetrahedrally coordinated to four bridging oxygen atoms forming TO_4 tetrahedra. The TO_4 tetrahedra are often referred to as the primary building units of zeolite structures. The primary building units are linked together to form secondary building units. The secondary building units consist of n-ring structures which can contain 4 to 20 tetrahedra. Structures consisting of 8, 10 or 12 tetrahedra are the most favoured ones. Zeolites are classified according to their pore size which depends on the number of oxygen atoms in the aperture ring. Small pore zeolites consist of 8-member rings, medium pore zeolites of 10-member and large pore zeolite of 12-member oxygen rings. The corresponding pore openings have diameters of 0.4, 0.55, and 0.73 nm, respectively. When Si^{4+} is replaced by Al^{3+} in the zeolite framework, the negative AlO_4-building block has to be compensated by a counter ion. The following formula gives the chemical composition of zeolites where M is the counter ion with the charge n^+.

$$M_{x/n}[(AlO_2)_x\,(SiO_2)_y] * zH_2O \qquad \textbf{eq. 4}$$

The Si/Al ratio in zeolites varies considerably, from 1 which is the lower ratio for zeolite X to near infinity in silicalites. Al-O-Al linkages are forbidden due to local charge restrictions, so that 1 is the lowest obtainable Si/Al ratio (Loewenstein rule) [72].

Brønsted acidity (H^+-donator) can be introduced if protons are the compensation ion for AlO_4^-, thus making the material to a solid acid. The concentration of Brønsted sites is directly related to the number of framework Al atoms per unit cell. The strength of the acid sites depends on the polarization of the OH band and therefore is influenced by the angle between the two bridging T-O bonds and the distance between the T-atoms connected to the bridging oxygen. Consequently, the acid strength depends on the structure of the three-dimensional network and on the local atomic environment [73]. At the same aluminium content, the strength of the Brønsted acid sites was found to follow the order:

H-ZMS-5 > H-Mor > H-BEA > H-Off, showing the influence of the structural factor [74]. Since aluminium atoms carry a lower charge than the silicon atoms, the electronegativity of the zeolite is strongly dependent on the ratio between the silicon and aluminium atoms in the framework.

Usually, the strength of the acid sites increases when the Si/Al ratio is increased. In parallel, the total amount of the acid sites is decreased. A higher electron density is donated by aluminium than by silicon, resulting in a higher oxygen charge and a stronger proton-oxygen interaction and therefore in a reduced acid strength. Generally, the catalytic activity for an acid catalyzed reaction goes through a maximum with increasing Si/Al ratio and is individual for each reaction. The optimum depends on the framework density of the zeolite [75].

Increasing the aluminium content of a zeolite leads to a decrease of the framework stability in the calcination process or the hydrothermal stability [76]. The reduced framework stability origins in the susceptibility of the Al-O bond to hydrolysis in acidic and basic media and under hydrothermal conditions. The dealumination leads to the formation of cationic aluminium species, which can act as Lewis acid sites. Therefore, the dealumination results in a reduction of Brønsted acid sites accompanied by an increase of the Lewis acid sites. Under serve condition, an extensive and uncontrolled removal of aluminium atoms from the zeolite lattice can take place, leading to a progressive collapse of the crystal structure.

The inductive effect, arising from the Lewis acid sites, on the neighbouring protonic acid sites increases their acid strength, resulting in a higher catalytic activity. Besides the Si/Al ratio and the degree of dealumination, the acid strength is also influenced by charge compensation ions. For a given cation valence, the influence depends on the cation size. For the cracking over FAU, the deactivation effect follows the order: $K^+ > Na^+ > Li^+$ [77].

Besides acid sites the zeolite structure consists also of basic sites. The basic sites in the zeolite are the oxygen atoms in the framework (T-O-T) bearing the negatively charges of the lattice. These sites are called structural basic sites and despite to the acidic protons, the oxygen is fixed to the lattice and therefore is not able to move to the reactants as protons can do. As a result, the reactant molecules have to approach the lattice oxygen in a configuration that is favourable for the formation of reaction intermediates [78].

As in case of the Brønsted sites, the basicity varies with the composition and the structure of the zeolite. The lattice oxygen atoms in the AlO_4^- tetrahedra have the highest negative charge, resulting in the strongest basicity. In line with the acid strength, the strength of the basic sites depends on the T-O-T angle and bond length but the basic properties increase in the opposite direction of the acid properties.

Furthermore, the hydrophilicity/hydrophobicity is determined by the Si/Al ratio. The aluminium content is the main parameter, influencing the ionic characters of the zeolite surface. Consequently, the ability of a zeolite to absorb either polar or non-polar molecules depends on its composition. Alumina rich zeolites can be used to remove water from organic solvents whereas silica rich zeolites can be used to adsorb non-polar molecules.

As mentioned above, zeolite based catalysts are widely used in industrial catalysis. In many applications, the "pure" zeolite is used as catalyst, e.g. in protolytic cracking or dehydrogenation.

Compared to amorphous supports such as alumina or silica, zeolites have a high crystallinity and a defined pore structure. This results in a high selectivity towards special products of zeolite-catalysed reactions. The concept of molecular shape-selective catalysis implies an intimate interaction between the shape, size, and configuration of the reactants, transition states and products, and the dimension, geometry and the tortuosity of the channels and cages of the zeolite [79]. Herein the selectivity of the zeolite is either determined by the reactant, the product or by the suppression of a transition-state. Reactant selectivity means that molecules which are too bulky to diffuse trough the pore structure towards the active centre, are prevented to react. This technique is applied e.g. in the Selectoforming process (Mobil) in which short paraffins are selectively hydrocracked from a mixture of paraffins and aromatics. Product selectivity means the suppression of the formation of bulky intermediates and products by the low dimensions of the cavities and the pores, resulting in a high selectivity towards one of the possible reaction products. Besides the suppression of transition states, product selectivity arises from the geometrical dimensions of the product molecule. Bulky product molecules are trapped by the pores and are further converted to the desired product molecule, which is less hindered and therefore able to leave the zeolite. This high selectivity plays an important role in the synthesis of para-aromatic compounds over ZMS-5 based catalysts. The selectivity is also dependent on the void fraction in the pores, since some transition states require more space than that available in the pores of the zeolite. For example, the transalkylation in the isomerisation of xylenes over ZMS-5 is suppressed because the bimolecular transition state for the transalkylation cannot be formed due to the geometric dimensions in the pores. Accordingly, the addition and substitution of bulky molecules as well as the oligomerisation is suppressed.

Despite of the huge variety of industrial and petrochemical reactions catalysed by zeolite-based catalysts, zeolites are only rarely used in commercialised environmental applications. One well established example is the catalytic decomposition and conversion of N_2O and NO_x

over iron or copper containing zeolites, e.g. in the Sued-Chemie/Uhde EnviNO_x-Process. Besides their utilization as catalyst, zeolites are also used as storage-components for example as cold-start trap for hydrocarbons in vehicles as due to their large void fraction, zeolites can absorb up to 50 % of their total solid volume.

Zeolite Beta:

Zeolite Beta (BEA), which is of primary interest in this work, was first synthesized by Mobil Oil Corporation in 1967. The high-silica zeolite was synthesized in 1967 from alkaline aluminosilicate gels in the presence of sodium and tetraethylammonium cations. In Figure 1 the structure of BEA is shown. The three dimensional channel system is constructed of 12-member rings constituted of perpendicular straight channels (0.66 x 0.67 nm aperture) and of sinusoidal channels (0.56 x 0.56 nm aperture) [80]. BEA is an intergrowth hybrid of two distinct structures, polymorphs A and B [80] containing of nine unique tetrahedral framework sites. Unsatisfied linkages are present in the transient region between the two polymorphs inducing a stacking disorder with a high concentration of internal defects [81]. H-BEA has at least two different types of Lewis acid sites, attributed to extra framework aluminium species and to aluminium in defect position and Brønsted acidic bridging hydroxyl groups.

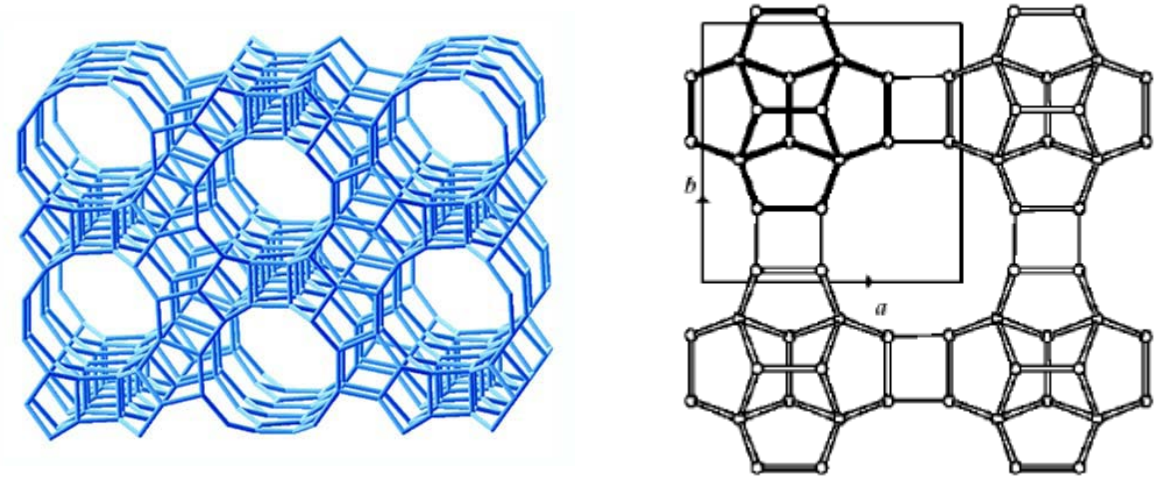

Figure 1:Framework of zeolite BEA along [100] (left) and periodic building unit (right) [82]

1.4.2. Precious metal containing zeolites catalysts

Besides the “pure” zeolite, metal exchanged zeolites are used as catalysts. The introduction of a precious metal opens new reaction pathways for the catalyst e.g. for isomerisation and (de)hydrogenation. Secondly, the metal function improves the catalyst stability against coke formation.

Precious metal nanoclusters encaged in the pore system of zeolites are of interest for catalysis because this approach combines the advantages of the zeolites, such as high surface area, temperature stability, acid/base properties and hydrocarbon storage capacity with the advantages of small precious metal clusters. The porous structure of the zeolite framework offers steric restrictions that limit the cluster size and influences the electronic structure of the encapsulated noble metal. One of the advantages of using metal exchanged zeolites is the improved selectivity towards special products. On the other hand, the effective exploitation of the expensive noble metal can be enhanced by decreasing the cluster size, so that most of the precious metal is exposed to the reactant and therefore can participate in the reaction. In respect to this, zeolites are suitable supports, because the steric constrains imposed by the cages an channels limit the cluster size [83]. The cages are small enough to exert solvent-like effects on clusters within them, and the cages may cause the cluster structures and properties to be different from those of clusters in solution or on the nearly planar surfaces of amorphous supports. The encapsulation of the clusters reduces the interactions between them and thus increasing their thermal stability as reported by Sachtler [84] and Gates [85].

Besides the mechanical trapping of these clusters in the zeolite matrix, the electronic structure of these nanoscale clusters is strongly influenced by the zeolitic support and thus resulting in unique catalytic properties. The changes in the catalytic activity are ascribed to the modification of the electronic properties of the metal particles induced by the support-metal interactions. Several models have been proposed to explain the influence of a zeolite upon the structure and performance of the noble metal cluster. In case of a zeolite support, an electron deficient cluster is formed by the interaction between the metal and the Lewis and/or Brønsted acid sites of the zeolite [86]. In case of an interaction of noble metal particle and the proton of a Brønsted acid site, a so called "*proton-metal adduct*" [86] is formed, resulting in an electron withdraw from the metal cluster towards the proton, thus forming an electron deficient cluster. The same is true for the interaction with other positively charged ions nearby the metal cluster, such as aluminium in case of zeolites [87]. On the other hand, electron-rich clusters are formed if electrons are donated from the basic oxygen towards the metal cluster. The electron richness of the oxygen in the lattice is predominately influenced by the ionic character of the cations in the oxide support; with electron rich oxygen in basic supports with alkaline cations and electron poor oxygen in acidic supports having protons or more covalent cations [88]. For these reason the changes in the electronic structure are more pronounced if the noble metal is deposited on zeolites than on other metal oxides, resulting in a higher activity, increased thermal stability and improved resistance to poisons such as sulphur. The

improved catalytic activity and thermal stability of electron negative of the clusters is ascribed the oxidation-resistance of those clusters by Yazawa et al. [33, 38] and Yao [29]. The same trend is described by Sugaya et al. [89] who established a linear correlation between the electronegativity support and the turnover frequency. It is suggested, that electronegative supports suppress the oxidation of Pt^0 to less active oxidized platinum species. The same explanation is given for the improved sulphur resistance.

Nonetheless a lot of work was focused on the influence of the support towards the reactivity of the precious metal deposited. Garetto et al. [90, 91] were the first who studied platinum containing zeolites for the deep oxidation of lower alkanes. In their studies, they compared platinum deposited on MgO, Al_2O_3 and zeolites KL, HY, ZMS-5 and BEA. They reported a drastic enhancement of the turnover frequency. The TOF over Pt/acetic zeolites were two orders of magnitude higher compared to Pt/Al_2O_3. They also found that the reactivity of Pt/KL is remarkably higher than of Pt/Al_2O_3, although these two carriers exhibit the similar acid sites density and strength. Contrary to the acid properties, both carriers differ in the propane up-take, which is one order of magnitude higher over the Pt/KL catalyst compared to the alumina based catalyst. They explained the increased reactivity of Pt/zeolite catalysts with the reported drastic increase of the density of adsorbed propane and proposed that the higher propane density promotes the oxidation. From their results, they conclude, that Pt/zeolite based catalysts offer two reaction pathways.

For the main reaction mechanism over Pt clusters it is assumed that the rate-determining step is the dissociative chemisorption of the alkane on Pt with the cleavage of the weakest C–H bond followed by the interaction of the intermediate with oxygen atoms adsorbed on adjacent sites. For zeolite based catalysts, they propose a parallel oxidation pathway in which propane is adsorbed and activated on surface sites in the metal-zeolite interfacial region and reacts with oxygen spilled-over from platinum. Propane oxidation via this latter mechanism will be promoted by increasing the density of adsorbed propane molecules in the interfacial region.

1.4.3. General synthesis methods for noble metal containing zeolites

In the synthesis of metal containing zeolites the three main steps usually are: (1) introduction of the metal, (2) calcination and (3) reduction. The techniques used for the introduction of metal compounds and/or ions can be classified in three groups: impregnation, ion exchange and vapour phase decomposition. The calcination step is normally performed under air at high temperatures to decompose the precious metal precursor and might be followed by a final

reduction step. Each of these steps affects the metal cluster dispersion, location and distribution and therefore affects structure of the metal cluster and the catalytic performance.

Ion exchange:

Ion exchange is the most commonly used technique to introduce metal ions into a zeolite [92]. For the ion exchange procedure of the acidic proton or any other counter ion, an intrinsic behaviour of the zeolite is exploited. The ion-exchange depends on the zeolite composition and structure, as well as on the ions involved. Ion exchange isotherms for most metal ions and zeolites have been reported [93]. The ion exchange requires special attention, since this process is sensitive to the condition under which the ions are exchanged, e.g. the pH value. The pH value of the slurry has to be adjusted in order to avoid the hydrolysis of the metal ions. Several multivalent ions exist as free ions only in very acidic slurry, in which the zeolite starts to decompose [94]. This problem can be overcome by using complex ions for the exchange. The most frequently used complexes are amine complexes e.g. tetramine ($Pt(NH_3)_4^{2+}$, $Pd(NH_3)_4^{2+}$), hexamine ($Rh(NH_3)_6^{3+}$) or pentamine-chloride ($Rh(NH_3)_5Cl^{3+}$) complex ions [95]. These complexes are more stable against hydrolysis and remain their cationic character. However, the decomposition of these complexes has to be performed very carefully to avoid migration and agglomeration of the metal cations. The ion-exchange process is limited by the exchange capacity of the zeolite, which increases with an increasing aluminium concentration in the lattice. For that reason the conventional ion-exchange procedure is not feasible to introduce larger amounts of metal into the zeolite. This problem can be overcome by the using solid state ion exchange. In this process, an intimate mixture of the zeolite and the metal salt is treated at high temperatures in order to incorporate the metal cations into the zeolite.

Impregnation:

With the impregnation method, both metal ions and neutral compounds can be introduced into the zeolite. The impregnation can either be performed as "*incipient wetness impregnation*" or as "*adsorption-impregnation"* of metal complexes. The ion exchange introduces only metal cations whereas if the metal is introduced via impregnation the counter anions are incorporated as well. Impregnation methods can only be applied, if the effect of the remaining anions is negligible or if the anions can be eliminated for example by calcination [92].

Generally, when impregnation methods are applied, a slurry comprising of the zeolite and an aqueous solution of the metal salt or complex, is heated under stirring until the water is evaporated. In this process, ion exchange takes place simultaneously with the impregnation.

The ion-exchange can only be suppressed, if the size of the metal complex restricts the entering of the pore openings or if the exchange of given ion-zeolite pair is not favoured. In general, metal containing zeolites, prepared by this method contain various metal clusters of different size which are distributed in the pores of the zeolite and on the external surface. The impregnation method is the only technique, to introduce quite large neutral metal complexes, such as organometallic compounds. To synthesize clusters, being homogeneously distributed in the pore system, the "*incipient wetness impregnation"* can be applied. Prior the incipient wetness impregnation, the zeolite is dried in order to remove the residual water from the pore system. For the impregnation, an aqueous solution of the metal is prepared. The volume of the solution has to correspond to the maximum water adsorption capacity of the zeolite and the metal concentration has to correspond to the desired concentration of the catalyst. If the metal solution is contacted with the dried zeolite material, the complete impregnation solution is adsorbed in the pore system of the zeolite. This process is driven by the capillary forces arising. Since the volume of the impregnation solution corresponds to the water adsorption capacity of the zeolite, the noble metal is exclusively located in the pore and channel system. This method is limited by the solubility of the metal salt, the size of the metal precursor and the water adsorption capacity of the zeolite.

Vapour phase decomposition:

The vapour phase decomposition is an additional route to introduce metals into the zeolite pores. Normally, metal carbonyl complexes are used for this method because of their high volatility. The advantages of this method are: volatile metal carbonyl distribute homogenously in the zeolite pores, after the decomposition of the carbonyl, the metal is in atomic dispersion [92].

Calcination and reduction:

Metal containing zeolites are calcined in order to decompose and to eliminate the counter ions or ligands of the metal complex or salt used for the introduction of the metal in order to transfer the precious metal into the active metal/metal oxide phase. Therefore, the minimum calcination temperature is given by the thermal stability of the metal precursor. Depending on the calcination temperature, calcination atmosphere, the thermodynamic stability of the precious metal the active metal is oxidized to the corresponding metal/metal oxide during the calcination. If it is necessary, the calcination step is followed by a reduction step to reduce the metal oxide to non-charged clusters. Both steps can have a major impact on the structure of the metal clusters and hence on the activity of the catalyst. The crucial parameters for the

calcination are especially the temperature used for the calcination, the heating rate and the atmosphere. The same is true for the reduction.

Calcination:

The calcination temperature and atmosphere crucially affects the precious metal distribution and particle size. Amongst others, Sachtler et al. [96] studied the effect of calcination temperature in air on platinum distribution and cluster size in Y zeolite. They reported that the calcination at lower temperature (360 °C) favours the formation of platinum ions being exclusively located in the supercages of the carrier. Contrary to that, if the calcination is carried out at 550 °C, the platinum ions are stabilized in the sodalite cages. At higher calcination temperatures (between 500 °C and 600 °C), the metal oxide can react with a nearby acid site of the zeolite, forming divalent platinum ions and water according to the reaction in eq. 5 [97].

$$PtO + 2H^{+}\text{-Zeo} \rightarrow Pt^{2+} - \text{Zeo} + H_2O \qquad \textbf{eq. 5}$$

Furthermore, the Pt^{2+} ions were observed to migrate from the supercages into the sodalite cages [98, 99] which cannot be entered by PtO due to the small apertures of these cages. Another factor affecting the metal distribution arises from the precursor used for the introduction of the metal. If amine containing precursors are used, auto-reduction may occur during the calcination procedure [100, 101].

$$Pt(NH_3)_4^{2+} + 2\ \text{Zeo} + 5/2\ O_2 \rightarrow Pt^{(0)} + 2\ H^{+}\text{-Zeo} + 2\ N_2 + 5\ H_2O \qquad \textbf{eq. 6}$$

The interaction of these zero valent clusters with the carrier are much weaker than the interactions of the divalent ions or metal oxides. The decreased interactions increase the mobility of the clusters and lead to migration and cluster grow. The formation of bigger clusters is accompanied with a reduction of the surface free energy and therefore is thermodynamically favoured. It is reported, that if amine containing precursors are used the calcination has to be performed very slowly with a heating rate of 0.5 K/min in an excess of oxygen to avoid migration and agglomeration of the metal [100]. However, this procedure cannot be generalized and depends on the metal used since it was found that $Ru(NH_3)_6^{3+}$ on Y-FAU forms bulk Ru-oxide upon heating in air [102].

Another calcination method for ZMS-5 zeolite impregnated with $(NH_3)_4Pt(NO_3)_2$ is proposed by Schüth et al. [103]. They found, that the calcination under inert gas atmosphere leads to the formation of nanoscale clusters in the pore system of the zeolite. They showed that the distribution of the clusters strongly depend on the calcination temperature and on the Pt concentration on the zeolite. They found, that a low calcination temperature (500 °C) and low concentration (1 wt%) favours the formation of nanoclusters in the matrix. Increasing the calcination temperature (800 °C) and/or the platinum concentration (3 or 6 wt%) favours the formation of bigger clusters on the outer surface of the zeolite. A bimodal distribution was found on the sample with 3 wt% calcined at 500 °C. Increasing the temperature to 800 °C an ongoing migration to the outer surface was reported. For samples impregnated with 6 wt%, most of the platinum is located at the outer surface even if the sample is calcined at 500 °C.

Reduction:

Besides calcination the metal distribution and particle size is sensitive to the reduction. The result of the reduction strongly depends on the concentration and kind of the reducing agent, temperature and heating. During the reduction, precious metal atoms or small clusters are formed, that start to migrate randomly through the zeolite since their interactions with the zeolite are weaker than the interaction of the metal oxide. The mobility of the clusters and atoms result in the migration, collision and coalescence of the precious metal and therefore in cluster growth. Creyghton et al. [83] described the influence of the hydrogen concentration on the cluster size and distribution. They conclude, that if an excess of hydrogen is used, small clusters (< 15 Å) are formed which are homogeneously distributed inside the zeolite matrix. This is explained by the rapid and homogeneous formation of a large number of nucleation sites. A high number of nucleation sites results in a short average mean free path of the atoms and thus in a rapid formation of small aggregates which will grow to small clusters. The maximal cluster size that can be reached is regulated by the largest void space of the zeolite [83]. If the cluster size is growing fast enough, the critical size at which the clusters are too big to traverse the apertures of the pores, is reached before the clusters arrive at the outer surface and hence the clusters are trapped in the pores of the zeolite. On the contrary to this, if the reduction is limited by the hydrogen supply, fewer nucleation sites are formed and consequently the average mean free path is longer and the atoms and clusters can migrate to the outer surface of the zeolite where bigger clusters are formed, since the cluster growth is not restricted by the zeolite structure. The final metal distribution is not only dependent on the hydrogen concentration but also on the metal distribution after the calcination. As described

above, the precious metal distribution depends on the calcination temperature. Clusters and ions in supercages are reduced at lower temperatures compared to those in sodalite cages. The reduced atoms start to migrate from the sodalite cages to the supercages and due to the absence of nucleation sites in these cages, resulting from the calcination procedure, they migrate to the surface and again big clusters are formed.

From what was said above, it can be concluded that one crucial point in the synthesis of matrix stabilized precious metal nanoclusters is the supply of an adequate amount of nucleation sites, which assures a fast cluster growth and consequently that the critical cluster size is achieved before the small aggregates and atoms migrated to the surface of the zeolite crystallite. Sachtler et al. [98] reported that the final dispersion depends in a surprising manner on the metal loading on the zeolite: the sample with the highest metal loading has the highest dispersion. This is contrary to the experiences with noble metal on amorphous supports, such as silica or alumina. On these carriers, the dispersion decreases with increasing metal loading. Furthermore, it is concluded, that the inverse behaviour is the consequence of the channel and cavity structure of the zeolite. This can be explained by the fact, that small primary particles in the low loaded sample can easily migrate over long distances and finally form large cluster on the surface. One the other hand, in high metal loaded samples, there is a high amount of small primary particles inside cavities which agglomerate inside the pores and as a result are trapped by the zeolite structure. Consequently, the critical size, at which the clusters are too big to travel through the zeolite, is reached in an early stage and in a high concentration resulting in the desired matrix stabilized clusters.

To design new precious metal nanoclusters stabilized by a zeolite matrix, in is necessary to consider all the influences arising from choice of the zeolite and its composition as well as the precious metal precursor. Additionally, the preparation method and the thermal treatment influence the structure of the clusters and therefore the catalytic properties of the catalyst.

1.5. Summary

In the introduction, the legal situation and the current “state of the art” catalysts as well as their weak points are discussed. Most of the catalysts applied in environmental catalysts are noble metals mainly, platinum and palladium deposited on metal oxide based carriers such as alumina and silica. The overall activity of the catalysts depends on the kind of the metal, the size and the shape of the clusters formed and their electronic properties e.g. the oxidation state or electron deficiency. Besides the activity, the thermal stability and resistance against

poisons, such as sulphur oxides, are crucial parameters for the successful utilisation of a catalyst.

Palladium and platinum are, due to their electronic structure, the most active noble metals for the oxidation of VOC in oxygen rich atmosphere. In general, the reactivity of platinum is superior to the activity of palladium. An exception is the oxidation of short chain alkanes in which palladium has a higher reactivity than platinum. The increased activity for this reaction is attributed to the formation of the more reactive PdO species under reaction condition. In contrast to PdO the oxides formed of platinum are less active in the catalytic oxidation. Additionally to the low activity, PtO and PtO_2 are volatile and therefore tend to sinter, resulting in bigger clusters accompanied by a loss of active sites. The oxidation to the inactive oxide species is more pronounced for high dispersed platinum than over medium and large clusters. The total oxidation of medium and large clusters is suppressed and the interactions with oxygen lead to the adsorption on the surface of the clusters, resulting in an active $Pt\text{-}O_s$ species. This activation of oxygen on the cluster surface is one of the elementary steps in the total oxidation of VOC and therefore has a crucial influence on the performance of the catalyst. Large clusters exhibit crystal planes that strongly interact with oxygen leading to self-inhibition by oxygen. Moreover, alkenes strongly adsorb on those planes, resulting in competitive adsorption with oxygen and consequently in a reduced reactivity. In conclusion, the catalytic performance of platinum based oxidation catalysts strongly depends on the cluster size, since small clusters are oxidised to inactive and volatile species and large clusters suffer from the inhibition of strongly adsorbed oxygen and/or pollutants such as alkenes on crystal planes. The reactivity of platinum clusters is not only dependent on its size but also on the electron density in the valence band. As described in 1.3.3 electron deficient clusters are more stable and exhibit higher resistance against thermal and chemical deactivation. The electronic structure is mainly influenced by the kind of support used and the interactions between the support and the noble metal cluster. On basic supports such as MgO the clusters are less electron deficient than over acidic supports such as Al_2O_3 or sulphated supports such as $ZrO_2\text{-}SO_4$ and $Al_2O_3\text{-}SO_4$. As a consequence, the support essentially influences the performance of the catalyst. Besides the acid/basic properties of the support and the resulting interactions with the clusters, the surface area influences the overall performance of the catalyst.

For a successful catalyst the consistency against the harsh conditions during the operation conditions is also important. The main sources of a decrease in the performance are the thermal deactivation and the exposure to poisons. In addition to the mentioned amorphous

metal oxide supports, zeolites are a well know catalyst support, mainly used in catalytic petrochemical processes. Contrary to their frequent use in industrial processes noble metal based zeolite catalysts are rarely used in environmental catalysis. Nevertheless, zeolites offer interesting properties because of their acid properties, the high surface area and the porous structure. Precious metal containing zeolites are mainly synthesised by ion-exchange or impregnation with the metal precursor followed by calcination and reduction procedure. These synthesis methods favour either formation of mono-atomic platinum species or small clusters in the pore structure of the zeolite. It is reported by Sachtler [84, 98, 104] and others [83, 105, 106], that noble metal clusters encapsulated in the pores of a zeolite have unique electronic and catalytic properties. Additionally the mechanical trapping and the spherical constrains favours the formation of small and medium size clusters. Additionally, the thermal stability is increased by the mechanical trapping. However, the preparation methods mentioned above are only suitable to introduce small amounts of precious metals into the pore structure and the synthesis of zeolites containing noble metal nanoclusters is still challenging.

2. Scope of the thesis

To meet the reduction of emitted pollutants from mobile and stationary sources as requested by the enforced legislative situation, new catalytic materials have to be developed, that can overcome the problems of the existing catalysts, mentioned in the introduction. The objective of this work is to develop new catalytic materials which exhibit improved low temperature activity and are able to withstand the harsh condition occurring under reaction condition and therefore can contribute to meet the given aims in reduction of emitted pollutants.

As described in the introduction, one approach is to combine the catalytic active noble metal and the outstanding properties of zeolites, exploiting their pore structure and thermal stability. The known zeolite based catalysts are not suitable to fulfil the given aims but it was already demonstrated that the combination of noble metal and zeolites can improve the catalytic performance. Nevertheless, until now, it is not possible to synthesise uniform matrix-stabilized nanoclusters evenly distributed over the whole zeolite crystallite. It is the aim of this thesis to develop an easy and robust synthesis of those matrix-stabilized clusters, which can be applied on industrial scale and to prove the hypothesis of the enhanced properties of such clusters entrapped in the porous structure of zeolites. Platinum, palladium and rhodium are the most frequently used noble metals in both, industrial and environmental catalysis, therefore this work will focus on these metal introduced in the large pore zeolite BEA. The BEA structure was chosen due to the large pores and large channel diameter to minimize transport limitation of both, the precious metal precursors and the reactant molecules. Moreover it is know that precious metal clusters have to exceed a certain size to be active in catalysis as discussed in chapter 1.3. On the other hand the pore structure of BEA is small enough to prevent the agglomeration of precious metal to large clusters. Moreover the BEA zeolite is known withstand the (hydro)thermal conditions occurring in operation conditions. Sulphite containing precious metal complexes such as platinum sulphite acid (PSA) and rhodium sulphite acid (RSA) had been chosen for the synthesis. These precursors were used to overcome several problems with other prominent precursors, for example tetramine complexes or nitrates as there is amongst others the NO_x release during the large scale production. Additionally the sulphite containing precursors have superior chemical properties such as strong chemisorption on Al_2O_3 resulting in the reduction of the chromatographic effects known from mentioned tetramine complexes.

In the first section, a new robust synthesis which offers the possibility to synthesise nanoscale clusters in high concentration and homogeneous distribution throughout a zeolite host is

presented. Besides classical analytic methods, such as X-ray diffraction and transmission electron microscopy, an IR method is developed to characterise the noble metal distribution. The idea of this method is based on the selective poisoning of clusters deposited on the outer surface of the zeolite by bulky nitriles. Additionally, the influence of the zeolite on the electronic structure of the noble metal is investigated by CO adsorption and FTIR. Moreover, the catalytic activity of the developed precious metal nanoclusters catalysts was compared with commercial catalysts and recent developments to prove the assumption that the inclusion of nanoclusters in a zeolite host leads to improved properties such as higher low temperature activity, thermal stability and enhanced resistance against poisons. The developed catalyst is compared with several reference catalysts with different cluster size to indentify the advantages of such nanoclusters over bigger clusters.

The influence of the cluster size upon the reactivity towards different educt gases was studied by the oxidation of different educt molecules, such as alkanes, alkenes, carbon monoxide and NO. To indentify the potential commercial applications of the developed catalysts, they were tested for special application such as diesel oxidation catalyst, NO oxidation catalyst and, in case of a rhodium zeolite, as three-way catalyst.

In the last part, the micro and macro kinetic parameters of the various catalysts are derived and the influences of the cluster size and support materials on these materials are discussed in detail. Diffusion limitation is of special interest, since the encapsulation might restrict the transportation of the reaction educts and therefore compensate the effect of enhanced catalytic activity.

The overall catalytic activity of encapsulated nanoclusters might be limited by the diffusion of the educt to the active center in the cavities and channel system inside zeolite. This aspect will be considered in the last section. To understand the diffusion processes and their influence on the results obtained in the previous section, the washcoat loading is varied to understand the transport processes and their influence on the overall performance.

3. Catalyst development and characterisation

To overcome the problems of the existing catalysts, described in the introduction, a new synthesis route for precious metal containing zeolite had been developed. This new synthesis route favours the formation of nanoscale noble metal and bimetallic clusters homogenously distributed in the pore system of zeolites. The synthesis and the characterization of those noble metal zeolites will be discussed in this chapter.

3.1. Catalyst preparation

For the synthesis, H-BEA-35 (Sued-Chemie), platinum sulphite acid (PSA) and rhodium sulphite acid (RSA) had been used. Rhodium sulphite acid (5.080 wt% Rh) and platinum sulphite acid (10.14 wt% Pt) are commercially supplied by Heraeus. Before the incipient wetness impregnation, the zeolite powder was dried. After the introduction of the precious metal by the incipient wetness method, the impregnated zeolite was again dried and calcined. Prior the catalytic test, a slurry was prepared consisting of the impregnated support and a silica binder (Bindzil 34 wt% SiO_2 from EKA Chemicals AB) to bind the zeolite to the ceramic support. This slurry was ball-milled and dip-coated on Corning ceramic honeycombs.

3.1.1. Synthesis of precious metal containing zeolites

Synthesis of PSA-BEA:

To synthesize 80 g of Pt-BEA with a Pt content of 3.3 wt%, 26.14 g PSA was mixed with 45.3 g of distilled water. This solution was used to impregnate 77.36 g of H-form of the BEA which was dried at 120 °C over night before and after the impregnation. In order to prove the hypothesis that the calcination atmosphere influences the cluster distribution and cluster size, 40 g were calcined under argon and the second half under air. The “argon calcination” was carried out in a flow through tube oven. The flow rate of the argon was 2 l/min. The “air calcination” was carried out in a muffle oven. Both samples were calcined at 800 °C for 5 h to ensure, that the precursor was completely decomposed. The heating rate was 2 °C/min. The argon calcined sample is denoted as PtB(Ar) and the air calcined sample as PtB(Air). To coat these two powders, 40 g of each Pt-zeolite was suspended in 120 g distilled water and 10 wt% silica binder is added to each suspension. The suspension was ball-milled to an average particle size of d_{50}~2 µm. Ceramic honeycombs were dip-coated with these suspensions. For the different catalytic tests, the washcoat loading was varied as described in the corresponding

chapters. After the coating, the honeycombs were calcined for 5 h at 350 °C in air. The preparation method as well as the platinum containing zeolite are patented in the patent applications DE102008023472 [107] and DE102009015592 [108].

Synthesis of Rh-BEA:

The Rh-BEA was prepared in the same manner as the Pt-catalyst. For the synthesis of 80 g of the Rh-zeolite, 47.152 g of the rhodium sulphite acid (5.05 wt%, Heraeus) is mixed with 24.15 g of distilled water. The Rh concentration of the impregnated zeolite is 3 wt%. One half of the Rh-zeolite was calcined in air and the second half under argon. The calcination procedure was the same as described for the Pt-zeolites. In analogy to the Pt-catalysts, the Rh-zeolites are denoted as RhB(Ar) and RhB(Air), respectively. The coating procedure is the same as described for the Pt-zeolites. To achieve a washcoat loading of 100 g/l and an Rh-concentration of 0.3 g/l the Rh-zeolite was diluted with ZrO_2. The synthesis and the resulting catalytic active material is patented by Hutt et al. [109].

Synthesis of $PtNO_3$-BEA:

The $PtNO_3$-BEA was synthesised as the PSA-BEA but instead of the platinum sulphite acid platinum dinitrate was used as platinum source. The impregnated zeolite powder was dried over night and then calcined at 800 °C for 5 h in analogy to the PSA-BEA catalyst.

Synthesis of PtEA-BEA:

The PtEA-BEA was synthesised as the PSA-BEA but instead of the platinum sulphite acid hydroxyethylammonium hexahydroxoplatinate (IV) (PtEA) (13.2 wt% Pt, Heraeus) was used as platinum source. The impregnated zeolite powder was dried over night and then calcined at 800 °C for 5 h in analogy to the PSA-BEA catalyst.

Synthesis of Pt-SH-27:

The synthesis described for the PSA-BEA catalyst was also applied for the SH-27 (Sued-Chemie) zeolite with MFI structure.

Synthesis of Pt/Pd-BEA:

A platinum/palladium containing zeolite was synthesised as described by Hutt et al. [110].

3.1.2. Synthesis of reference catalysts

To investigate the influence of the metal precursor used for the impregnation several reference catalysts were prepared with different precursors. The support material was varied to proof the predicted advantages of a zeolite support.

Pt-Al_2O_3 (EnviCat 2520):

The EnviCat 2520 is prepared as described in the corresponding patent [111]. The washcoat loading was 50 g/l honeycomb. The Pt-concentration is 1 g per litre catalyst.

Pt-Siralox (PtEA):

For the synthesis of the comparative catalyst PtEA, an Al/Si mixed oxide (Siralox 5/155 from Condea) is impregnated with PtEA solution (13.2 wt% Pt, Heraeus). Prior to the incipient wetness impregnation, the oxide powder is dried at 120 °C over night. For the synthesis of 40 g of the Pt-catalyst, a Pt-solution consisting of 9.98 g (1.32 g Pt) of the PtEA diluted in 30.8 g H_2O was prepared. This Pt-solution is used for the incipient wetness impregnation of 36.88 g of the dried carrier. The platinum concentration of the impregnated Siralox is 3.3 wt%. After the impregnation the support is calcined at 450 °C for 5 h in air and coated onto the same honeycomb as described above.

Fe-BEA/Pt-Alumina (reference DOC):

The Fe-BEA/Pt-alumina catalyst is synthesized as claimed by Sued-Chemie in WO 2009/068289 A2 [112]. This catalyst compromises of a hydrocarbon storage component and a catalytically active material. An iron-exchanged H-BEA-35, with an iron concentration of 3.6 wt%, is employed as hydrocarbon trap. Iron-sulphate was used as precursor for the exchange. For the synthesis of catalytically active material, an Al/Si mixed oxide (Siralox 5/155 from Condea) was used, which was impregnated with platinum from 2-hydroxyethylammonium hexahydroxoplatinate(IV) solution (13.2 wt% Pt, Heraeus). The Pt-concentration is 5 wt% of the impregnated Siralox. These two powders are used to produce a washcoat, which then is coated on a 400 cpsi ceramic honeycomb. The washcoat loading is 120 g/l while the Pt-concentration is 3.5 g/l.

Pt/Pd-Catalyst:

67.39 g of PtEA solution (13.2 wt% Pt, Heraeus) are diluted with 58 ml water. This solution is used for the impregnation of 186 g of an alumina/silica mixed oxide (Siralox 5/140 Type C large pore 5 % Si, Condea). In a second impregnation step 17.4 g palladium nitrate solution in 58 ml water are added to the platinum impregnated Siralox. The impregnated powder is dried at 80 °C and finally calcined at 550 °C.

Rh-Zircon (three-way catalyst):

To investigate the improvements of the Rh-zeolites, a “state of the art” Rhodium catalyst was synthesized. The zirconium carrier is dried at 120 °C for 12 h. The rhodium is then introduced by incipient wetness impregnation with rhodium nitrate (12.8 wt%, Heraeus). After the impregnation, the catalyst is calcined at 550 °C for 5 h. The Rh concentration is 3 wt% as well. To achieve the same rhodium concentration and washcoat loading as in case of the Rh-zeolites, the Rh/ZrO_2 is diluted with pure ZrO_2. The coating procedure is analogous to the procedures described before. The Rh-concentration on the coated honeycomb is 0.3 g per litre honeycomb and the washcoat loading is 100 g/l.

3.2. Physico-chemical characterisation

The performance of a catalyst strongly depends in its chemical composition, the accessibility of the catalytically active sites and the dispersion and distribution of the active metal. The sulphur content of the catalyst is determined with atom adsorption spectroscopy (AAS). The influence of the calcination procedure upon the structure of the carrier is analyzed by BET, pore volume measurement (PV) as well as by XRD. Ammonia-TPD and TGA are used to study the influence of the different calcination atmospheres towards the acid site concentration and the decomposition of the precursors. For the determination of the cluster size, XRD and TEM were used. Additionally to these standard methods, an IR spectroscopy method was developed to determine the precious metal distribution throughout the zeolite.

3.2.1. Textural characterization (BET, PV, TEM, XRD, AAS)

Atom adsorption spectroscopy:

The sulfur and precious metal content of the impregnated and calcined zeolites was determined by atomic adsorption spectroscopy (AAS) with an *UNICAM 939 AA-S*pectrometer.

Transmission electron microscopy:

The precious metal particle size was determined by transmission electron microscopy (TEM). For TEM images a JEM-2010 Jeol transmission electron microscope operating at 120 kV was used. The catalysts samples were grinded and suspended in ethanol and ultrasonically dispersed. Droplets of the dispersions were deposited on a copper grid supported carbon film.

X-Ray powder diffraction:

For the XRD measurements, a Bruker Endeavor diffractometer with a Cu 2Kα x-ray tube was used. The step width was 0.03 deg 2 °Theta and the step time was 0.500 s. The Scherrer equation (eq. 7)

$$\tau = \frac{K\lambda}{\beta cos\theta} \qquad \textbf{eq. 7}$$

where *K* is the shape factor, λ the x-ray wavelength, β the line broadening at half the maximum intensity (FWHM), and θ the Bragg angle, was used to calculate the average cluster size τ.

Temperature programmed experiments:

TPD:

The thermal decomposition of the precious metal precursor was studied by temperature programmed desorption. For these experiments, a Netzsch STA 409 PC/PG equipment with a Netzsch QMC mass spectrometer was used. To study the influence of the different gas atmosphere used for the calcination, helium (Linde 99.999 %, 5.0) and synthetic air (Linde 20 % O_2 in N_2) were used. The samples were heated from 40 °C to 900 °C with a heating rate of 10 K/min. The reactant gas flow was 50 ml/min.

Ammonia-TPD:

The acidity of the catalysts was determined by NH_3-TPD with Thermo TPDRO 1100 equipped with a Pfeiffer OMNISTAR GSD detector. Prior to the ammonia adsorption the sample was heated to 550 °C with a heating rate of 1 K/min and held at this temperature for 1 h under helium atmosphere. After this conditioning, the sample was cooled down to 110 °C and ammonia was dosed. For the ammonia desorption, the sample was heated with a heating rate of 5 K/min to a final temperature of 750 °C.

3.2.2. FTIR Spectroscopy

In the study of zeolites, IR spectroscopy can be used to provide information about the nature of surface hydroxyl groups, like Brønsted acid sites and silanols. In Table 4 the position and assignment of the different bands are listed. Two main types of OH groups are present in the protonic form of zeolites: silanols (SiOH) and bridging hydroxyl groups (Si(OH)Al). Silanols are mainly found at external surfaces, where they saturate silicon dangling bonds associated with framework truncations. Nevertheless, silanols also occur at internal lattice defects, arising mainly from partial dealumination. In this case a local cluster of silanols can be formed, called "silanol nest". Isolated silanols on external surfaces are characterized by a sharp IR absorption band in the 3750-3745 cm^{-1} range. When silanols occur at internal sites, weak electrostatic perturbations normally cause a downward shift (and broadening) of the IR stretching band, which then typically appears at 3720-3700 cm^{-1}. Stronger, hydrogen-bonded interactions (e.g. in hydroxyl nests) result in a very broad absorption band in the 3650-3200 cm^{-1} range [113]. In BEA this absorption band was assigned to bridged hydroxyl groups which are perturbed by hydrogen bond interactions with the zeolite framework [114]. Bridging hydroxyl groups, which are the acid sites, can be found in two different wavenumber ranges: 3650-3600 and 3580-3530 cm^{-1}. The high frequency range corresponds to OH groups vibrating in large cavities, formed by pores larger than eight-membered rings, whereas in smaller voids the low-frequency range is observed. This is typical for faujasite-type zeolites (FAU), which show OH bands around 3650 and 3550 cm^{-1} [115]. After thermal dehydration, or steaming, a new band usually was observed in the range 3680-3660 cm^{-1}. On the basis of ^{1}H-MAS NMR studies, this band was assigned to AlOH groups of extraframework aluminium species [116]. A band at 3782 cm^{-1} can also be present in the IR spectrum of dealuminated zeolites, called VHF (very high frequency). This band was observed for dealuminated H-ZSM-5 and calcined BEA [117, 118]. It was also observed in spectra of MOR [119]. This feature has been assigned to various aluminium-containing species, such as terminal AlOH

groups bound to a single aluminium in the form of AlOOH [118] or to AlOH moieties of transient species leaving the framework associated to the octahedral ^{27}Al-NMR resonance [120].

Table 4: IR stretching frequencies of the possible hydroxyl groups on a zeolite surface [113-115, 117-119]

ν_{O-H} (cm^{-1})	Hydroxyl group
3790-3780	Unperturbed Al-OH
3750-3745	External Si-OH
3660-3670	Perturbed Al-OH
3650-3530	Bridging Si(OH)Al
3600-3300	H-bonded silanols or perturbed Si(OH)Al groups

Adsorption of probe molecules:

A widely spread technique to characterize the surface properties of a solid catalyst, such as the acid or base strength and distribution, is to adsorb appropriate probe molecules. To investigate the acid/base properties, the probe molecule should have suitable acid/base properties to induce optimal interaction. Probe molecules can therefore be classified on the basis of the principle of the Lewis HSAB model [121, 122]. Regarded as potential probe molecules ammonia and pyridines are classified as hard bases followed by nitriles, ethers ketones and aldehydes with intermediate hardness and finally soft bases such as CO, dinitrogen and dihydrogen. Besides the acid/base properties of the probe molecule the size of the molecule is a crucial parameter. Small molecules such as ammonia or carbon monoxide are able to penetrate small pores and therefore can provide information of the whole surface whereas other molecules such as substituted pyridines or nitriles are sterically hindered, cannot penetrate into the pores and therefore can be used to study the external surface of porous materials.

A detailed list of criteria for the selection of probe molecules have been formulated by Paukshtis and Yurhchenko [123], Knözinger [124] and Lercher [125].

Adsorption of carbon monoxide:

Carbon monoxide is an almost ideal probe molecule, that can discriminate between aprotic [123, 125-129] and protic [115, 127, 129]acid sites with a high specificity for sites with different acid strength [1, 130].For sites with different acid strength it is one of the most commonly used probe molecules in IR spectroscopy. According to its size it can enter the channels and cavities of a zeolite and therefore interacts with all defect sites in the zeolite independent of their location. CO forms donor-bonds with prevalent σ-character to metal centres via its 5σ orbital. Considerable contribution to the metal-carbonyl bond may come from the interaction of the metal d-orbitals and the antibonding π*-orbitals of the CO ligand (π-back-donation). The increased electron density in the antibonding orbitals of the C=O bond is the origin of the decreased C=O bond order, the stretching force constant and hence, the stretching frequency [1]. The carbonyl stretching frequency responds very sensitively to the coordination onto cationic sites, leading to a positive frequency shift of up to 90 cm^{-1} relative to the gas phase frequency of 2143 cm^{-1}, when CO is coordinated to the hardest d^0-cation site such as low-coordinated Al^{3+}. According to the bonding mechanism, the frequency is shifted to lower wavenumbers, when the CO is coordinated to low-valent transition metal centres with finite d-electron density.

Due to the sensitivity of the C=O-bond towards electron transfer, carbon monoxide is an appropriate molecule to investigate the oxidation state and the dispersion of noble metals such as platinum or rhodium. For CO adsorbed on platinum, the C=O stretching vibration is either red or blue shifted compared to the stretching vibration of the free CO molecule. In case of neutral $Pt(CO)_n$ clusters the stretching vibrations are red shifted, since the presence of the 4d-AO of Pt leads to an increase of the electron population in the antibonding π* orbital of CO [131]. The bond strength is weakened by the increased electron density in the antibonding orbital and consequently, the excitation energy is reduced. Contrary to neutral complexes, positively charged complexes, for example $Pt(CO)_n^{m+}$, are characterized by a significant blue shift of the CO stretching vibrations. In presence of a positively charged metal cation, the CO ligand is polarized, which leads to a higher iconicity and its strengthening compared to the free CO. Therefore, CO is a proper molecule to investigate the electron density of the precious metals. As the electron density corresponds to the oxidation state, the CO adsorption provides a possibility to analyse the oxidation state of the precious metal clusters deposited on a carrier.

Furthermore, the high sensitivity of CO to the electronic state of the precious metal cluster, allows to study the electron transfer from the metal cluster to the carrier indirectly [86]. The

electron transfer is also dependent on the cluster size. Therefore, the position of the Pt-C=O vibration can be used to determine the cluster size. But nevertheless these results have to been treated with caution since the band position is influenced by many parameters, e.g. the adsorbed carbon monoxide can interact with the zeolite lattice which results in a shift of the CO band [1]. These interactions differ with the diameter of the channel and thus the comparison of two different types of zeolite has to be done carefully. Besides the interaction of the CO molecule and the zeolite, a dipole moment can be introduced by dipole-dipole interaction of two neighbouring CO molecules [132, 133].

Adsorption of ammonia and pyridine:

Ammonia is one of the most commonly used probe molecules in the characterization of acid properties of solid surfaces. It is a hard Lewis base and small in its size. Ammonia is bonded to the surface acid sites in various manners, namely coordinated, H-bonded and protonated NH_3. These different bonds can be detected by infrared spectroscopy and can be discriminated by their characteristic normal vibrations. Due to its strong basicity, ammonia is unselectively bonded to a wide variety of different surface sites. Therefore, it has to be considered as an unspecific probe molecule. Besides ammonia, pyridine and substituted pyridines are frequently used probe molecules, which are classified as weaker bases than NH_3 and are therefore more specific than ammonia. Pyridine can undergo coordination to aprotic sites; it can either be protonated to form the pyridinuim ion (PyH^+) on acid OH groups or H-bonded on less acidic OH groups. The alkylation of pyridine in the 4-position increases the basicity via the inductive effect. The same is true for the substitution in the 2- and 6-postition. Contrary to the substitution in the 4-position the alkylation in the 2- and 6- position results in a sterical shielding of the nitrogen lone pair. The influence of the introduction of various substituents such as methyl and tert-butyl-groups was first studied by Benesi [134] Jacobs [135] and Knözinger [136]. In these studies it was demonstrated that steric hindrance of di-tert-butylpyridine is so pronounced that the interaction with Lewis acid sites is impossible, resulting in a high specific probe molecule for protic acid sites.

Adsorption of nitriles:

Nitriles are a 3rd class of frequently used probe molecules which are softer bases compared to ammonia but harder than carbon monoxide, dihydrogen or dinitrogen. The sterical shielding in the vicinity of the lone electrons of the nitrogen atom is less compared to pyridines. As a result, nitriles are considered to be attractive probe molecules.

As discussed for the substituted pyridines, the same is true for nitriles. Busca and his group [137] proposed to use a set of hindered nitriles to approach the problem of accessibility of active species in zeolites. Small molecules, such as carbon monoxide or ammonia can access almost all active sites in the zeolite but cannot give any information of their location. Especially for the zeolites the knowledge of the location of the active sites is crucial for a detailed understanding of the catalytic activity. For example, morphoselective catalysis can only be realized at the internal surface, whereas in other processes the external surface properties play an important role. Areán et al. [138] proposed to use small nitriles such as acetonitrile that can penetrate the inside of the pores and cavities of a zeolite and adamantane-carbonitrile (see Figure 2), which according to its size cannot. By using these two probe molecules they could discriminate between internal and external OH groups. Based on the results of those studies a method to discriminate between external and internal Pt-clusters was developed.

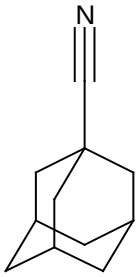

Figure 2: Adamantane-carbonitrile ($C_{11}H_{15}N$, M_w: 161.24 g/mol d_M ~ 0.6 nm [139])

Determination of the PM-distribution on zeolite: carbon monoxide and nitrile adsorption:

For the determination of the precious metal distribution a method based on the idea of the two studies describes above was developed. As described by Busca [137], sterically hindered nitriles, such as adamantane-carbonitrile selectively bond to precious metal clusters on the outer surface since due to their steric hindrance they are not able to access the pore system of the zeolites. Contrary to this, CO is suitable to enter the small cavities of a zeolite and additionally can be used to discriminate between ions and zero valent platinum clusters. By

comparing the CO adsorption bands of the pure Pt/BEA and AdaCN poisoned Pt/BEA the ratio between surface clusters and clusters located in the pore system of the zeolite can be obtained. A similar method was used by Montanari et al. [140] to investigate the cobalt distribution on MFI zeolites. They also showed that the adsorbed nitriles are not substituted by adding a subsequent dose of CO which is crucial for the comparison of the nitrile adsorption before and after the CO addition. For this method it is of crucial importance that the adsorbed nitrile species is not eliminated by the second adsorption of carbon monoxide. Since nitriles are the stronger bases compared with CO and the platinum clusters are electron deficient the bonding between the platinum cluster and the nitrile probe molecule is stronger than between the noble metal cluster and the CO molecule. Therefore, the adsorbed nitrile is not displaced by the second adsorption of carbon monoxide.

The detailed procedure is the following: To determine the Pt-distribution throughout the zeolite, CO is adsorbed to measure the overall CO adsorption on platinum. After the reference spectrum is recorded, the CO is desorbed by heating up the sample to 400 °C in vacuum for 30 min. After the sample was cleaned in this way, AdaCN vapour was dosed to the sample, which results in a selective nitrile adsorption and blocking of the Pt-clusters on the outer surface, whereas the Pt-species in the cavities as well as in the channels are still unblocked. A second dose of CO was injected which will selectively adsorb on accessible Pt sites which are located inside the pores of the zeolite since the Pt on the outer surface is already blocked by the bulky nitrile [106]. The subtraction of the two CO peak areas, measured before and after the poisoning with adamantane-carbonitrile, will correlate to the Pt-distribution on the zeolite.

In this work, FTIR spectra were recorded using a Mattson Galaxy 6020 spectrometer equipped with a MCT detector. 128 scans were recorded with a resolution of 2 cm^{-1}. Prior to the IR experiments, the zeolites were pressed in self-supporting wafers and were pre-treated at 400 °C for one hour in vacuum to remove water and other impurities on the surface.

3.3. Results

3.3.1. Physico-chemical characterisation

The noble metal content and the residual sulphur content of the catalysts prepared with sulphur containing precursors was determined by AAS and the results are summarized in Table 5.

For the platinum as well as for the rhodium impregnated catalysts, the precious metal content is around 3 wt% on the impregnated support and does not dependent on the calcination, indicating that no volatile species are lost during the calcination procedure. Contrary to the noble metal content, the amount of residual sulphur is strongly dependent on the calcination atmosphere. In case of the platinum zeolite, the argon calcination resulted in a nearly sulphur free Pt-zeolite whereas the air calcined sample contains remarkable amounts of sulphur. The opposite is true if rhodium sulphite is used as precursor. In this case, the sulphur removal is significantly higher if the sample is calcined in air than under inert gas atmosphere.

Table 5: Chemical composition of the impregnated supports

	PM [%]	S [%]
PtB(Ar)	2.9	0.004
PtB(Air)	2.9	0.155
RhB(Air)	3.1	0.003
RhB(Ar)	3.1	0.014

The changes of the surface area and the pore volume due different calcination atmosphere are listed in Table 6.

Table 6: Physical properties of the support

	Pore volume [cm³/g]	NH_3-TPD [µmol/g]
H-BEA	0.21	963
PtB(Ar)	0.20	665
PtB(Air)	0.17	617
RhB(Air)	n.a.	283
RhB(Ar)	n.a.	532

The results of the NH_3-TPD show, that the reduction of the NH_3-uptake is independent of the calcination procedure in case of the platinum containing zeolite. The NH_3-uptake the two rhodium zeolites is strongly reduced compared to the fresh H-form of the zeolite.

3.3.2. Precious metal distribution and dispersion

To understand the influence of the calcination atmosphere upon the precious metal dispersion and distribution the prepared catalysts were characterized with X-ray powder diffraction, infrared-spectroscopy and transmission electron microscopy. The decomposition of the precursors under the different gas atmospheres was studied by thermogravimetric analysis.

The thermal decomposition of platinum and rhodium-precursors impregnated on the zeolite is shown in Figure 3 and Figure 4, respectively.

Under both gas atmospheres, the thermal ligand decomposition proceeds in two steps. The first decomposition takes place at ~325 °C, the second at around 680 °C in case of inert gas calcination and at 775 °C, if the calcination is carried out under air. The main decomposition product is SO_2 in both calcination atmospheres and no relevant SO_3 peak can be found. The AAS results listed in Table 5 show that in case of the air calcination the sulphur concentration is remarkably higher compared to the inert gas calcination. These results together with the thermogravimetric studies indicate, that the sulphite ligand is oxidised to sulphate which is bond to the zeolite.

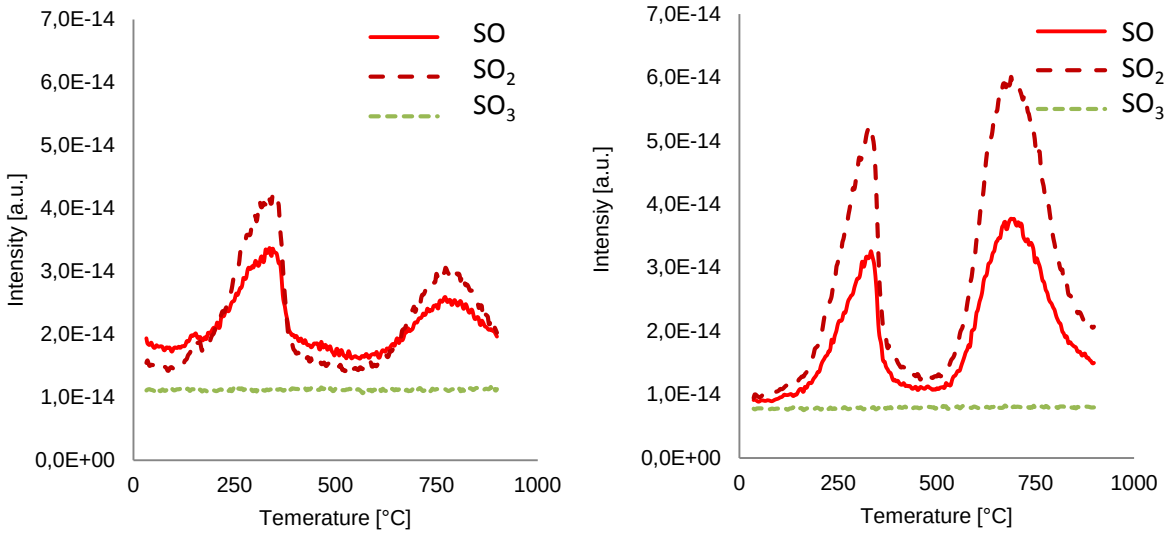

Figure 3: Decomposition of platinum sulphite acid on BEA in air (left) and in inert gas (right)

The same is true for the rhodium containing zeolite, but the decomposition takes place at lower temperatures of 290 °C and 590 °C.

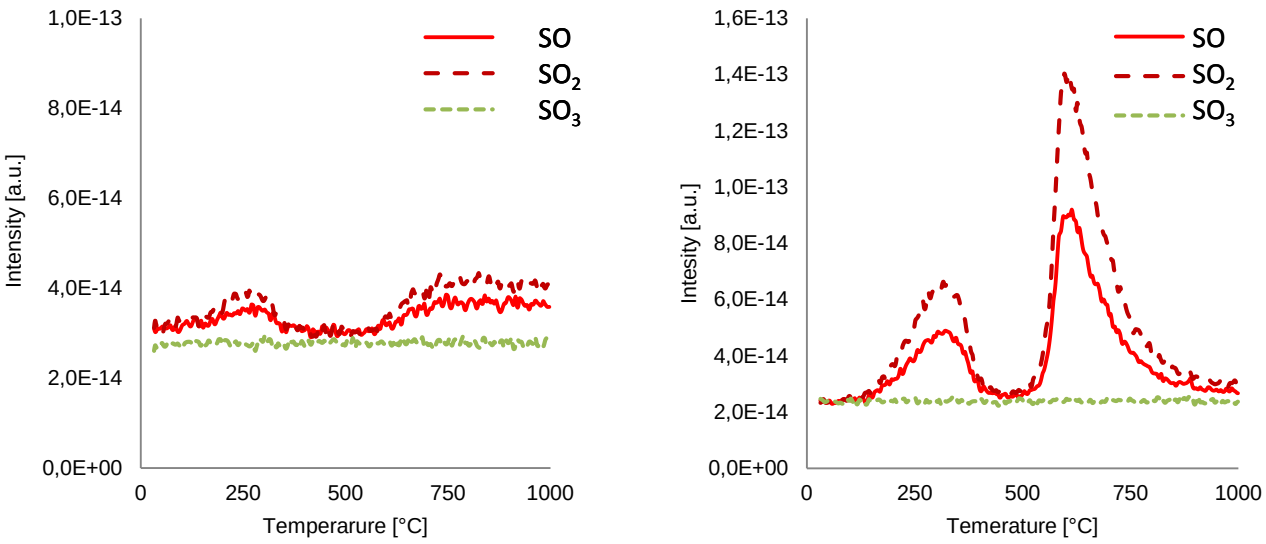

Figure 4: Decomposition of rhodium sulphite acid on BEA in air (left) and in inert gas (right)

XRD:

XRD experiments were carried out to study the influence of the calcination atmosphere upon the platinum clusters size and distribution. The patterns are shown in Figure 5. Besides the typical reflections of the zeolite, the sample calcined in air shows reflections at 39.7 °, 46.2 °, 67.4 ° and 81.2 °. These reflexions are assigned to the (111)-, (200)- and (112)-planes of platinum, respectively [141]. Despite this, if the Pt-zeolite is calcined under inert gas atmosphere, no reflexion can be seen in the diffractogram although the Pt concentration is 3 wt%. The absence of these reflexions indicates that the clusters are too small to be detected or that they are incorporated in the zeolite pores and therefore no diffraction can be detected. The size of the clusters in the air calcined sample is calculated according to the Scherrer equation (eq. 4) and is found to be approximately 25 nm.

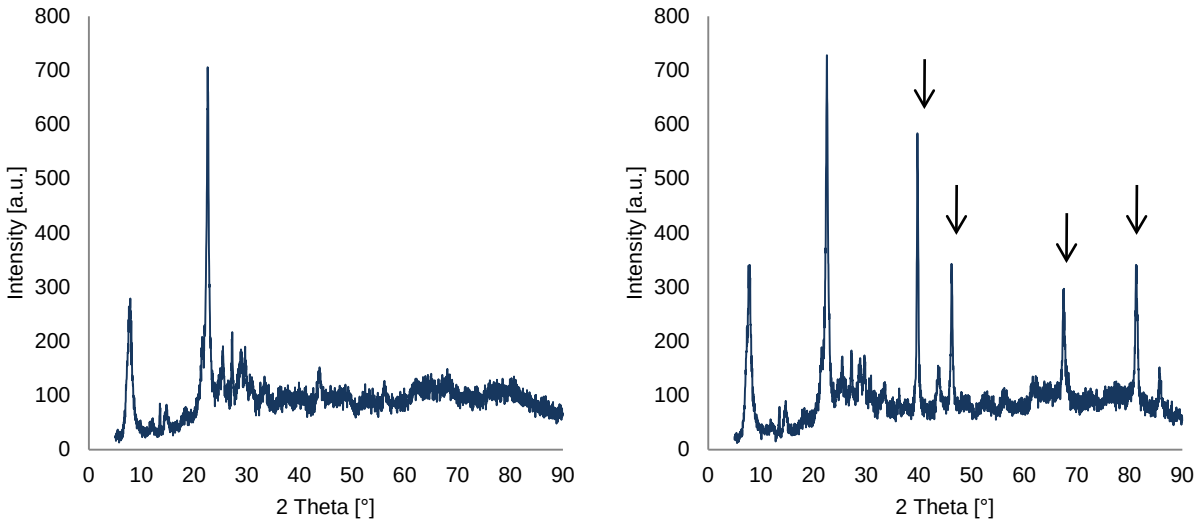

Figure 5: XRD pattern of the argon (left) and air (right) calcined platinum containing zeolite powders. The reflexes attributed to platinum are marked with an arrow

The XRD patterns of the calcined Rh-zeolites are shown in Figure 6. The argon calcined sample (left) differs from the air calcined one on the right. Contrary to the calcination of PSA-BEA, the calcination under inert gas atmosphere favours the formation of Rh clusters with diffraction angles (2θ) of 47.1 and 41.0 corresponding to the Rh (111) planes [142]. Instead of Rh-clusters, small Rh_2O_3 particles are formed during the calcination in air. Weak reflexion at diffraction angles of 34.5 and 34.9 ° indicated the formation of such clusters. The size of the Rh-cluster after the inert gas calcination is estimated to be ~12 nm. The Rh_2O_3 clusters on the air calcined sample are around the detection limit and therefore have a size about 5 nm.

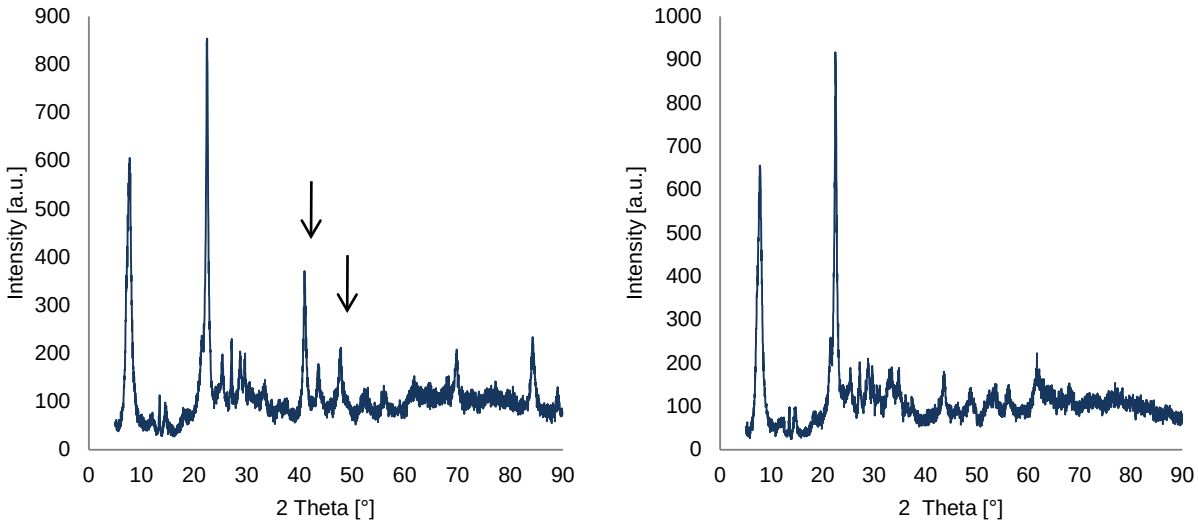

Figure 6: XRD pattern of the argon (left) and air (right) calcined rhodium containing zeolite powders. The reflexes attributed to rhodium are marked with an arrow

IR Studies: Influence of the calcination atmosphere on the zeolite:

OH-Region of H-BEA, PtB(Ar) and PtB(Air):

In Figure 7, the spectra of H-BEA-35 and the two platinum containing zeolites in the OH-stretching region are shown. The reference spectra of the blank zeolite shows three main IR adsorption bands, which peak at 3608, 3741 and 3780 cm^{-1}, respectively. There is general agreement, that the band at 3608 cm^{-1} corresponds to the O-H stretching mode of bridged Si(OH)Al groups (Brønsted acid sites). The main band at 3739 cm^{-1} has to be assigned to Si(OH)Si groups. This main peak consists of two different maxima at 3744 and 3733 cm^{-1}. The band at 3744 cm^{-1} is assigned to external silanol groups on the outer surface of the zeolite crystallite. The latter vibration is due lattice defects, which arise from silicon or aluminium vacancies in the lattice. These defects are generally terminated with OH-groups, responsible for the band 3733 cm^{-1} [120]. To assign the very high frequency band (VHF) observed at 3781 cm^{-1}, Wang [143] proposed, that this band is attributed to O-H attached to various aluminium-containing species, such as terminal AlOH leaving the lattice due to hydrothermal dealumination. Therefore, the occurrence of this band is accompanied by a broadening of the internal silanol band.

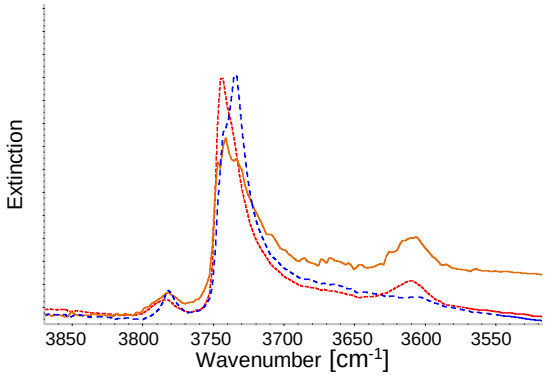

Figure 7: OH vibration region (H-BEA solid line, PtB(Ar) dashed and PtB(Air) dotted line, respectively)

The spectra of the PtB(Ar) has the same peaks as they are in the reference spectra, indicating that the impregnation with PSA and calcination under inert gas atmosphere at 800 °C does not affect the structure of the zeolite. The situation is different, if the impregnated zeolite is calcined at 800 °C in air. In this sample, the band at 3608 cm^{-1}, representing the Brønsted acid sites, disappeared. This dealumination was accompanied by an increase of the band at 3733 cm^{-1}. After the impregnation and the air calcination procedure, the intensity of the band, assigned to the internal silanols, exceeds the intensity of the band denoting the external silanol groups, indicating that these silanols are blocked by the platinum. The opposite is true for the argon calcined sample.

CO adsorption PtB(Ar) and PtB(Air):

After the reference spectra of the Pt-zeolites were recorded, a pulse of 20 mbar CO was adsorbed on the samples. The subtracted spectra are shown in Figure 8. The spectra of PtB(Ar) reveals a main adsorption band at 2100 cm^{-1} and one band at 2225 cm^{-1}. The band at 2100 cm^{-1} is assigned to Pt^0-clusters [103, 131, 144]. In addition to these bands, the air calcined sample shows supplementary peaks at 2167, 2135 and 2124 cm^{-1}. The band at 2124 cm^{-1} is attributed to monoatomic Pt^0 by Stakheev et al. [145]. The high wavenumber of the adsorbed CO indicate that the Pt is strongly electron deficient, and probably exists as $[Pt\text{-}H_{zeo}]^+$ adducts. The band at 2135 cm^{-1} corresponds to $Pt^{\delta+}$-CO and the one at 2167 cm^{-1} to CO adsorbed on Pt^{2+}. The main band at 2094 cm^{-1} is shifted by 6 cm^{-1} with respect to the corresponding band in the spectra of the argon calcined sample. Additionally, the peak is broaded towards lower wavenumbers and has two shoulders at 2088 and 2077 cm^{-1}. The bands in this region are assigned to Pt^0-CO [146].

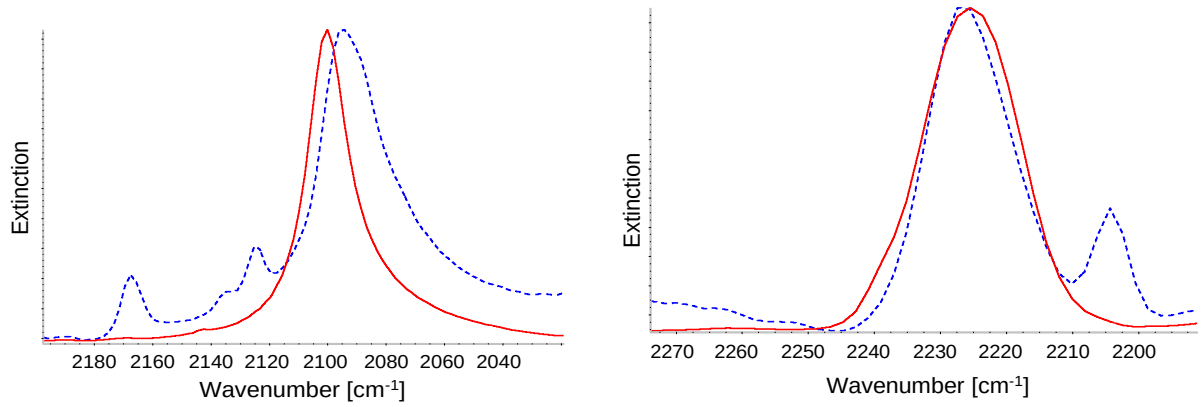

Figure 8: CO adsorption on PtB(Ar) (solid) and PtB(Air) (dashed); CO on Pt (left) and CO an Al (right)

The effect of the different calcination procedures can also be seen in the CO adsorbed on alumina. In both spectra, the main peak arises at 2225 cm^{-1}. This peak is the only one, if the sample is calcined under inert gas atmosphere. If the sample is calcined in air, a second peak appears at 2205 cm^{-1}. The band at 2225 cm^{-1} is denoted to Lewis acid sites and the latter one to extraframework alumina [147] showing the dealumination during the air calcination procedure as mentioned above.

Adamantane-carbonitrile adsorption on PtB(Ar) and PtB(Air):

Following the CO adsorption, the probe molecule was thermally removed in vacuum at 400 °C from the zeolite prior the adsorption of the nitrile, to assure that the platinum is accessible for the nitrile. After pulsing approximately 5 mbar of adamantane-carbonitrile, the sample was equilibrated for 20 min. Before the measurement, the cell was evacuated. The AdaCN adsorptions on the two samples, as well as the reference spectra, taken prior to the adsorption, are shown in Figure 9.

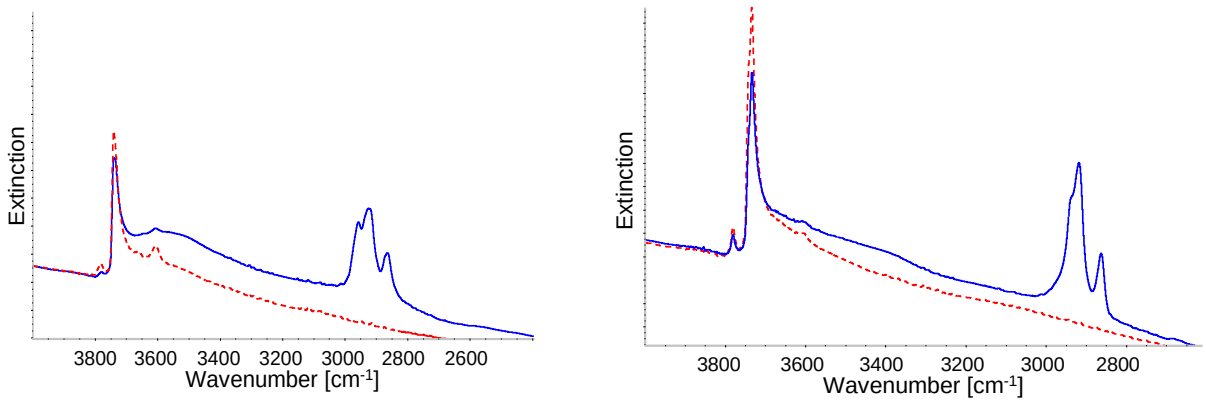

Figure 9: AdaCN (solid) on PtB(Ar) left and PtB(Air) right and the reference spectra (dashed)

In both experiments, the AdaCN adsorbs on the external silanol groups. Simultaneously to the reduction of the silanol band, a broad band in the 3650-3300 cm^{-1} region is formed. In both cases the VHF band is slightly eroded by the nitrile adsorption. According to Areán [138], the Brønsted acid OH groups at 3608 cm^{-1} was not significantly affected by the absorption; the fluctuations observed are due to the broad band of perturbed silanol and the relatively low intensity of the Si-(OH)-Al band.

Simultaneous adsorption of Adamantane-carbonitrile and CO:

To study the influence of the calcination process towards the distribution of the Pt-clusters, the change of the intensity of the Pt-CO vibration at 2100 cm^{-1} before and after selective poisoning of extra porous platinum with AdaCN is examined. Therefore, a second dose of carbon monoxide was dosed to the sample on which the nitrile was adsorbed. For the air calcined sample a dramatic decrease of the peak was observed as shown in Figure 10. Contrary to this, the changes in the CO peak was marginal for the argon calcined Pt-zeolite. This experiment clearly shows that the two materials noticeably differ in the distribution of the platinum. In case of the air calcination, nearly the entire platinum is accessible for AdaCN

and almost no CO can be adsorbed after the exposure to the nitrile. Therefore, it is concluded that the clusters are located on the outer surface of the zeolite crystallite. If the sample is calcined under inert gas atmosphere, most of the platinum is still accessible for the carbon monoxide molecule and not blocked by the nitrile, that leads to the conclusion that most of the platinum is located in the pores and channels of the zeolite.

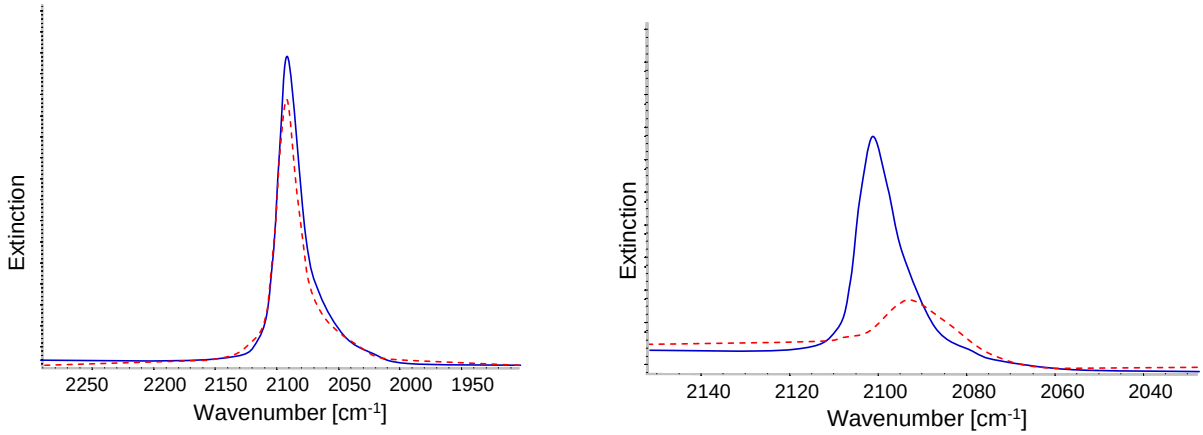

Figure 10: Influence of nitrile adsorption on the Pt-CO intensity, PtB(AR) left and PtB(Air) right, respectively (solid line: CO adsorption; dashed line CO adsorption after AdaCN poisoning)

IR experiments over Rh-BEA:

The IR spectra of the two rhodium impregnated zeolites and the H-BEA-35 are shown in Figure 11. As in the spectra of the Pt-zeolites the main bands representing the Brønsted acid sited at 3608 cm^{-1}, the silanol bands at 3745 cm^{-1} and the very high frequency band at 3782 cm^{-1} are found. After the high temperature treatment at 800 °C in air, the zeolite was found to be dealuminated, which was indicated by the disappearance of the Brønsted acid sites. Contrary to the calcination in air, this band is not affected by the calcination under inert gas atmosphere. The different calcination gas atmosphere has no influence on the structure of the silanol groups, but the intensity of this band is reduced by the impregnation and calcination. The intensity of this band is more pronounced if the impregnated zeolite is calcined in inert gas atmosphere. Despite to the spectra of the Pt-zeolite, only one band representing the silanol groups at 3744 cm^{-1} is found in the spectra of the Rh-zeolite.

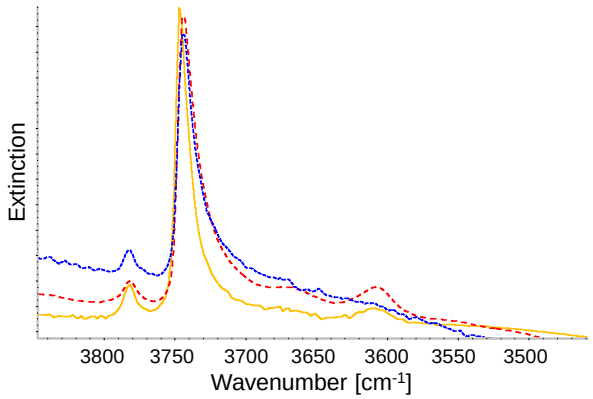

Figure 11: OH-vibration region (H-BEA solid, Rh-BEA(Ar) dashed and Rh-BEA(Air) dotted

CO adsorption on Rh-BEA:

After the adsorption of 20 mbar carbon monoxide, three main bands were found. These bands and their assignments are listed in Table 7. In case of the argon calcined sample, the broad band between 2130 and 2105 cm^{-1} consist of two bands, one band peaking at 2123 cm^{-1} and another band at 2115 cm^{-1}, corresponding to $Rh^{(I)}$ differently bond to the zeolite. The most significant impact of the calcination atmosphere is the degree of reduction, which is more pronounced in case of the argon calcined sample, indicated by the intensity of the band at 2058 cm^{-1} which is correlated to CO linearly adsorbed on $Rh^{(0)}$.

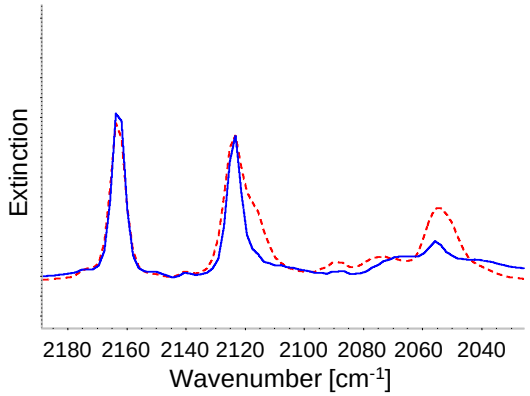

Figure 12: CO adsorbed on RhB(Air) (solid) and RhB(Ar) (dashed)

The minor bands of the spectra can be assigned to $Rh_4(CO)_{12}$ and $Rh_6(CO)_{16}$ clusters [148].

Table 7: CO frequencies adsorbed on Rh-BEA

Frequency [cm^{-1}]	Rh(Air)	RhB(Ar)	Species
2163	+	+	Rh^{3+}-CO [149]
2123	+	+	$TO_2Rh^{(I)}$-$(CO)_2$ [150]
2115	+	-	T-O-$Rh^{(I)}(CO)_2(OH)$ [151]
2058	-	+	Rh^0-CO [151]

Simultaneous adsorption of adamantane-carbonitrile and CO:

As in case of the platinum containing zeolite, the carbon monoxide was thermally removed by heating the zeolite up to 400 °C in vacuum. After 30 min, the CO was completely removed and adamantane-carbonitrile was adsorbed. After an equilibration time of 20 min, CO was adsorbed to investigate the precious metal distribution.

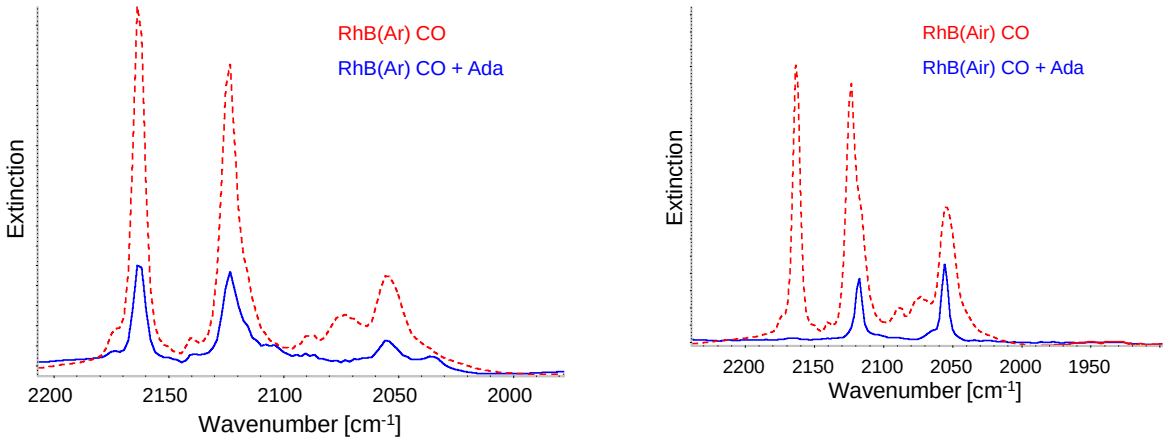

Figure 13: Adsorption of CO (dashed) and simultaneous adsorption of AdaCN and CO (solid) on RhB(Ar) (left) and RhB(Air) (right)

In both samples, after the nitrile adsorption, the amount of CO that still can absorb on the sample is strongly reduced. In case of the argon calcined sample, all the main bands of the initial CO spectra can be detected, but the intensity is significantly reduced, indicating that most of the precious metal is located on the external surface of the zeolite and therefore accessible for the AdaCN. These results are in line with the XRD pattern of the corresponding zeolite, which exhibits large reflexes corresponding to $Rh^{(0)}$-clusters on the outer surface. In case of the air calcined sample, the band at 2163 cm^{-1}, corresponding to $Rh^{(3+)}$ ions completely disappears, whereas the other two bands, corresponding to the inert gas calcined sample, are strongly decreased.

To round the analysis of the influence of the calcination atmosphere, transmission electron microscopy micrographs had been taken of the air and argon calcined platinum zeolite. The micrographs are shown in Figure 14. The left micrograph shows the argon calcined sample, whereas the air calcined sample is shown on the right one.

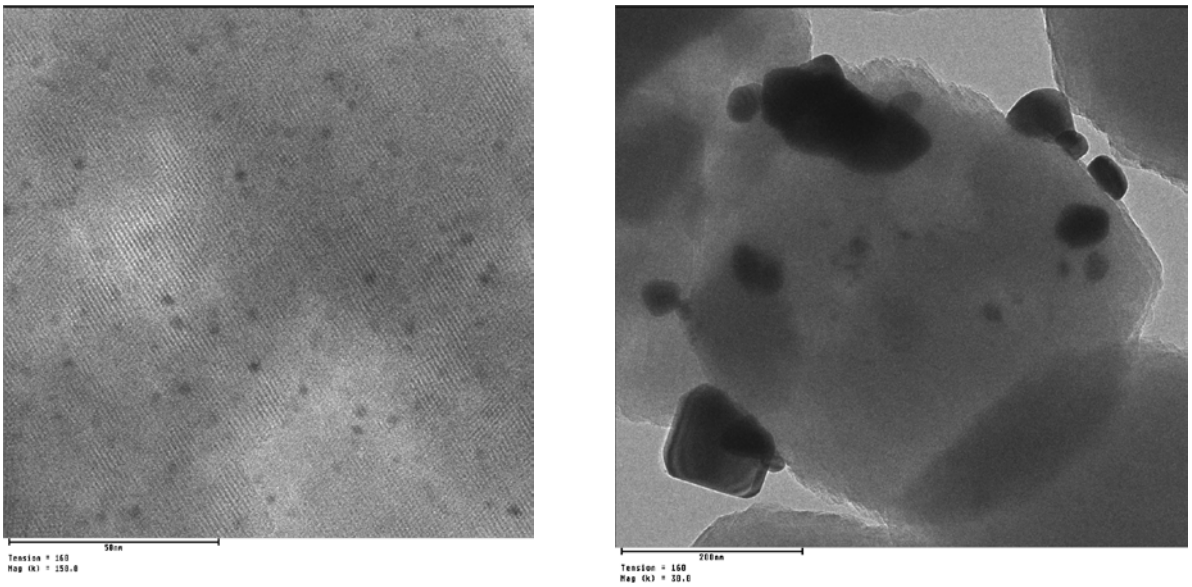

Figure 14: TEM micrograph of the Ar (left) and air (right) calcined PtB

The effect of the calcination procedure can be seen clearly by the comparison of the two micrographs. If the Pt impregnated zeolite is calcined under inert gas atmosphere, small Pt clusters, which are homogenously distributed throughout the zeolite, are formed. Their average cluster size is determined to be around 3 nm. These small clusters can hardly be found, if air is used for the calcination. Contrary to the argon calcination, the air calcination favours the migration of platinum to the outer surface of the zeolite crystallite and along with this migration, the formation of large clusters on the outer surface. The mean particle size after the air calcination is 100 nm, with a large number of particles exceeding 500 nm. Nevertheless, small cluster still can be found in the pores of the zeolite. These results are in good agreement with the results obtained by the XRD and IR experiments.

Additional zeolite based catalysts according to the developed synthesis route:

The platinum distribution and dispersion of the zeolite based reference catalysts was studied with XRD, since the results of the IR experiments are in line with the XRD experiments and hence XRD experiments are a fast and robust method to determine the cluster size and distribution.

In Figure 15 the XRD pattern and the decomposition of the nitrate precursor of the $PtNO_3$-BEA are shown.

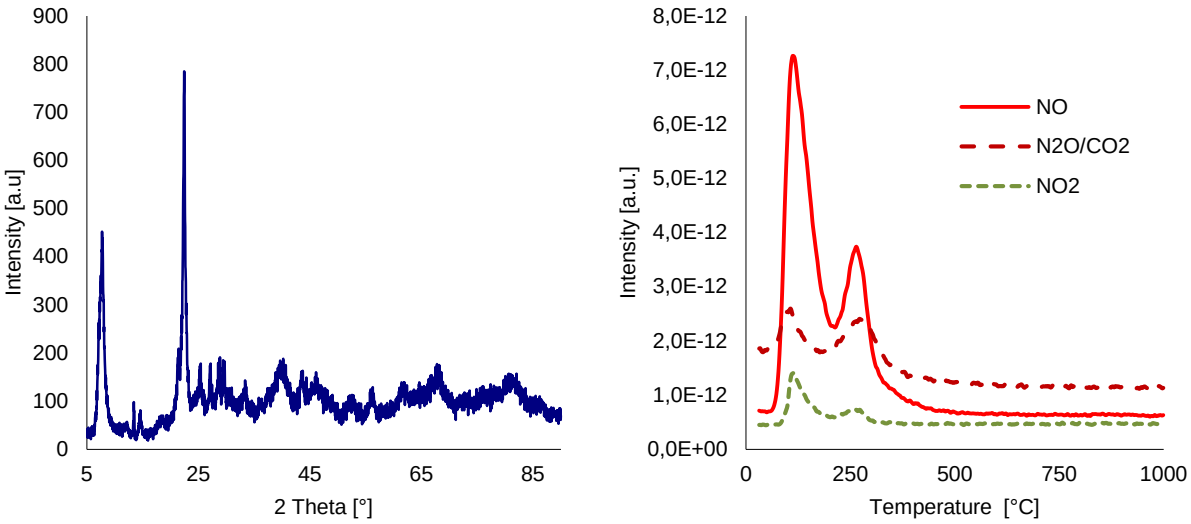

Figure 15: XRD pattern and TPD of the $PtNO_3$-BEA

In Figure 16 the XRD pattern of the platinum impregnated SH-27 and the PtEA-BEA are shown.

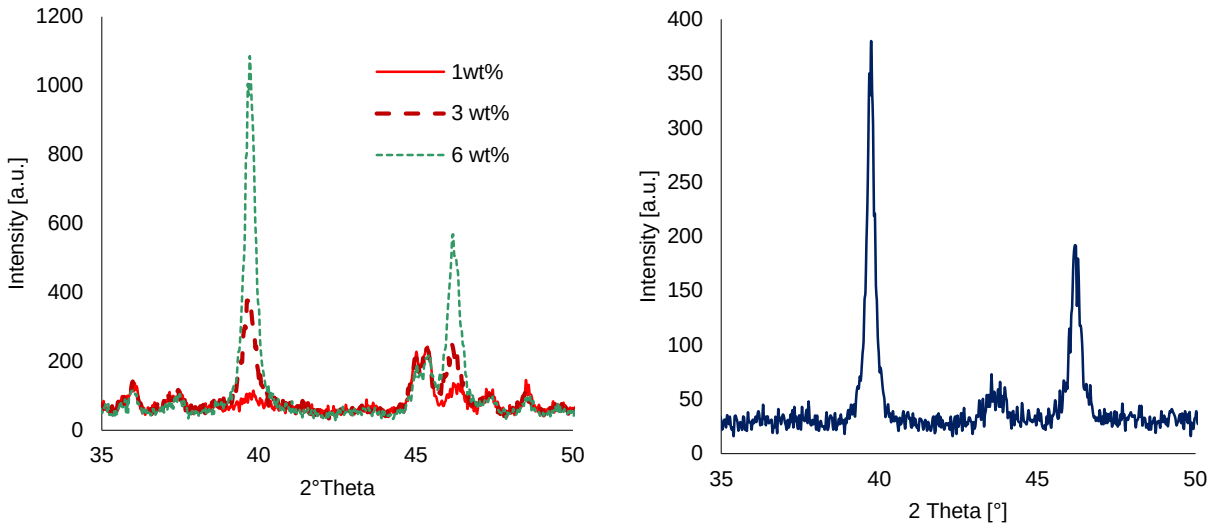

Figure 16: XRD pattern of platinum impregnated SH27 (left) and PtEA-BEA (right)

All three zeolite based catalysts show small reflexions of platinum at 39.7, 46.2 67.4 and 81.2 °. As mentioned above, these reflexions are assigned to the Pt (111)-, (200)- and (112)-plane, respectively [141]. The cluster size is calculated with the Scherrer equation and given in Table 8.

Reference catalysts (PtEA and EnviCat2520):

The cluster size of the reference catalysts on alumina are determined by transmission electron microscopy. The two micrographs in Figure 17 show platinum deposited on Siralox (left) and on alumina (right).

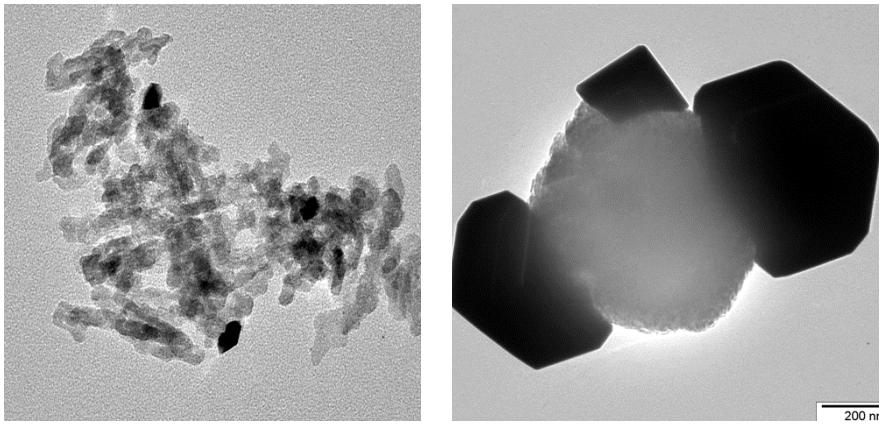

Figure 17: TEM micrographs of PtEA (left) and EnviCat2520 (right)

Table 8: Platinum concentration and cluster size

	Pt concentration [wt%]	Cluster size
$PtNO_3$-BEA	3	detection limit
Pt-SH27	1-6	detection limit, 15 nm and 60 nm
PtEA-BEA	3	15 nm
EnviCat2520	1	250 nm
PtEA	3	10-20 nm

3.4. Discussion of the synthesis

3.4.1. Influence of the calcination gas atmosphere:

The results show that the gas atmosphere used for the calcination of Pt-zeolite impregnated with platinum sulphite acid has a strong influence on the remaining sulphur as well as on the distribution and dispersion of the resulting Pt-clusters. The influence of the calcination towards the sulphur content and the cluster size and distribution will discussed here:

Sulphur content:

The differences in the sulphur content found by AAS can be explained by the thermogravimetric analysis of the sulphur desorption and the IR experiments.

The TGA experiments show that most of the SO_x desorbs as SO_2, independent of the gas atmosphere used for the calcination. The desorption profiles of the two calcination procedures show nearly the same SO_x release at ~300 °C but differ clearly in the temperature range between 700 and 800 °C. Temperatures above 400-600 °C [6] and an oxidizing calcination atmosphere favour the oxidation of SO_2 to acidic sulphur-containing species such as sulphate. The oxidation of SO_x can be suppressed by the utilisation of an inert gas atmosphere. Nevertheless, SO_3 was not detected in the TGA experiments. The most likely explanation for the sulphur retention during the high temperature treatment in oxidizing atmosphere is the interaction of the carrier with oxidation products such as sulphate. This explanation was given by Regalbuto et al. [152] who first evaluated platinum sulphite acid as precursor for supported Pt catalysts. The IR experiments (Figure 7 and Figure 8) reveal the dealumination of the zeolite during the calcination in air. This dealumination leads to the formation of extra-framework alumina and to Al_2O_3. As discussed in chapter 1.3, alumina is well known to strongly interact with sulphur, forming $Al_2(SO_4)_3$. Therefore, the oxidation of SO_x to SO_3 or to any acidic sulphur-containing species and the simultaneous dealumination coming along with the formation of Al_2O_3 and the high temperatures necessary for the reaction of sulphate and Al_2O_3 to $Al_2(SO_4)_3$ are the most likely reason for the retention of the sulphur in the Pt

zeolite during the calcination in air. If inert gases such as argon are used for the calcination these problems can be overcome since both effects, the oxidation of SO_2 and the dealumination are suppressed, resulting in a sulphur free zeolite prepared with a sulphur containing precursor.

Platinum cluster distribution and dispersion:

Additionally to the sulphur content and the dealumination, the platinum distribution and the particle size are influenced by the choice of the calcination atmosphere. The XRD pattern taken from the two differently calcined samples clearly show that the formation of large clusters is favoured if the sample is calcined in air whereas no platinum reflexes can be found if argon is used for the calcination. These results are in line with results of the IR measurements in which only marginal amounts of CO can be adsorbed after selective poisoning with adamantane-carbonitrile in case of the inert gas calcination. The opposite is true if the zeolite is calcined in an oxidizing atmosphere. The different distribution of the clusters can be explained by the different chemical and physical properties of the different Pt oxidation states and their reactivity towards the carrier. It is well know that PtO is formed at 100 °C and is further oxidized to PtO_2 at 300 °C [20]. The formation of these platinum oxide species is responsible for the cluster growth on the external surface of the zeolite crystallites. PtO_2 is known to be highly volatile and instable. As result of these properties, PtO_2 migrates from the inner surface to the outer surface and big clusters are the result of the coalescence of the mobile PtO_2 species. The $Pt^{(0)}$-clusters result from the thermal instability of PtO_2 that decomposes [50].

$$\mathrm{Pt_{disp}} \xrightarrow{300°C} \alpha - \mathrm{PtO_2} \xrightarrow{600°C} \beta - \mathrm{PtO_2} \xrightarrow{600°C} \mathrm{Pt_{cryst}} \qquad \textbf{eq. 8}$$

Furthermore, it is reported that PtO formed by the high temperature treatment reacts with the acid sites of the zeolite [82].

$$\mathrm{PtO} + 2\mathrm{H^+} \rightarrow \mathrm{Pt^{2+}} + \mathrm{H_2O} \qquad \textbf{eq. 9}$$

Pt^{2+}-ions are known to migrate through the zeolite and therefore can contribute to cluster growth. Another reaction between the zeolite and platinum which has to be taken into consideration is reaction of Pt^{2+} and Pt^{4+} ions and the zeolite at the surface forming Pt-(O-Si≡)$_y^{2-y}$ as mentioned by Jimerez et al. [153]. The IR spectra of CO adsorbed on the air

calcined sample (see Figure 8) prove the existence of all species mentioned above. However, the situation is completely different if the calcination is carried out under inert gas atmosphere. No Pt reflexes can be detected in the XRD pattern. The CO adsorption after selective poisoning with adamantane-carbonitrile as well as the TEM micrographs clearly show that nearly no platinum clusters are formed at the outer surface of the zeolite. The mechanism leading to the formation of those clusters is not fully understood yet. But it is obvious, that the lack of oxygen favours the formation of nanoclusters in the pore system of the zeolite. One possible explanation for the formation of homogenously distributed nanoclusters is that the sulphite ligand decomposes to H_2SO_3 at 300 °C followed by the decomposition of H_2SO_3 to H_2O and SO_2 at 400 to 450 °C indicated by the formation of water in the TGA experiment. The formed Pt species might interact with the internal silanol groups of the zeolite which is indicated by change of the ratio internal/external silanol-groups in the IR spectra. An interaction with the Brønsted acid is not likely since these sites still exist after the calcination. These Pt-zeolite sites are potential nucleation sites for volatile Pt-oxide species that also might be formed during the inert gas calcination by the decomposition of the precursor. The high concentration of nucleation sites lowers the mean free path of the volatile species and results in a rapid formation of small aggregates that grow to small cluster. An analogous mechanism is described by Creyghton et al. [83] but correlated to the influence of hydrogen supply for the reduction of Pt ions. If the calcination is carried out in an oxidizing atmosphere the oxygen suppresses the possibility of such a reaction pathway. Nevertheless the detailed mechanism is not clear and has to be an issue of further studies.

For further understanding of the synthesis of matrix stabilized precious metal nanoclusters, H-BEA zeolite was impregnated with different commonly used Pt-precursors such as tetraammineplatinum (II) dinitrate and platinum (II) nitrate and 2-hydroxyethylammonium hexahydroxoplatinate (IV). Additionally, an H-ZMS-5 zeolite was impregnated with platinum sulphite acid to investigate the influence of the zeolite structure upon the synthesis. The incipient wetness impregnation of a ZMS-5 with $(NH_3)_4Pt(NO_3)_2$ followed by inert gas calcination was first published by Kubaneck et al. [103]. They impregnated the zeolite with 1, 3 and 6 wt% and calcined at 550 and 800 °C. They found that it is possible to synthesise matrix stabilized nanoclusters at low temperatures and low concentrations and concluded, that the auto-reduction at higher temperatures and the resulting migration of the formed $Pt^{(0)}$-clusters lead to the formation of large crystallites on the external surface. The same was found here for the impregnation of BEA. PtEA was used to see the effect of a Pt(IV) precursor but again large clusters on the outer surface were formed. The only precursor leading to

comparable results is $Pt(NO_3)_2$ (see Figure 15). The similarity between both platinum nitrate and platinum sulphite is the electronegativity of the ligands, leading to the conclusion that beside the inert gas calcination, the electron-deficiency of the Pt is a crucial parameter for the successful synthesis of zeolite stabilized nanoclusters.

Based on the TGA, XRD and IR experiments the successful synthesis of matrix stabilized platinum clusters is achieved. For the synthesis it is necessary to use strongly adsorbing precursors such as platinum sulphite acid or platinum nitrate. The precious metal has to be introduced into a large pore zeolite such as BEA by incipient wetness impregnation. The impregnated zeolite has to be calcined under inert gas atmosphere at temperatures which are suitable to completely decompose the precursor. In case of the PSA a final temperature of 800 °C has to be reached (see Figure 3) whereas 300 °C are enough in case of the impregnation with platinum nitrate (see Figure 4).

The application of the developed synthesis with H-ZMS-5 zeolite showed, that it is in principle possible apply the method for other zeolite structures but that the amount of platinum that can be stabilized inside the pores of the zeolite depends on the zeolite structure, especially on the pore diameter (see Figure 16).

3.4.2. Rhodium impregnated BEA:

The same synthesis, as successfully applied for the generation of platinum nanoclusters mainly located in the pore system of H-BEA, was carried out with rhodium sulphite solution, in order to proof the hypothesis that the crucial parameter is the application of sulphite containing ligands. Compared to the AAS results and the XRD pattern of Pt-BEA, rhodium impregnated BEA shows opposite behaviour. In case of the rhodium zeolite the calcination in air favours the sulphur removal and the formation of small nanoclusters close to the detection limit of the XRD. Additionally, these results are in line with IR experiments, which show that independent of the calcination method the CO adsorption after selective poisoning is dramatically reduced. As in case of the Pt-zeolites, the Brønsted acid sites vanish after calcination in air due to the dealumination. But contrary to the Pt-zeolites, the silanol groups are not affected by any of the impregnation methods. The CO adsorption reveals the presence of various Rh-species independent of the calcination procedure. In both samples, Rh^{3+} and bidental zeolite bonded Rh^{+} are detected, whereas linear bonded Rh^{+} exclusively appeared in the air calcined sample and $Rh^{(0)}$ was only detected in the argon calcined sample. After the selective poisoning with adamantane-carbonitrile the intensity of all CO adsorption bands is noticeably decreased but besides the bands representing Rh_2O_3 in the air calcined sample,

they are still detectable. Therefore it can be concluded that both catalysts consist of an uneven distribution of the precious metal in different oxidation states. Although the Rh_2O_3 clusters are exclusively located on the external surface of the zeolite crystallite, as proofed by the IR experiments and the high temperature treatment, sintering is suppressed since they a slightly above the detection limit of the XRD. The high thermal stability can only be explained by intimate interaction between the carrier and the Rh_2O_3 clusters. One possible explanation is that the dealumination and the simultaneous migration of Rh_2O_3 lead to the formation of a "Zeolite-Al_2O_3-$RhAlO_4$-Rh_2O_3" structure, in which the dealumination and Rh-aluminate formation occur at the same time and that this species is the nucleation site for Rh_2O_3. Analogous to the Pt-BEA zeolites the processes leading to the temperature resistant Rh clusters are not understood yet and need to be further studied.

The experiments with rhodium sulphite acid clearly showed that the utilisation of sulphite containing precocious metal precursors not necessarily favours the formation of nanoclusters exclusively located within the pore system of zeolites. This hypothesis seems to be limited to divalent precious metals such as platinum [107, 108], palladium [110] and platinum/palladium alloys [110].

4. Comparison of the catalytic performance

The activity of precious metal catalysts is mainly influenced by the cluster size of the employed noble metal and the support used to dispense the active components. To study these influences towards the activity, catalysts with different cluster size and on different carriers were investigated.

In the first case study the oxidation of propane, ethylene and CO over PtB(Ar), PtB(Air), PtEA, and the EnviCat2520 were investigated. This study consisted of two parts. First, the initial activities of the various catalysts were compared. In the second part, the ramification of thermal stress to the Pt-zeolite catalyst was compared with the commercial EnviCat2520. Additionally, the thermal stability of the zeolite-stabilized platinum clusters and the accompanying cluster growth was investigated.

To complete the understanding of the developed Pt-zeolite catalyst, the simultaneous oxidation of propylene, CO and NO under humid condition was tested, in the second case study and compared with commercial catalysts. In addition to the activity of the fresh catalysts, the behaviour of hydrothermally aged and sulphur dioxide poisoned catalysts was investigated. The aim of the second case study is to evaluate the potential application of the developed zeolite based catalyst as a Diesel oxidation catalyst (DOC). For this application, the oxidation of NO to NO_2 and the cold start trap properties of the catalyst are of crucial importance. These characteristics will be highlighted in the second case study.

In the third case study, the effect of stabilization of rhodium in the pores of BEA is investigated. The most known catalytic application of rhodium in environmental catalysis is the simultaneous conversion of NO with CO and hydrocarbons in three-way catalysts (TWC). Thus, the simultaneous reaction of CO, NO and propylene was chosen to test this catalyst.

4.1. Description of the test units

The three different cases studies were carried out on three different test units. The experiments of the first case study (Chapter 4.2) and of the kinetic considerations (Chapter 5) were carried out on the Test unit H02 of the department of “Stationery Emission Control”. For the two other case studies, test units of the department of “Automotive” named WTU and LTUA were used. These three test units will be described only briefly and schematically since the details are property of Süd-Chemie AG (Clariant Produkte (Deutschland) GmbH).

All test units applied have the same principal structure. The educt gases are supplied from the in-house media supply or local gas cylinders. The desired flow rates were adjusted by

electronic mass flow controllers (Bronkhorst). Then the individual gas flows were mixed and preheated before entering the reactor with the catalyst. For all experiments the test unit was heated to the maximum temperature and was then stepwise cooled down, meaning all experiments were carried out form high to low temperature, to ensure comparability to already existing data. Preheater and catalyst zone were separately heated to the desired temperature. The inlet and outlet gas composition was analysed by the analytical equipment, mainly by a FTIR Spectrometer, and the obtained data were saved and evaluated on the control computers of the test units. The analytical equipment was calibrated on a regularly with calibration gases. The schematic set-up of the test units is shown in Figure 18 and Figure 19.

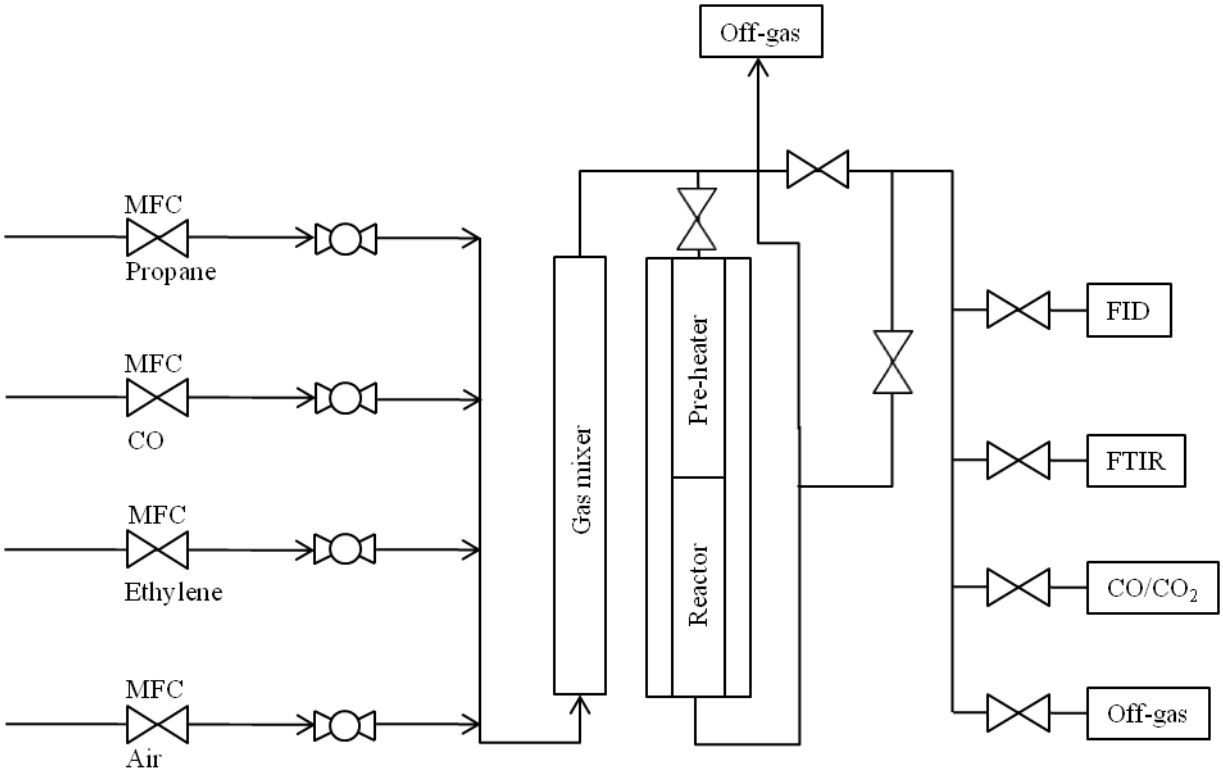

Figure 18: Schematic drawing of the test unit H02

Details of the H02 test unit:

The coated honeycomb catalyst (20 mm diameter) was fixed with quartz wool inside a quartz tube, installed in a vertical stainless steel reactor tube. Quartz as fixing and reactor wall material has the advantage to avoid undesired reaction as it can appear in case of a stainless steel reactor. For heating up the reactant gas and the catalyst homogenously the test unit is equipped with three hot air blow heaters. After changing the temperature the whole system was equilibrated for 15 minutes. Prior and after a test run the inlet gas composition was

analyzed. For gas analysis, the test unit is equipped with a Flame Ionisation Detector (ABB), FTIR Spectrometer (Thermo Fisher) and CO/CO_2-Analyzer (ABB).

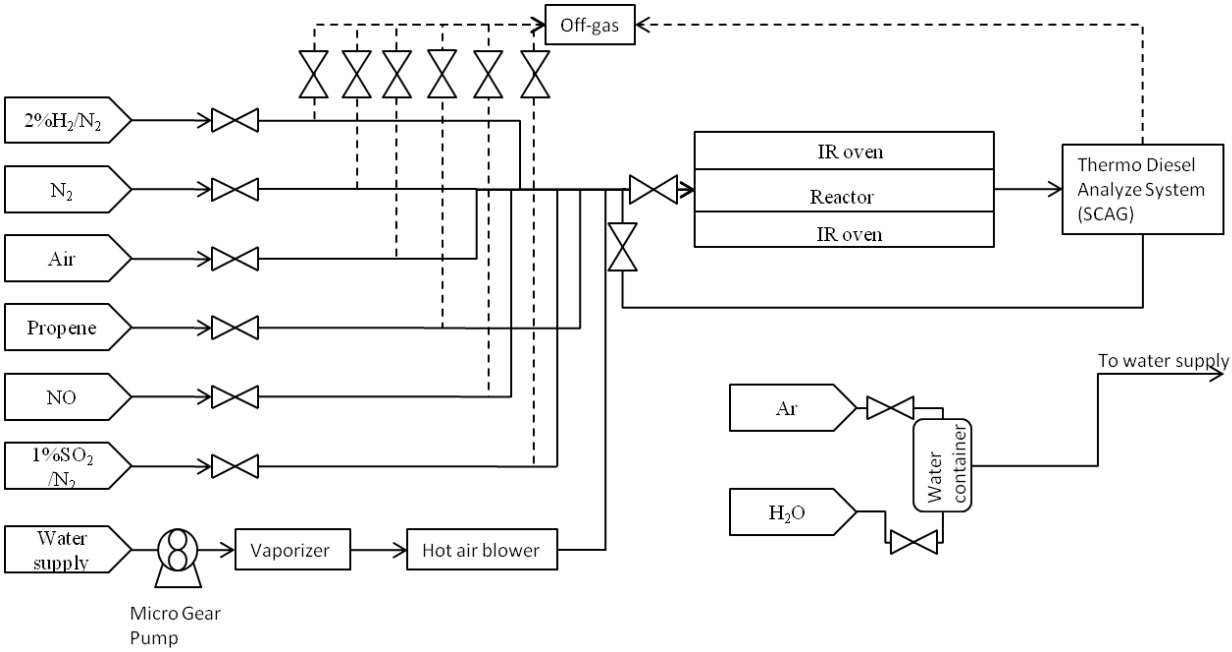

Figure 19: Schematic drawing of WTU and LTUA test unit

Details of the WTU and LTUA test units:

In both test units, the honeycomb catalyst was fixed with quartz wool in a horizontal quartz plug flow reactor tube with was heated by a radiation oven. This oven provides the possibility of fast changes in the reaction temperature and of high heating rates as typically occurs under real automotive operations. The two units were equipped with a vaporizer unit to add water in percentage range to the feed. Condensation of water was prevented by heating all piping with heating bands. The reactant and product gas composition was analyzed by a Thermo Fisher FTIR Spectrometer.

4.2. Case study I: Pt-BEA as VOC and CO combustion catalyst

To study the influence of Pt-cluster size and distribution on a zeolite support, two zeolite based catalysts, PtB(Ar) and PtB(Air), were prepared. In the case of the PtB(Ar), small platinum clusters are homogenously distributed throughout the zeolite. In contrast to this, the PtB(Air) contains mainly very large Pt-clusters on the outer surface of the zeolite. In order to investigate the effect of the carrier and the cluster size, two reference catalysts were prepared as described in chapter 3.1. The PtEA catalyst contains medium size Pt-clusters, whereas the EnviCat2520 consists of big clusters. Before the test, the various supports were coated onto 20 mm long, 200 cpsi ceramic honeycombs with a diameter of 25 mm. The Pt loading was 1 g

per litre of the honeycomb volume. The washcoat loading was 100 g/l in all cases except the EnviCat2520, where the washcoat loading was 50 g/l. All catalysts, except the PtEA, were aged at 550 °C for 12 h prior to the test, to ensure that the results are not altered by any changes during the test procedure. For the PtEA catalyst the aging temperature was only 450 °C and the catalyst was tested in a temperature range not exceeding this temperature. The lower temperature was chosen to ensure, that the platinum dispersion is not affected and the influence of the noble metal dispersion on the reaction can investigated.

Table 9: Test conditions

	Concentration [ppm]	Temperature [°C]
Propane	100	500→350
Ethylene	600	160→100
CO	600	160→100
Oxygen	20.5 vol%	

The GHSV[1] was 150 000 h^{-1}.

4.2.1. Comparison of the catalytic activity

In Figure 20 the conversion as a function of the temperature of the different catalysts and the three reactants gases are shown. For the deep oxidation of propane, the platinum stabilized in the zeolite matrix shows the highest activity in the whole temperature range, whereas the Pt-zeolite catalyst calcined in air hardly oxidizes any propane. Over the PtEA catalyst approximately 7 % less propane is oxidized compared to the PtB(Ar) catalyst at the corresponding temperature. The propane conversion over the EnviCat2520 is between 10 % and 15 % lower than the conversion of the argon calcined platinum catalyst.

[1] The GHSV is calculated by dividing the gas flow rate by the volume of the sample at standard conditions.

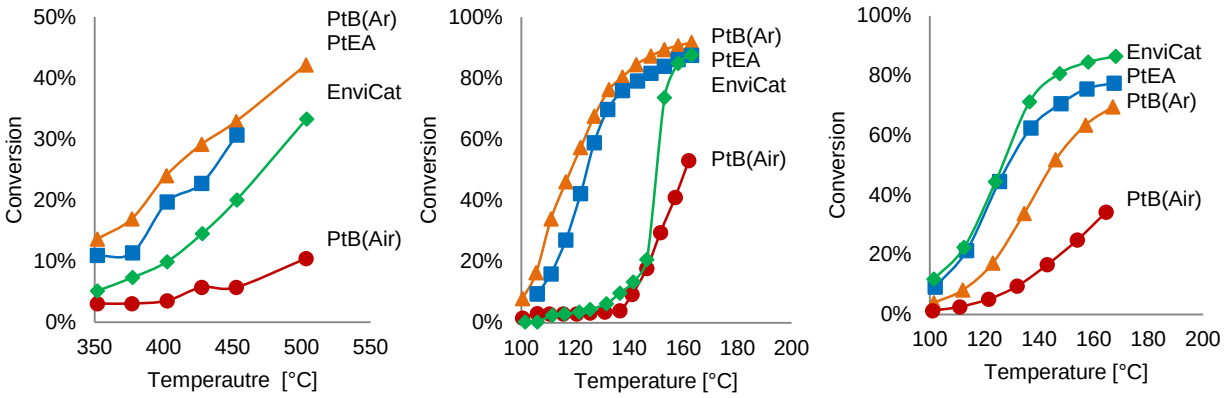

Figure 20: Conversion as a function of the temperature plot: propane (left) CO (middle) and ethylene (right)

The oxidation of CO and ethylene was investigated in a temperature range from 160 °C to 100 °C. For the oxidation of CO, the same order of reactivity is found as for the oxidation of propane. The two catalysts consisting of small platinum clusters (PtB(Ar) and PtEA) have nearly the same activity for the oxidation of CO. The light-off temperatures[2] over these two catalysts are 116 °C and 123 °C, respectively. In contrast, the reaction over the commercial EnviCat2520 did not ignite until 150 °C. The light-off over the air calcined catalyst is further increased to 160 °C.

Contrary to the oxidation of propane and CO, the two catalysts based on alumina are the most active ones for the oxidation of ethylene. The PtB(Ar) catalyst has a lower activity compared to the two others. Again, the PtB(Air) catalyst has the poorest activity and reaches a maximum conversion of 45 %. The light-off temperatures for the oxidation of 600 ppm are 123 °C, 128 °C and 141 °C for PtEA, the EnviCat2520 and the PtB(Ar), respectively.

[2] In this thesis the light-off temperature is defined as the temperature at which 50 % conversion is reached.

4.2.2. Comparison of the thermal stability of the platinum catalysts

As explained in the introduction, the thermal stability is one of the crucial aspects for a catalyst used in environmental catalysis. In stationary applications, sudden temperature rises can be caused by hot-spots, which can originate from oscillations in the feed's pollutant concentration. To test the hypothesis that the inclusion of precious metals leads to an improved thermal stability, the PtB(Ar) and the commercial catalyst EnviCat2520 were thermally aged and their remaining activity compared. In the first experiment the two catalysts were aged under reaction condition up to 25 h. In a second experiment, the two samples were thermally aged in a muffle oven at 650 °C stepwise up to 100 h. For these tests, the PtB(Ar) was coated on a 75 mm long, 200 cpsi cordierite honeycomb. The total washcoat loading was 100 g/l and the Pt concentration was 1 g/l. The platinum loading of the EnviCat2520 the washcoat loading was 50 g/l but the Pt-concentration was kept constant at 1 g/l. The test condition are summarised in Table 10.

Table 10: Test conditions

C_3H_8	Air	Temperature	GHSV
180 ppm	balance	550 °C	40 000 h^{-1}

The two different catalysts clearly differ in the thermal stability under reaction conditions, as illustrated in Figure 21 and Figure 22. The activity for the fresh catalyst is nearly identical, for both the EnviCat2520 and the PtB(Ar) catalyst. The initial conversions for the EnviCat2520 and the PtB(Ar) catalyst, are 97 % and 95 % , respectively. After five hours on stream, the situation is completely different for the two catalysts. The alumina based EnviCat2520 deactivates dramatically, with a relative drop down to ~60 %. After the deactivation within the first five hours, the performance of the catalysts stabilizes at that level. In contrast to the EnviCat2520, the PtB(Ar) catalyst is stable under reaction condition during the first five hours and only decreases its activity slightly. After 25 hours, a conversion of 91 % can still be achieved.

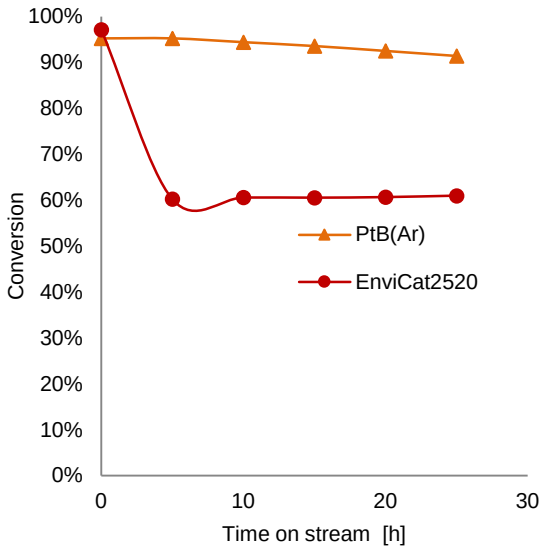

Figure 21: Time on stream at 550 °C

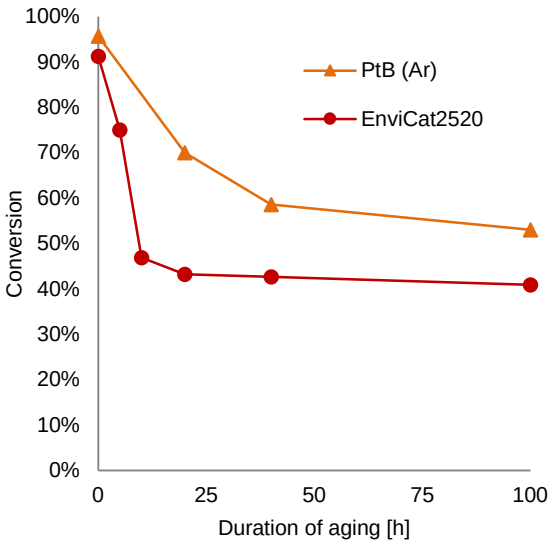

Figure 22: Deactivation at 650 °C

For further investigation of the thermal stability, both catalysts were aged at 650 °C in a muffle oven. The propane conversions over both catalysts after this thermal treatment are shown in Figure 22. The EnviCat2520 shows nearly the same behaviour as in the previous experiment. After been aged at 650 °C for 10 hours, only 47 % of the propane is oxidized. After aging for 100 hours, the conversion drops down to 40%. In comparison, the deactivation of the PtB(Ar) is slower and less pronounced. Nonetheless, the catalyst clearly deactivates. After aging for 20 hours the conversion drops to 70 % (47 % in case of the EnviCat2520) and after 100 hours at 650 °C, 53 % can still be achieved, which is 13 % more propane conversion than obtained by the commercial catalyst.

Thermal deactivation of PtB(Ar):

The Pt-BEA the was aged in a muffle oven successively at 600 °C, 650 °C and 700 °C for 12 h, to further investigate the thermal stability. After the aging procedure, the test as described above was repeated. Besides the catalytic activity, the cluster growth due to thermal treatment was investigated by TEM and XRD. The catalytic activities of the fresh and aged catalysts are shown in Figure 23 to Figure 25. The ongoing cluster growth is shown by the XRD pattern in Figure 26 and the TEM micrographs (Figure 27 to Figure 30).

The data illustrates, that the oxidation of propane is strongly affected by the thermal treatment (Figure 23). After aging the catalyst at 600 °C a maximal conversion of approximately 35 % can still be achieved. But at higher aging temperatures the maximal conversion is 20 % after aging at 650 °C and 10 % after 700 °C. The oxidation of CO is less affected by the thermal treatment (Figure 24). Up to 600 °C the aging has no influence on the performance of the

catalyst. After aging at 650 °C and 700 °C the light-off temperature is shifted from 120 °C to 135 °C and 145 °C, respectively. The effect of the thermal treatment on the catalytic conversion of ethylene is even less pronounced than for the two other educt gases (Figure 25). The catalytic activity is nearly unaffected for aging temperatures up to 650 °C. After a thermal treatment at 700 °C the conversion of ethylene is somewhat decreased (5-10 %).

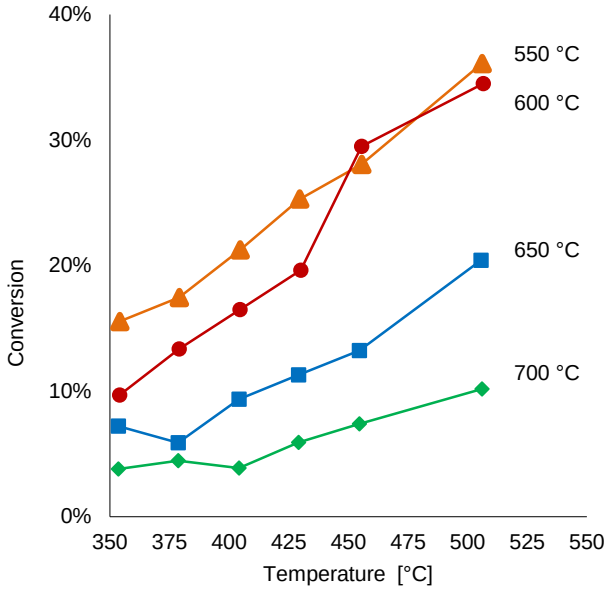

Figure 23: Propane conversion

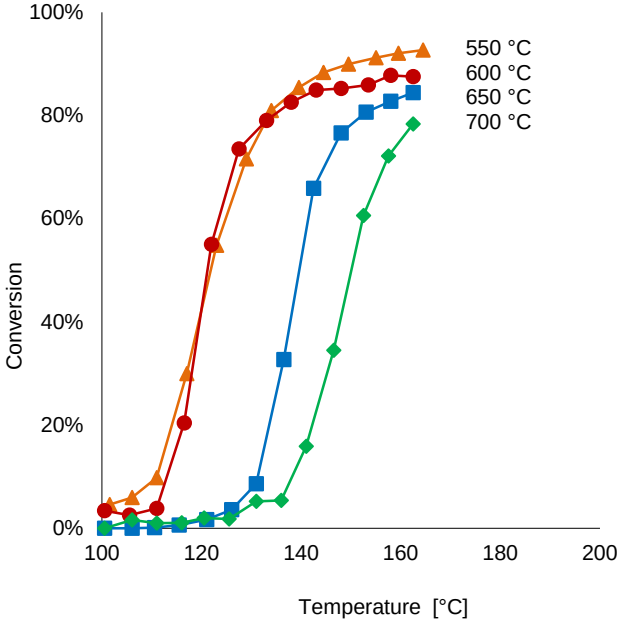

Figure 24: CO conversion

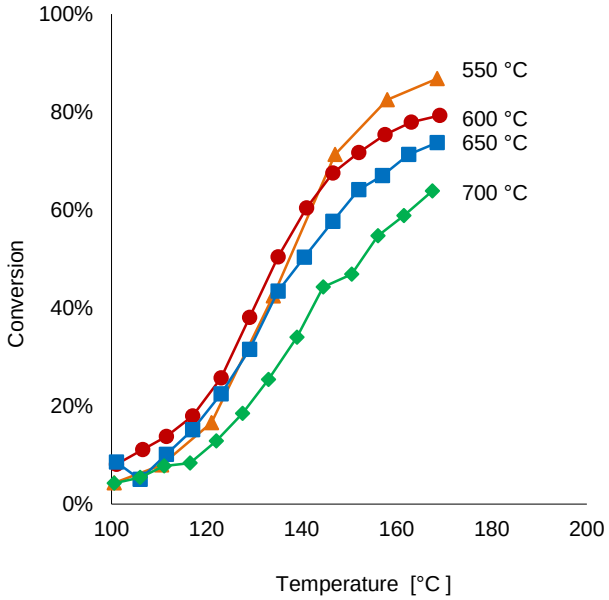

Figure 25: Ethylene conversion

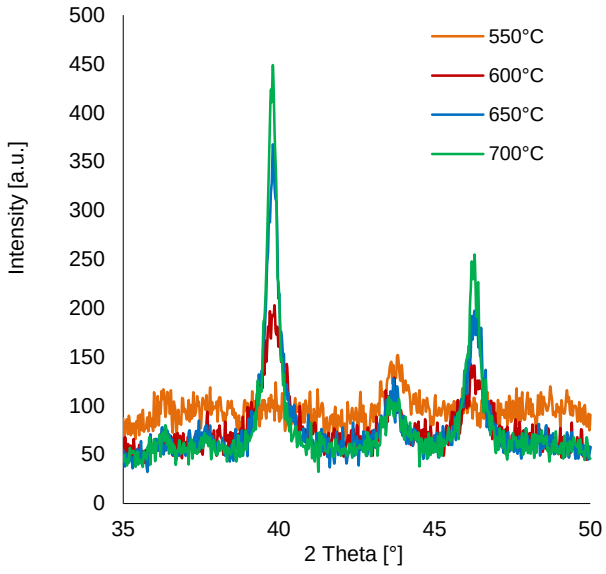

Figure 26: XRD pattern of the aged Pt-BEA

The XRD patterns show the sintering of the Pt-cluster by the thermal treatment. For the fresh catalyst, no Pt-reflexions can be detected in the XRD pattern. After the aging at 600 °C, small reflexions appear which constantly grow with the aging temperature. From the line

broadening the cluster sizes were determined to grow from 15 nm, after aging at 600 °C, up to 45 nm after aging at 700 °C.

Since the XRD method can only be used to determine the mean particle size, TEM micrographs were recorded. The crystal growth is confirmed by the TEM analysis, but additionally, the micrographs show an uneven cluster size. Besides the bigger clusters on the outer surface of the zeolite, small clusters still are present inside the porous system of the zeolite after aging at 700 °C.

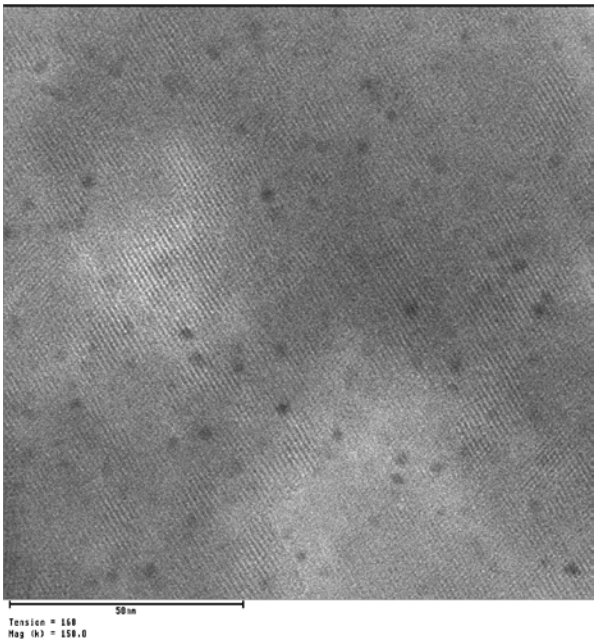

Figure 27: Fresh PtB(Ar)

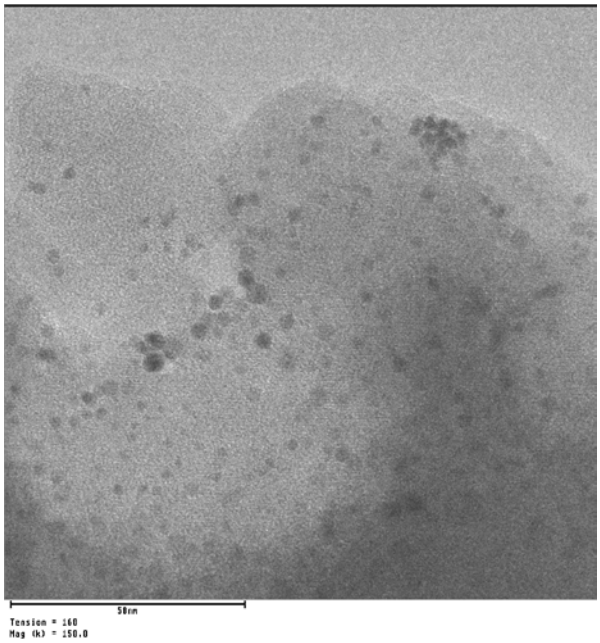

Figure 28: PtB(Ar) aged @ 600 °C

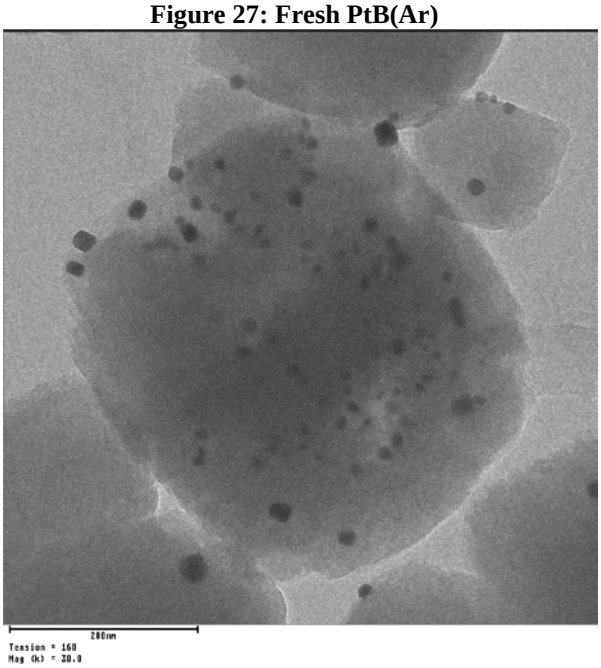

Figure 29: PtB(Ar) aged @ 650 °C

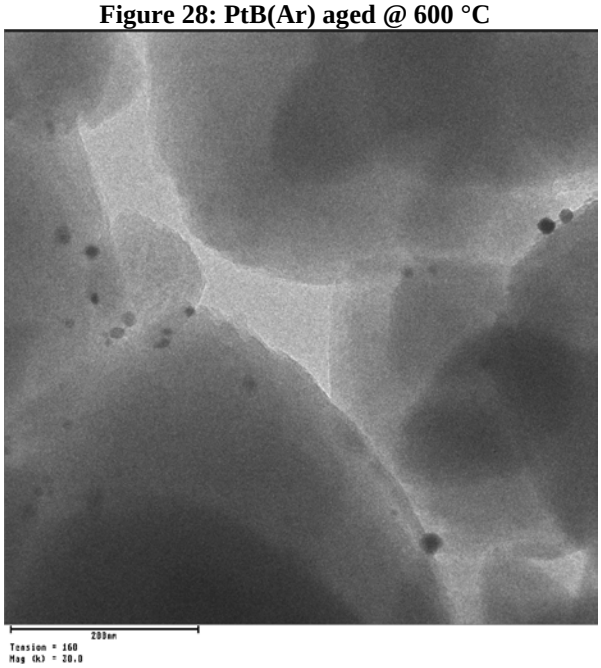

Figure 30: PtB(Ar) aged @ 700 °C

4.3. Case study II: Pt-BEA as Diesel-Oxidation Catalyst

4.3.1. Introduction

In the second case study, the applicability of the developed catalyst as a diesel oxidation catalyst (DOC) for automobiles is tested. In automotive applications, the catalyst has to handle fast changes of the operation conditions (e.g. temperature, feed composition) as explained in detail in the introduction. Among the key properties for a catalyst are low-temperature activity for the oxidation of the pollutants, resistance against thermal and hydrothermal treatments at temperatures above 700 °C, and resistance against catalytic poisons such as SO_2.

Another approach to reduce the amount of pollutants is the so called hydrocarbon adsorption trap on which the cold hydrocarbons are absorbed and retained until the downstream catalyst reaches the light-off temperature and is able to convert the released hydrocarbons. Hydrocarbon trap materials considered to date have been mainly various types of zeolites such as mordenite, Y-type, ZMS-5 and BEA [52]. Since the developed catalyst is zeolite-based and impregnated with a high concentration of active platinum site the PtB(Ar) is as well tested for its capability to be used as hydrocarbon cold start trap. To investigate the catalytic properties as well as the HC trap properties the developed PtB(Ar) and PtB(Air) catalysts were compared with a commercial DOC catalyst, designed to fulfil these requirements.

4.3.2. Catalyst and test procedure

The synthesis of the catalysts tested in this case study is described in chapter 3.1. The washcoat slurry of the reference DOC catalyst consists of a catalytically active component and a HC storage component. The catalytically active component is Pt deposited on silica doped alumina (Siralox by SASOL); the storage component is an iron exchanged BEA (further denoted as reference DOC). The mass ratio of catalyst/storage component is 1/1.

Three 5 cm long 400 cpsi ceramic honeycombs were coated with a washcoat loading of 100 g/l, resulting in a platinum concentration of 3.5 g/l for the reference DOC and the two Pt-zeolite based catalysts.

To study the initial activities and hydrothermal stability, as well as the resistance against sulphur, the following procedure was carried out: After a performance testing of the fresh catalyst, as described in Table 11, the coated honeycombs were aged at 750 °C with 10 % water in air for ten hours and tested again. After this hydrothermal treatment and a subsequent performance test (see Table 11), the same catalysts were exposed to 20 ppm SO_2 in air at

250 °C for two hours and then tested again under the previous conditions. Following the latter performance test, the catalysts were once more hydrothermally treated at 750 °C with 10 % water in air to remove the sulphate. Finally a fourth activity test was carried out. Since the Pt-zeolite calcined in air deactivated harshly after the hydrothermal aging, only the argon calcined Pt-zeolite and the reference DOC catalysts were exposed to sulphur and the following desulphurisation procedure.

To determine the HC storage capacity and the desorption characteristics; the catalysts were exposed to 220 ppm propylene in nitrogen at 80 °C for one hour. After the adsorption, the catalysts were heated up to 400 °C under nitrogen with a rate of 10 K/min to desorb the propylene.

Table 11: Test conditions

CO	C_3H_6	O_2	H_2O	CO_2	N_2	Temperature	GHSV
500 ppm	500 ppm	5 vol%	10 vol%	70-90 ppm	balance	390-110 °C	70 000 h^{-1}

4.3.3. Determination of the catalytic activity and thermal stability

As already demonstrated in the first experiment, the incorporation of the active precious metal into the pore structure of the zeolite increased the performance of the catalyst. In Figure 31 the light-off temperatures for the simultaneous oxidation of propylene and CO over the fresh, hydrothermally aged, sulphated and desulphated catalysts are shown. The PtB(Ar) and the reference DOC catalyst show the same activity for the oxidation of CO and propylene. The light-off temperatures for these reactions are nearly the same and differ only by a few Kelvin. For the CO oxidation, the light-off temperatures of the fresh, hydrothermally aged and sulphated catalyst are identical. The PtB(Ar) catalyst converts 50 % of the CO at temperatures of 196 °C, 225 °C, 237 °C, and 218 °C, corresponding to the fresh, hydrothermally aged, poisoned and regenerated catalyst, respectively. In comparison, the LOTs of the reference DOC are 203 °C, 226 °C, 232 °C and 236 °C. Significant differences can only be seen after the regeneration procedure, as the reference DOC is not affected by the regeneration. In contrast to that, the LOT of the PtB(Ar) decreases by 20 °C after this procedure. The PtB(Air) catalyst has the poorest activity of all the catalysts prepared. The light-off temperatures of the fresh and hydrothermally aged catalyst are 245 °C and 277 °C, respectively (not shown). These temperatures are approximately 50 K higher than the LOTs of the other two catalysts. Due to this poor performance, this catalyst was not exposed to sulphur poisoning and consequently also not regenerated.

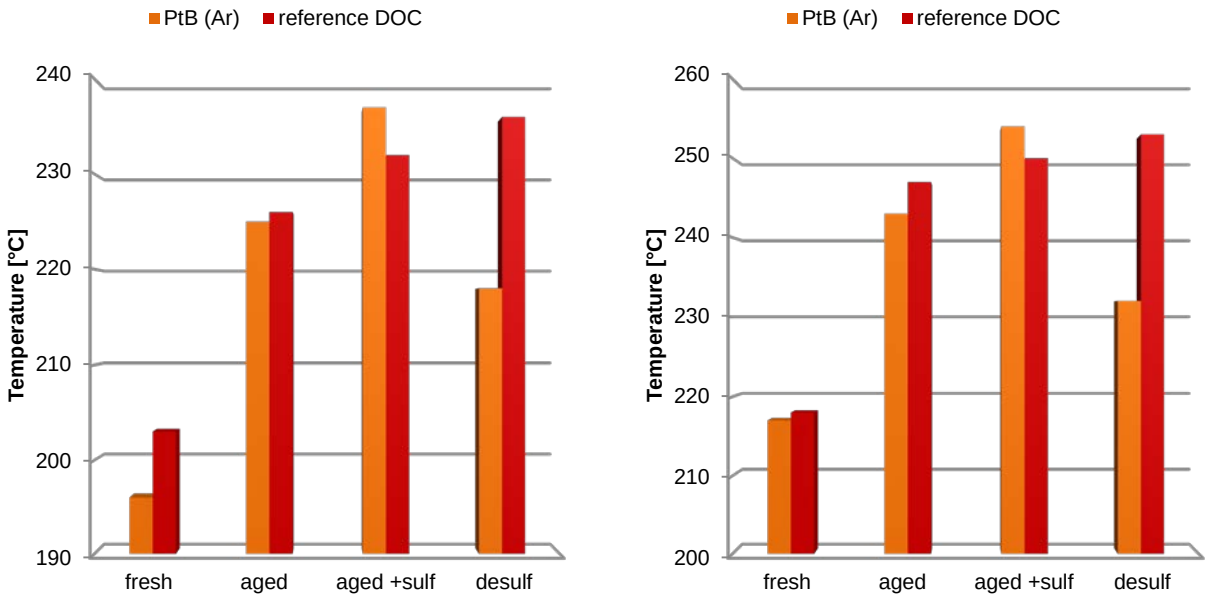

Figure 31: Light-off temperatures for the oxidation of CO (left) and propylene (right)

For the oxidation of propylene the same trends as in the CO oxidation were found. Over fresh PtB(Ar) catalyst, 50 % propylene conversion is reached at 217 °C and the LOT is increased to 243 °C by the aging. After the sulphur poisoning the LOT is further increased by 10 K. However, the poisoning is reversible, as the LOT is decreased by the regeneration to 232 °C. The reference DOC catalyst has the same catalytic activity in the fresh and aged state. The sensitivity to sulphur is less pronounced as the LOT of the poisoned catalyst is only slightly increased by 3 K instead of 10 K as in the case of the PtB(Ar) catalyst. Also, and in contrast to the PtB(Ar), the poisoning of the reference DOC is partly irreversible, as the LOT of the regenerated catalyst does not improve. In analogy to the CO oxidation, the fresh PtB(Air) (254 °C) and the hydrothermally aged catalyst (282 °C) have the lowest activity and are therefore not further investigated.

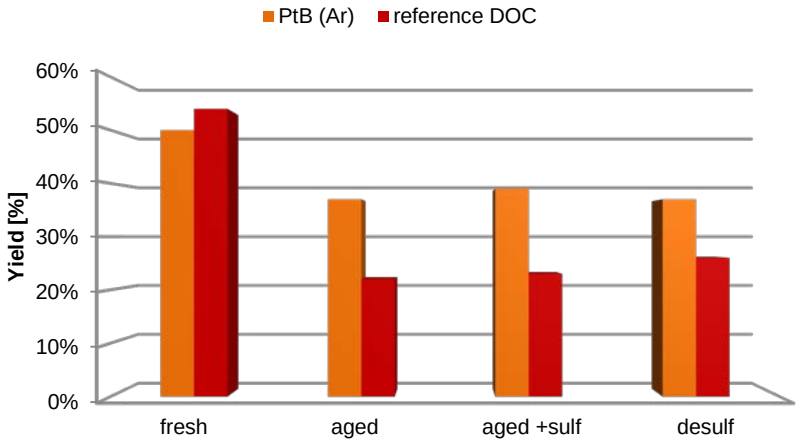

Figure 32: Maximum NO_2 Yield

Besides the oxidation of unsaturated hydrocarbons and CO, the oxidation of NO to NO_2 was investigated and the catalysts show a notably difference to the oxidation of propylene and CO. For this comparison, the maximal NO_2 yield, instead of the LOT is used. In this reaction, the fresh reference DOC catalyst reaches a maximum yield of 54 % and is followed by the PtB(Ar) catalyst, which achieves a conversion of 50 %. Once again, air calcined Pt-zeolite shows the poorest activity of all three catalysts tested. Its maximum NO_2 yield is only 32 %. After the hydrothermal aging, the ranking of the two superior catalysts is turned around. The maximal yield of the PtB(Ar) is reduced by 13 % to 37 %, whereas, the NO_2 yield, achieved by the commercial catalyst is only 22 %, and 15 % for the PtB(Air) catalyst. None of the catalysts tested is further affected by the sulphatation and regeneration.

To further investigate the advantages of the incorporated platinum clusters into the pore system of a zeolite, the PtB(Ar) is compared with a Pt/Pd catalyst, prepared as described in chapter 3.1.2 and coated on a honeycomb similarly to the PtB(Ar) catalyst. Catalysts, in which platinum is alloyed with palladium are known to withstand sulphur poisoning much better than pure platinum or pure palladium catalysts [154]. The results are summarized in Table 12.

Table 12: Comparison of the NO-oxidation

Catalyst	Maximum NO_2-yield [%]			
	fresh	750 °C aged	250° C 2 h + SO_2	750 °C 15 min reg.
PtB(Ar)	50	37	39	37
Pt/Pd catalyst	51	43	38	28

The initial yields of both of the catalysts are identical, while the deactivation due to the hydrothermal treatment is more pronounced for the PtB(Ar) than for the Pt/Pd catalyst. After the sulphur poisoning the two catalysts reach the same yield again. As mentioned above, the PtB(Ar) catalyst is neither influenced by the poisoning nor by the regeneration. However, the Pt/Pd catalyst is sensitive to the hydrothermal treatment after been contacted with sulphur and is further deactivated by this treatment.

4.3.4. Desorption and activity

For a catalyst designed for automotive applications, a low light-off temperature is only one of the key properties. For a good performance, a high hydrocarbon storage capacity, as well as desorption temperature close to or higher than the light-off temperature of the absorbed hydrocarbon is required. The closer the release temperature and the light-off temperature match, the better are the cold-start-trap properties of the catalyst.

The adsorption/desorption properties of the PtB(Ar) and the reference DOC catalyst are shown in Figure 33. The solid lines represent the desorption of propylene and the dashed lines the conversion of the desorbed hydrocarbon. The conversion data are taken from the previous measurements.

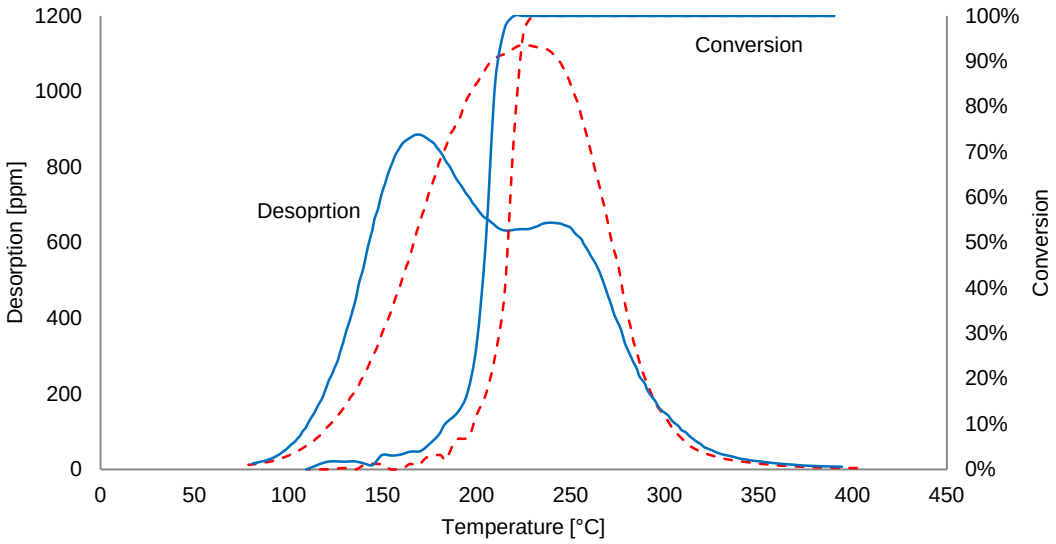

Figure 33: Desorption and conversion of propylene (PtB dashed, reference DOC catalyst solid)

The two catalyst clearly differ in their desorption properties. As detailed above, the reference DOC catalyst consists of two different components. On the one hand, platinum deposited on alumina as catalytically active component and an iron exchanged BEA zeolite as hydrocarbon trap. Due to the two components, the hydrocarbon desorb in two steps. At 175 °C, the HC

desorbs from the platinum containing alumina and at 270 °C from the Fe-zeolite. In case of the platinum containing zeolite, the hydrocarbons are released at approximately 225 °C.
In case of the reference DOC catalyst, the first desorption is at ~175 °C. The release temperature is below the light-off temperature of 205 °C and therefore the catalyst is not able to convert the released VOCs. At the 2nd desorption step, at 270 °C, 100 % conversion is achieved. In case of the PtB(Ar) catalyst, the situation is clearly different. Even though the LOT is 10 °C higher than in case of the reference DOC catalyst, fewer hydrocarbons are released before the temperature of maximum conversion is reached. At the temperature of maximum desorption, the catalyst is already able to convert the released propylene.

4.4. Case study III: Rh-BEA as NO reduction catalysts

The rhodium based catalysts were tested for the oxidation of propylene and CO and the simultaneous reduction of NO under slightly oxygen rich condition. The two rhodium zeolites catalysts and a "state of the art" Rh/ZrO_2 catalyst were tested under the conditions given in Table 13 and the conversion was measured from 450 °C down to 250 °C. After the test, the catalysts were thermally aged at 900 °C for 1 h in a muffle oven and the test was repeated. For the catalytic test, the rhodium impregnated washcoat were deposited on a 50 mm long 400 cpsi honeycombs as described for the platinum based catalyst. Prior the coating the slurry was diluted with zirconia in order to achieve a final metal loading of 0.3 g/l on each honeycomb. The washcoat loading was 35 g per litre honeycomb for all catalysts.

Table 13: Reaction conditions

CO	C_3H_6	NO_x:	O_2:	CO_2	N_2	Temperature	GHSV
1.5 vol%	110 ppm	2000 ppm	1 vol%	10 vol%	balance	450-250 °C	70 000 h^{-1}

The conversion as a function of the temperature plot of the simultaneous conversion of the pollutants over the three catalysts is shown in Figure 34.
In this experiment, the order of reactivity differs from the order given for the oxidation of hydrocarbons and CO over platinum based catalyst. In contrast to the results reported in the chapters 4.2 and 4.3 the catalytic activity is not the highest over the catalyst with the highest dispersion (RhB(Air)) but over the argon calcined sample with an average cluster size of 12 nm (determined by XRD line broadening). The RhB(Ar) catalyst has the lowest LOT of all catalysts tested and for all pollutants of interest. The LOTs are 283 °C, 281 °C and 286 °C for CO, NO and propylene, respectively, whereas the LOTs are 300 °C, 289 °C and 302 °C (again

CO, NO and propylene) over the air calcined catalyst with the smallest clusters. The “state of the art” catalyst with rhodium deposited on zirconia has the poorest catalytic activity towards all the reactants. The light-off temperatures over this catalyst are 317 °C, 314 °C and 318 °C, respectively for CO, NO and propylene.

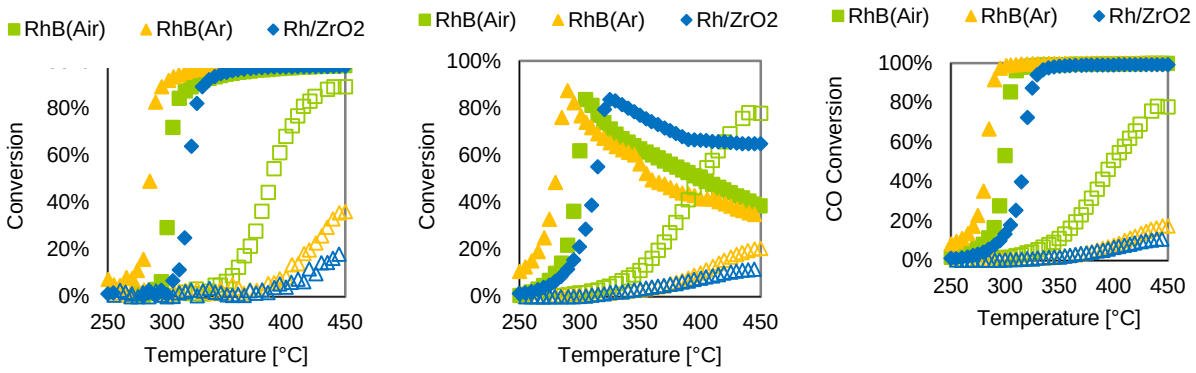

Figure 34: Conversion as a function of the temperature plot for the oxidation of propylene (left), NO (middle) and CO (left). Fresh catalyst full symbols, aged catalyst empty symbols

The impact of the thermal treatment on the three catalysts is shown in Figure 34. It is evident, that the three catalysts react very differently to the thermal treatment. The zirconia based catalyst and the argon calcined zeolite catalyst are strongly deactivated by the thermal treatment and achieve maximum conversions of 17.6 % (CO), 20.5 % (NO) and 36.1 % (propylene) over the latter one and 10.9 % (CO), 11.8 % (NO) and 18.0 % (propylene) over the Rh/ZrO_2 catalyst, respectively. In contrast to this, the RhB(Air) catalyst exhibits an improved stability towards thermal aging. The light-off temperatures are shifted by 99 K, 106 K and 81 K, to 399 °C, 404 °C and 383 °C for CO, NO and propylene, respectively.

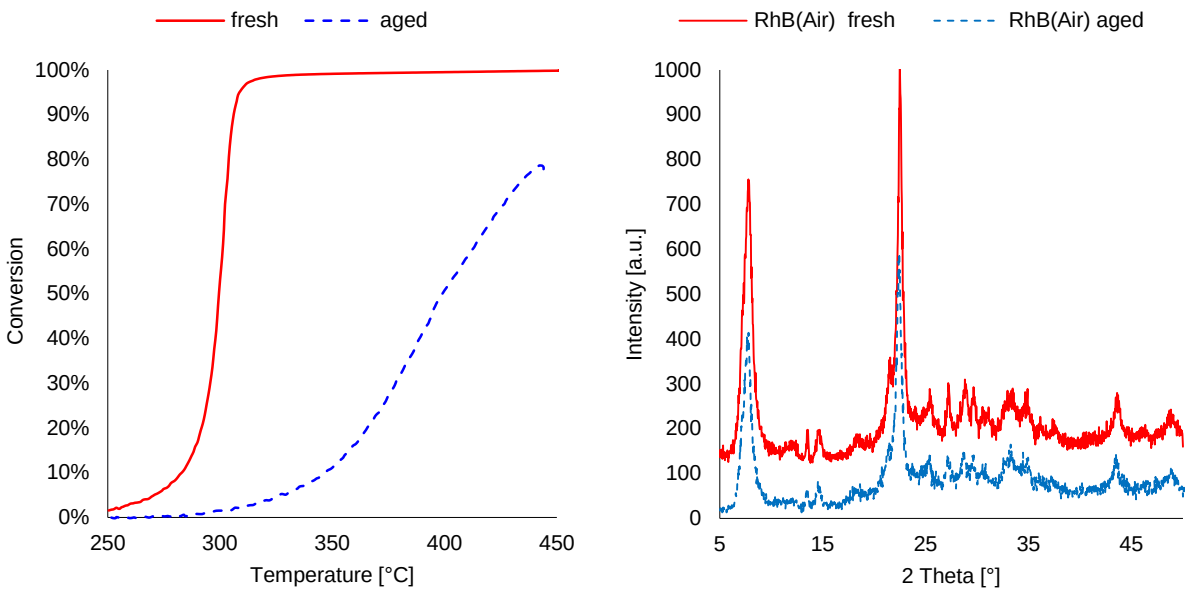

Figure 35: Deactivation of RhB(Air):CO Conversion as a function of the temperature plot (left) and XRD (right)

In Figure 35 the deactivation of the RhB(Air) is shown. The XRD pattern reveals that the deactivation of the catalyst is not caused by sintering of the noble metal, since no reflexions corresponding to bulk rhodium or rhodium oxide occur. The decrease of the reflexion at 7.8 and 22.5 2θ to approximately 60 % of the original value are due to structural changes in the zeolite which are responsible for the lower activity of the aged catalyst. This is further confirmed by the changes of the conversion as a function of the temperature plot.

4.5. Discussion

The developed catalyst synthesis favours the formation of platinum and rhodium nanoclusters located within the pore structure of zeolites as discussed in chapter 3. The influence of the particle size, distribution and interactions with the support will be discussed in this chapter. The reactivity of the different catalysts towards propane, ethylene, CO and NO differs for each educt and they will therefore be discussed separately. Moreover, the reactivity and thermal stability of the rhodium based catalysts for the reduction of NO and simultaneous oxidation of propylene will be discussed.

4.5.1. Case study I: Influence of structural and electronic properties on the reactivity and thermal stability

In the first case study, the reactivity and thermal stability of the developed catalyst were studied and compared to a commercial catalyst. The improved reactivity and increased thermal stability will be correlated to the platinum cluster size and distribution on the zeolite. Moreover the stabilizing effect influence of the zeolitic support will be discussed here.

Propane oxidation:

The light-off temperatures for the oxidation of propane follows the order:

$$Pt(Air) << EnviCat2520 < PtEA < Pt(Ar) \qquad \textbf{eq. 10}$$

Whereas, the cluster size decreases in the order of increasing activity. The influence of the cluster size on the oxidation of propane was investigated by Garetto et al. [91]. They reported a linear increase of the reactivity with decreasing clusters size for the oxidation of propane over Pt/Al_2O_3 catalysts. This correlates to the results found in this work. However, not only the cluster size has to be taken into consideration, but also the support material used. The surface area and the acid properties of the support are the crucial parameters that influence the catalytic properties. Garetto et al. [91] first reported a drastic enhancement of the turnover frequencies if zeolites instead of oxide carriers are used for the oxidation of aliphatic HC. They reported that the turnover rates are two orders of magnitude higher over acidic Pt/H-zeolites than over Pt/Al_2O_3. Nevertheless, they found a drastic increase by using a non-acid zeolite like KL instead of Pt/Al_2O_3, which has the same acid site concentration and strength as the alumina. Therefore it was concluded, that the effect of an increased surface area is more important for the reactivity of the catalyst than the acid properties of the zeolite. Again these results are comparable with the results found in this work. The EnviCat2520 with the lowest dispersion has the lowest propane combustion activity. The activity is clearly increased if the platinum is deposited on a high surface alumina as in case of the PtEA catalyst. The activity is further increased if an acid zeolite is used, with the propane oxidation activity of the PtB(Air) catalyst being an exception. This catalyst has a comparable cluster size as the EnviCat2520 and nearly the same acidity as the PtB(Ar) catalyst.

The cluster size and distribution in the zeolite influences the electronic structure of the platinum clusters and as a result of this, its catalytic activity. It is generally agreed, that the catalytic activity of supported platinum is improved by the acid strength of the support.

Yazawa et al. [33, 34], Ishikawa et al. [32] and Gelin et al. [20] reported this effect for the oxidation of propane over various metal oxides platinum catalyst. Yazawa et al. [34] correlated the adsorption frequency of CO, linearly adsorbed on platinum clusters which were deposited on various carriers, with the acid strength of the support and the propane conversion. MgO has the lowest adsorption frequency (~2050 cm^{-1}) resulting in the lowest conversion whereas the highest adsorption frequency (~2080 cm^{-1}) was found for Pt/SO_4-ZrO_2 [34], the catalyst with the highest propane conversion. From these results, they concluded, that the variations in the catalytic activity depend on the differences in the electronic structure of the platinum caused by the electronegativity of the support. Platinum on acid support materials is less oxidized than on basic materials, resulting in a higher oxidation resistance and therefore the oxidation to less active species such as PtO and PtO_2 is suppressed. For both PtB catalysts, the shift of the CO frequency is even more pronounced than over Pt/SO_4-ZrO_2 [33]. The adsorption band of linear bonded CO is shifted to 2099 cm^{-1} for the PtB(Ar). The interaction between platinum and zeolites (H-ZMS-5) is more complex than the interaction with metal oxides and are described by Treesukol et al. [106]. As in case of acid metal oxides, the interactions with the zeolite carrier lead to an electron withdrawal from the platinum, resulting in an electron deficiency of the clusters. Electron transfer from the metal particles to the Brønsted protons was given as explanation for the electron deficient state of Pt by Sachtler et al. [155]. Nevertheless, Treesukol et al. [106] concluded from their theoretical studies, that besides the Brønsted protons, nearby lattice oxygen is involved in the interactions between the platinum particles and the zeolite. This results in electron redistribution in the Pt-cluster leading to a higher electron density in the s-orbital and a lower density in the d-orbital.

Besides the electronic state of the platinum clusters, influenced by the acidity of the carrier, the surface area and the resulting propane uptake are important factors enhancing the propane oxidation rate as mentioned above. However it could be shown for the PtB(Air) catalyst, that these two parameters can be overcompensated by the distribution of the clusters, since the hydrocarbon can penetrate into the zeolite cavities. Consequently the catalytically active species has to be evenly distributed at the surface of the catalyst. Garetto et al. [91] conclude form their results that the area normalized propane uptake is more significant than the electronegativity of the support. They propose that zeolites provide the possibility of a second reaction pathway. Besides the widely agreed reaction pathway in which the rate determining step of the propane oxidation is the dissociative chemisorption of the alkane over the Pt-species accompanied by the breakage of the weakest C-H bond followed by the interaction

with an oxygen atom adsorbed on adjective sites, they propose an alternative reaction pathway in which the alkane is adsorbed and activated on a surface site in the metal-zeolite interfacial region where it can react with oxygen spilled over from platinum.

CO Oxidation:

In contrast to the clear order of reactivity given for the oxidation of propane which (PtB(Ar) > PtEA > EnviCat2520 >> PtB(Air)), the reactivity of the catalysts for the oxidation of CO can be splitted into two groups. The first group contains the small cluster catalysts and the second one the catalysts with big clusters. Both small cluster catalysts, the PtB(Ar) and the PtEA catalyst, have similar activity for the oxidation of CO which clearly differs from the performance of the EnviCat2520 and the PtB(Air) catalysts (large clusters). The two latter catalysts show the typical light-off curves known for platinum based oxidation catalyst, with a strong S-shape. At low temperatures the reaction is self-inhibited by CO, resulting in low conversion. The light-off region, in which the reaction rate increases rapidly from 10 % conversion to nearly its maximum, is in a very narrow temperature range of 10 K. Finally, there is the high temperature region, where the conversion is high and the surface coverage with CO is low [156]. In contrast to the well-known shape of the reaction profile of the EnviCat2520, the PtB(Ar) and PtEA catalyst show a completely different behaviour. The conversion increases nearly linear from 100 °C to 130 °C. At temperatures exceeding 135 °C (70 % conversion) this increase is reduced, indicating a limitation by transportation of the educt molecules. The self-poisoning by carbon monoxide is reduced on smaller clusters in the low temperature region and the activation of oxygen is more pronounced on these clusters. This difference can again be explained by the different electronic structure of the catalyst and the educt molecules. As explained in chapter 3.2.2, the bond strength of CO adsorbed on platinum is sensitive to the electron density of the platinum. The electron transfer in small electron deficient clusters is less pronounced than in the bigger and therefore electron rich clusters. The transfer results in a weakening of the σ-bond between Pt and the carbon atom of CO and a stronger stretching of the CO π-bond, leading to a transition state closer to the product molecule CO_2. Additionally, as detailed in the discussion of the propane oxidation, oxygen species adsorbed on electron deficient clusters are more active in the oxidation of propane and CO than oxygen on large clusters. However, support effects such as surface area and the acid sites need further investigations.

Oxidation of ethylene:

The order of reactivity for the ethylene oxidation differs from the order of reactivity of propane oxidation. As for the oxidation of propane, the reaction rate is the lowest for the PtB(Air) catalyst. The PtB(Ar) catalyst has medium activity but considerably lower than that of the two alumina based catalysts PtEA and EnviCat2520. An apparent increase of the reaction rate with increasing cluster size is discussed in several publications [11, 156-158]. In all these publications it is postulated that increased activity of the bigger clusters is the result of easier activation of oxygen on those clusters. Further, the absorption of ethylene or generally of unsaturated hydrocarbons is more preferred on the smaller clusters than the adsorption of oxygen, leading to the self-inhibition of the oxidation on smaller clusters. This is in line with the differences in the electronic structure discussed previously. However, if the cluster-size exceeds approximately 10 nm an ongoing increase in size does not further affect the reactivity of the catalyst. This explains the difference between the PtB(Ar) (~3 nm) and the two alumina based catalyst which have the same activity but differ in their particle size (10-20 nm for PtEA and 250 nm for EnviCat2520).

Thermal stability:

For industrial application the resistance against thermal deactivation and poisons is as important as the initial activity of a catalyst. To understand the influence of the matrix stabilization of the nanoclusters, the developed PtB(Ar) catalyst is compared with the commercial EnviCat2520. In Figure 21 and Figure 22 the thermal deactivation of the two catalysts is shown. It is obvious that the matrix stabilization of the nanoclusters can lead to enhanced thermal stability compared to Pt/Al_2O_3 catalysts. Nevertheless, the catalyst deactivates at temperatures exceeding 600 °C, as shown in the XRD pattern (see Figure 26) and the TEM micrographs (see Figure 27). Both reveal the ongoing cluster growth initiated by temperatures above 650 °C. The influence of the progressive cluster growth on the activity of the catalyst is shown in Figure 23 to Figure 25 and in agreement with the discussion above. The conversion of propane is significantly decreased with increasing cluster size, and after being exposed to the highest aging temperature of 700 °C only approximately 10 % of the pollutant is oxidized. The decrease of the catalytic activity can be ascribed to the migration of the small clusters from the internal pore structure of the zeolite to the outer surface and the subsequent coalescence to large particles as indicated by the XRD pattern (Figure 26) and the TEM micrograph (Figure 30). The high temperature treatment is accompanied by a dealumination of the zeolite but does not lead to a structural collapse. In Figure 25 the influence of the thermal treatment towards the CO conversion is shown. The light-off

temperature is shifted by 15 K after the catalyst was exposed to 650 °C. The shape of the temperature versus conversion plot is not affected, indicating that the deactivation of the catalyst is due to the loss of active sites as discussed in chapter 1.3.3. This is in line with the XRD pattern and the TEM micrographs, which clearly reveal the extensive cluster grow and migration towards the surface of the zeolite crystallite at a thermal treatment at 650 °C. In contrast to the oxidation of CO and propane, the reactivity of ethylene is less affected by the thermal aging of the catalyst. As discussed in the previous section, the oxidation of ethylene is favoured on clusters exceeding 10 nm. Therefore, the loss of active sites seems to be partly compensated by the higher reactivity of the larger clusters.

In addition, to the thermally induced change of the cluster size, the zeolite starts to be dealuminated, which further influences the catalytic activity. Moreover, the high temperature and the dealumination provide the possibility of platinum aluminate formation which also influences the activity of the catalyst by loss of active sites. Although the catalyst starts to deactivate at 650 °C, the incorporation of nanoclusters in the pore system of a zeolite clearly stabilizes the clusters, resulting in an improved thermal stability of the catalyst. The improved thermal stability is ascribed to the electron deficiency of the nano-size clusters and their reduced reactivity towards oxygen since the suppressed reactivity to oxygen retards the formation of inactive and volatile Pt-oxide species.

4.5.2. Case study II: NO oxidation: reactivity, hydrothermal stability and sulphur resistance

In the second case study, the reactivity, hydrothermal stability and sulphur resistance of the developed catalyst were studied and compared to an in-house “state of the art” catalyst. The results for the oxidation of CO and propylene are in line with the results obtained in the first case study, and will therefore not be discussed here any further. Thus, the discussion will be focused on the NO oxidation, the hydrothermal stability and the sulphur resistance of the developed catalyst.

For the oxidation of CO and propylene, the initial light-off temperatures over the Pt(Ar) catalyst are slightly lower than over the reference DOC catalyst. This is in line with the results of the previous experiments discussed above. The initial NO_2 yield of the reference DOC catalyst is higher over the Pt/Siralox catalyst. In literature the reactivity of platinum based oxidation catalyst is correlated to the cluster size. This effect is amongst others discussed by Vaccaro [159] for the conversion of NO over Pt/Al_2O_3 and over Pt/SiO_2 by Jayat [30]. Both

reported a maximum reactivity of the supported clusters at an intermediate cluster size, while small clusters were found to be inactive for the oxidation of NO. This is explained by the abundance of ionic oxygen associated with small oxidized platinum particles (< 2.7 nm). The metallic character of larger platinum particles is increased resulting in atomic oxygen, which is active for the oxidation of NO. The inactivity of the smaller cluster is explained by the irreducibility of the Pt-O due to the strong interaction between oxygen and platinum, resulting in a high number of surface platinum which cannot participate in the reaction. As shown by Wang et al. [160] oxygen is stronger adsorbed on step sites of platinum clusters than on terraces, which leads to relative concentration increases with the cluster size. Additionally, the lower activity of larger clusters is related to the low reducibility of these clusters by Vaccaro et al. [159]. Jayat et al. [30] studied the reactivity of platinum particles with a cluster size from < 3 nm to 23 nm on silica and found an optimal cluster size between 4.1 and 6.6 nm with the lowest light-off temperature and a maximum conversion of NO to NO_2 of 60%. For bigger clusters, the light-off temperatures are reported to be increased with a simultaneous decrease of the maximal NO_2 yield.

The results obtained by Vaccaro et al. [159] and Jayat et al. [30] are in line with the results obtained in this thesis and the initial activities of the two catalysts compared here can be explained with the activity dependency on the cluster size. The PtB(Ar) catalyst comprises relatively small platinum clusters of 2-3 nm, resulting in a lower reactivity for the oxidation of NO to NO_2, compared to the reference DOC catalyst. Hydrothermal aging and sulphur poisoning increase the light-off temperatures for the oxidation of propylene and CO over both the PtB(Ar) and the reference DOC catalyst in the same manner. The effect of sulphur poisoning is more pronounced for the PtB(Ar) catalyst. In contrast to this, the oxidation of NO over the PtB(Ar) is less affected. The maximum NO_2 yield is decreased from 50 % to 37 % whereas only 23 % yield is achieved over the reference DOC catalyst. From these results in can be concluded that after the hydrothermal treatment the initially homogeneous platinum dispersion on both catalysts has changed to a bimodal dispersion with bigger clusters which are known to be less effective for the NO oxidation and smaller clusters still existing after the hydrothermal aging. Overall, the deactivation is more pronounced over the reference DOC catalyst than over the zeolite based catalyst. The enhanced stability of the zeolite based catalyst can be explained by the incorporation of Pt into the pore structure of the zeolite and the electronic deficiency of the clusters as discussed previously. The bimodal dispersion and distribution of clusters is also shown to behave differently in the reactivity towards CO and propylene, and NO. Sulphur poisoning further decreases the reactivity over both catalysts,

while the NO oxidation is not affected by the sulphur addition. This shows that both catalysts consist of two different platinum species. The first consists of larger clusters which are responsible for the CO and propylene oxidation, and which are further affect the sulphur poisoning. The second species consists of small cluster that effectively oxidize NO and are not affected by SO_2 addition. The encapsulation in the zeolite stabilizes the small clusters at higher concentration than on the high surface Al_2O_3 support, resulting in improved thermal stability.

4.5.3. Case study III: Rhodium based catalyst for three way catalysis

The catalytic activity of the rhodium based catalyst is somewhat different to the reactivity of the platinum based catalysts. This is caused by the different chemistry of rhodium compared to the chemistry of platinum and palladium. Among the main differences are the lower ionisation potential, resulting in a more oxidized surface, most probably as Rh_2O_3 in excess of oxygen. As discussed by Yao et al. [29] the formation of Rh_2O_3 results in a negative reaction order towards oxygen and a positive reaction order with respect to olefins. This is in accordance with the catalytic results shown in Figure 34, where the argon calcined, rhodium based catalyst has the lowest light-off temperatures for CO, NO and propylene under slightly oxidising atmosphere. This is due to the composition of the catalyst which contains a certain amount of Rh^0-clusters which are highly active for the conversion of CO and olefins under rich conditions. The air calcined, rhodium based zeolite catalyst has medium activity due to the formation Rh_2O_3 during the calcination procedure which is equivalent to strong oxygen adsorption and resulting in a reduced reactivity. Figure 34 shows that the situation of the aged catalysts clearly differs from the fresh ones. The RhB(Ar) catalyst as well as the Rh/ZrO_2 catalyst strongly deactivate after being exposed to air at 900 °C for 1 h. For the air calcined, zeolite based catalyst, the light-off temperatures are significantly increased after the thermal treatment, and nevertheless, good conversion can still be achieved in the temperature range investigated. The XRD pattern shown in Figure 35 reveals that the structure of the rhodium clusters is not changed and no sintering occurs, but that the reduced catalytic activity is caused by a collapse of the zeolite structure as shown by the reduction of the corresponding reflexes. The activation energy for the oxidation of CO over the fresh catalyst is ~70 kJ/mol and drops to ~35 kJ/mol over the aged catalyst. According to the classical theory, the apparent activation energy drops to half of the initial value, if the reaction is limited by pore diffusion [161]. The thermal stability of this catalyst is clearly not dependent on the stability of noble metal as in case of the zeolite platinum based catalyst developed in this work or

published so far but on the stability of the zeolite support. The reason for the remarkably high thermal resistance under oxidising atmosphere might be due to the "Zeolite-Al_2O_3-$RhAlO_4$-Rh_2O_3" structure discussed in chapter 3.4 but needs to be further investigated.

4.6. Conclusions

In this thesis, a new approach for the synthesis of precious metal containing zeolite catalyst had been developed. The synthesis route comprises the incipient wetness impregnation of the zeolite with precious metal complexes with electron withdrawing ligands, preferably sulphite and nitrate, followed by calcination at temperatures of 800 °C, whereas the gas atmosphere was found be crucial for the success of the synthesis. The synthesis results in a zeolite based catalyst which is characterized by a high concentration of noble metal nanoclusters exclusively located in the pores system of the carrier.

4.6.1. Synthesis and catalytic performance

The developed platinum zeolite can be prepared by a fast and cheap incipient wetness impregnation of the zeolite support with strongly adsorbing platinum precursors such as platinum sulphite acid or platinum dinitrate (see Figure 15). Wide pore zeolites with a low silica/alumina ratio such as BEA-35 are the preferred supports, but it is also possible to vary the zeolite structure (see Figure 16). For BEA-35 the synthesis method provides the possibility to load the zeolite with up to 6 wt% of platinum. If other zeolites such as MFI or a higher Si/Al ratio are used, the amount of platinum has to be reduced. The incipient wetness impregnation is followed by inert gas calcination at temperatures suitable to decompose the precursor used. For platinum sulphite acid, the calcination is carried out at 800 °C to ensure complete decomposition. In case of a less robust precursor such as $Pt(NO_3)_2$ lower temperatures might be sufficient (see Figure 15). This is the first easy and fast preparation method for platinum nanoclusters in a zeolite matrix and differs from other methods by the amount of platinum which is located in the zeolite matrix. Other methods achieve lower concentrations and require more time consuming preparation methods.

The nanoscale clusters have unique catalytic properties, which is a result of the electron deficiency of these clusters. Among those properties the thermal stability and sulphur resistance have to be highlighted, especially for the oxidation of NO to NO_2.

Besides the above-mentioned platinum clusters, the same synthesis route provides the possibility to introduce palladium and platinum/palladium clusters into a zeolite matrix (see Figure 16), Hutt et al. [110] and Wanninger et al. [162]. Additionally, a new Rh-zeolite

material was developed by using rhodium sulphite solution for the incipient wetness impregnation followed by calcination at 800 °C. This material consists of highly active high temperature resistant nanoclusters.

4.6.2. Industrial relevance

The most apparent industrial application of the platinum based zeolite catalytic material is its application as Diesel oxidation catalyst. The high temperature resistance, the sulphur tolerance and especially the (hydro-) thermal stability of the NO oxidation make this catalytic material a promising candidate for this application. In addition to these properties, the high concentration of active metal on a material which is used as a hydrocarbon-trap allows to use of only one component in the DOC instead of a catalytically active component and a material to store hydrocarbons. This simplifies, and thereby, reduces the cost for the production of diesel oxidation catalysts.

Moreover, the developed Pt catalyst shows nearly no thermal deactivation up to 600 °C, which is a clear improvement compared to the catalysts on the market.

The developed rhodium impregnated catalyst is stable even up to 800 °C under oxidizing conditions and thus, a promising new material for three-way catalysis.

5. Kinetic considerations

5.1. Introduction

The fundamental of any chemical reaction is its kinetics. The kinetics of a given reaction describes the correlation between the reaction rate and the various reaction parameters, such as temperature, pressure and educt concentration, and in case of a catalysed reaction, the concentration and the kind of catalyst used. In most of the catalytic applications, a solid catalyst is used and the reactants are in gas or liquid phase. If the system consists of different phases, as it is the case in heterogeneous catalysis, the rate of the reaction may be influenced by film diffusion. To be converted, the reactant has to be first transported from the surrounding gas phase to the outer surface of the catalyst and then, as in case of zeolites, through the transport pores (macro pores) to the catalytically active site in the reaction pores (meso and micro pores). Consequently, convection and diffusion occur in parallel with the reaction. Interface gradients confine the diffusion within the catalyst particle to the local reaction sites; therefore, pore diffusion occurs in addition to the reaction. Consequently, the overall measurable reaction rate depends on the kinetics of the reaction (micro kinetics) itself but also on the kinetics of the film diffusion (macro kinetics).
For any catalytic reaction, the following physical and chemical steps have to occur:

1. Diffusion from the gas phase through the laminar boundary layer to the surface of the washcoat (film diffusion)
2. Diffusion of the educts through the porous network of the washcoat and support to the active sites of the catalyst (pore diffusion, including macro, meso and micro pores)
3. Adsorption of the educts on the active sites
4. Catalytic conversion
5. Desorption of the products
6. Diffusion of the products through the porous network (pore diffusion)
7. Diffusion from the catalyst surface through the laminar boundary layer to the gas phase (film diffusion)

Steps 1 and 7 represent the film diffusion, which depends on the conditions of the feed and the geometry of the honeycomb. The steps 2 and 6 correspond to the pore diffusion which primarily depends on the size and shape of the pores, the reactants and the products. The third, fourth and fifth step are related to the reaction itself and the active sites, as well as the

interactions of the reactants, products and the active material. The overall reaction rate might be either limited by the diffusion or the catalytic conversion or it is determined by both processes. The influence of the micro and macro kinetics will be discussed in the following chapter.

5.1.1. Micro kinetics

The IUPAC definition of the reaction rate of a catalyzed reaction is:

$$r = \frac{1}{v_i} * \frac{dn_{Educt}}{m_{cat} * dt} \qquad \textbf{eq. 11}$$

Where is *r* is the reaction rate, v_i is the stoichiometric coefficient of the component i, m_{cat} is the mass of the catalyst, *n* the amount of the educt and *t* the time.
For the total oxidation of a hydrocarbon the rate is given as:

$$r = \frac{k}{m} * c_{O_2}^m * c_{HC}^n \qquad \textbf{eq. 12}$$

Where *k* is the rate constant, m the mass of the catalyst and *c* is the concentration of the hydrocarbon and the oxygen. The reaction order of the reactants is given by *m* and *n*. For a large excess of air, it is assumed that the rate is independent of the concentration of air and therefore n = 0 and eq. 12 can be simplified to

$$r = \frac{k_{(n)}}{m} * c_{HC}^n \qquad \textbf{eq. 13}$$

For further simplification but on the cost of accuracy, it can be assumed that the reaction rate is first order (n=1) in the HC concentration and eq. 14 is derived.

$$r = \frac{k_{(1)}}{m} * c_{HC} \qquad \textbf{eq. 14}$$

The rate constant k of the reaction depends on the reaction temperature, which is given by the Arrhenius equation (eq. 15).

$$k = k_0 * e^{-E_A/RT} \qquad \textbf{eq. 15}$$

With these equations, the kinetic parameters such the rate constant and the activation energy can be calculated from the experimentally obtained data.

To maximize reaction rates, it is essential to ensure accessibility of all the reactants to the active sites in the internal porous network of the catalyst which can be achieved by using a large pore support, which on the other hand, results in a reduction of the catalytically active surface and therefore in a loss of activity. Therefore, the structure of the support has to be optimized for each reaction. In general, diffusion processes have a small temperature dependency (low activation energy). For this reason, diffusion controlled processes can easily be distinguished from chemical controlled reaction (strong temperature dependency and high activation energy).

The simplest method to get an idea of the rate limiting step of the reaction is the determination of the activation energy by using the Arrhenius equation (eq. 15):

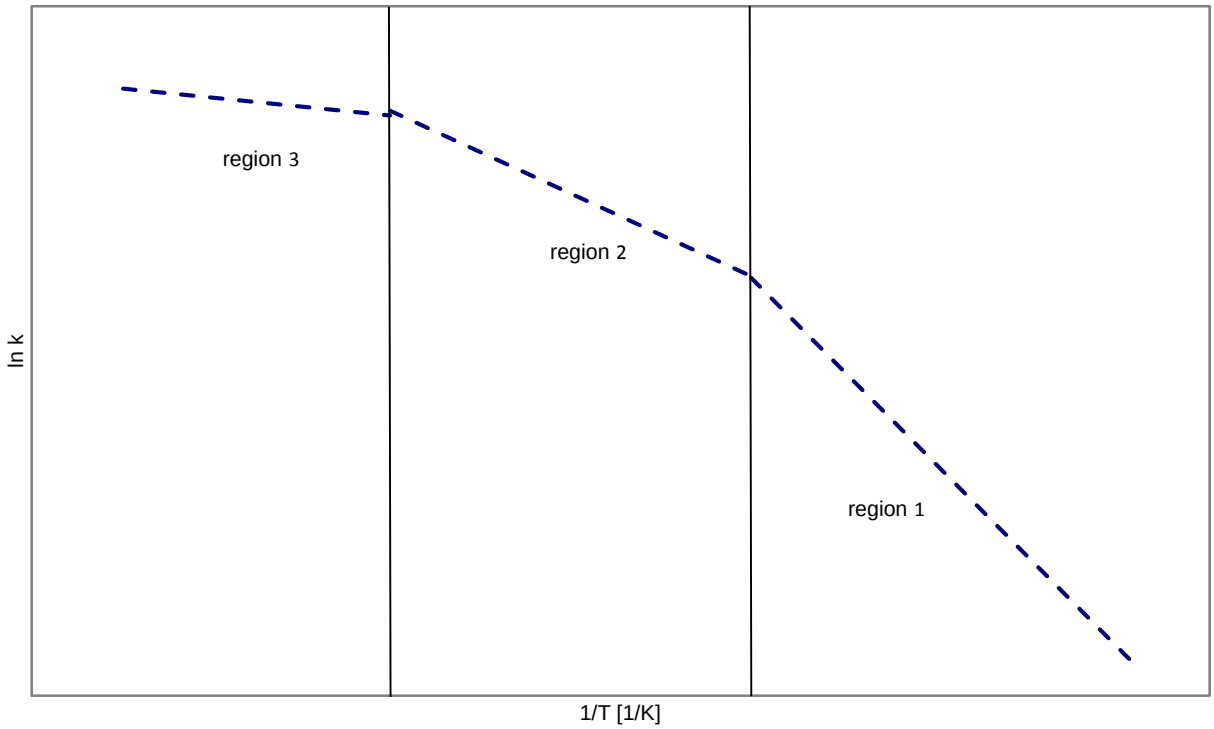

Figure 36: Typical Arrhenius plot

By taking the natural logarithm of the Arrhenius equation and plotting ln k vs. 1/T, a straight line is obtained, whose slope represents the activation energy as shown in Figure 36. In the chemical controlled regime (region 1) the slope gives the activation energy of the reaction. In

the pore diffusion controlled regime (region 2), the apparent activation energy drops to half of the initial value. For limitation by boundary layer diffusion (region 3) the apparent activation energy only is 5 to 10 kJ/mol [46].

5.1.2. Transport limitation

Diffusion effects become dominant and the intrinsic kinetics of the catalyst will not be determined accurately, if experiments are carried out at too high diffusion length or too narrow pores. As a consequence, the activation energy will decrease as pore diffusion and film diffusion become significant.

Mass transport limitation in the honeycomb

A simple model for the approximation of the influence of the mass transport in honeycombs is given by Farrauto [46]:

$$Fractional\ conversion = 1 - e^{-(\frac{N_{Sh}(a/\varepsilon)L}{N_{Sc}N_{Re}})} \quad \textbf{eq. 16}$$

With a the geometric surface area, ε the void fraction of the honeycomb, L the length of the honeycomb and the dimensionless numbers N_{Sh} (Sherwood number), N_{Sc} (Schmidt number) and N_{Re} (Reynolds number):

$$N_{Sc} = \frac{\mu}{\rho * D} \quad \textbf{eq. 17}$$

$$N_{Re} = \frac{\rho * u * d_{ch}}{\mu} \quad \textbf{eq. 18}$$

$$N_{Sh} = 2 * Re^{0.5} * Sc^{0.5} * \left(d_{ch}/L\right)^{0.5} \text{ [161]} \quad \textbf{eq. 19}$$

Where μ is the dynamic viscosity, ρ the density, D the mass diffusivity, d_{ch} the channel diameter, L the length of the channel, and u the mean velocity of the gas.

With eq. 16, the maximum conversion and the influence of the diffusion limitation for a given coated honeycomb catalyst under certain conditions can be estimated.

Film diffusion:

When a reaction is limited by the diffusion through the boundary layer, the educt gas concentration decreases in the film between the fluid and the surface of the washcoat and is constant in the washcoat layer. This is the so called film diffusion and occurs for example at high gas velocities and large pores in the washcoat, or if the reaction is fast in comparison to the diffusion process (region 1 in Figure 36). For such processes, the concentration of the reactant is almost zero at the outer surface of the washcoat. This scenario is illustrated in Figure 37.

Diffusion in porous materials:

The diffusion of the reactant gas molecules in a porous material might have strong effect on the efficiency of a catalyst since the concentration of the reactant gases might be limited by transport processes from the feed to the active surface.

The influence of the transport limitations on the gas concentration in the solid catalyst is shown in Figure 37. In the case 1) the diffusion of the educt gas is only marginally limited by the boundary layer and the washcoat and can be considered as not to be influenced by transport processes. This situation correlates to the region one shown in the Arrhenius plot.

Since various pores exist in a washcoat layer, the diffusion might either be limited by the diffusion (region 2 in Figure 36) through the pores in the washcoat (interparticular diffusion) or by the diffusion in the pores of the porous material (intraparticular diffusion) as shown by 2) and 3) in Figure 37. In the first two cases, the concentration decreases in the washcoat layer, indicating the reaction of the educt gases with the outer surface of the zeolite particles. In case of a very dense washout layer or a highly porous washcoat material, such as in case of zeolites, the reaction might be limited by pore diffusion.

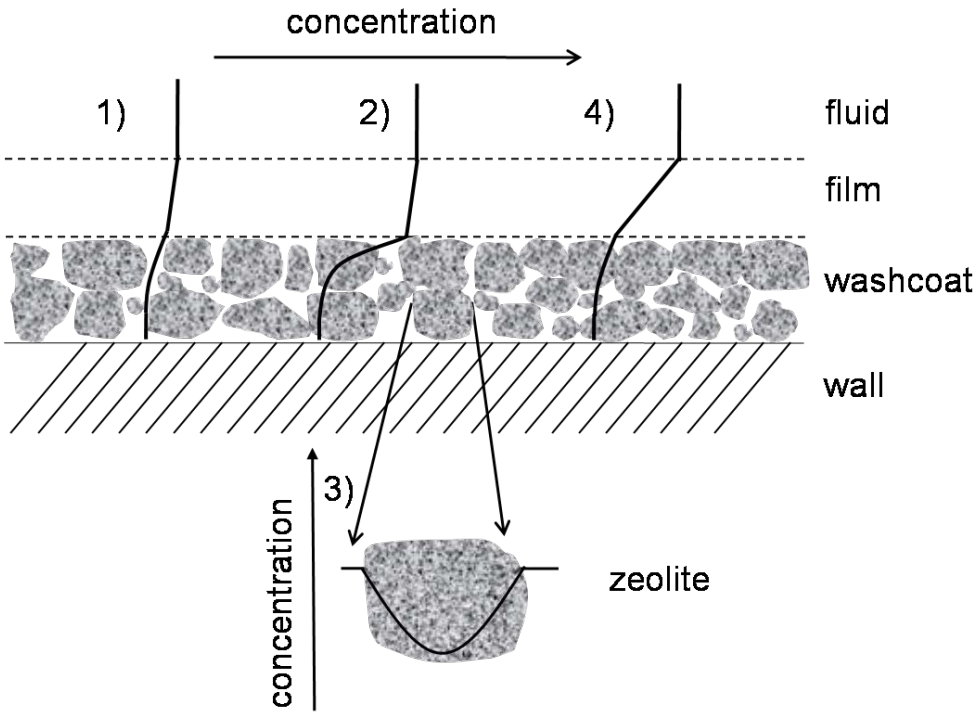

Figure 37: Decrease of the educt concentration in different diffusion regimes

In a real system the all these effects might occur in parallel and affect the efficiency of the catalyst since the transport of the educts might be slower than the rate of the reaction.

The diffusion in a porous material strongly depends on the pore diameter d_p and the mean free path of the molecule λ. In accordance to the pore diameter the pores are defined as micro pores, meso pores and macro pores (see Table 14). The different diffusion regimes are listed in Table 15.

Table 14: Definition of pores [163]

	Pore diameter
Micro pores	< 2 nm
Meso pores	2-50 nm
Macro pores	> 50 nm

Table 15: Diffusion regimes [163]

Molecular Diffusion	$\lambda << d_p$
Knudsen Diffusion	$\lambda > 10\ d_p$
Configurational Diffusion	$\lambda >> d_p$; 0.3 nm < d_p< 1 nm

Molecular diffusion:

If the mean free path of the molecule is small compared to the pore diameter, the free molecular diffusion is dominant and the binary diffusion coefficient can be calculated with the equation derived by Fuller et al. [164].

$$D_{AB} = \frac{T^{-1,75}\left(1/M_A + 1/M_B\right)^{0,5}}{p[(\Sigma_A v_i)^{1/3} + (\Sigma_B v_i)^{1/3}]^2} \qquad \textbf{eq. 20}$$

Where T is the temperature, p the pressure, M the molecular mass and v_i special diffusion parameters given in the mentioned publication.

In a porous material the geometry of the pores has to be considered and the formula is extended by the porosity ε and the tortuosity τ. The effective diffusion coefficient can be calculated the following formula:

$$D_{AB,eff} = \frac{\epsilon}{\tau} * D_{AB} \qquad \textbf{eq. 21}$$

Knudsen diffusion:

In smaller pores, when the mean free path of the molecule is longer than the diameter of the pores, the probability of a collision between a molecule and the carrier is higher than the probability of a collision between two gas molecules. This phenomenon is the so called Knudsen diffusion. The effective Knudsen diffusion coefficient is calculated by the following equation:

$$D_{Kn,eff} = \frac{\varepsilon}{\tau} * D_{Kn} = \frac{\varepsilon}{\tau} * \frac{d_p}{3} * \sqrt{\frac{8RT}{\pi M_i}} \qquad \textbf{eq. 22}$$

Where d_p is the pore diameter.

Diffusion in the transient region:

Both diffusion phenomena might occur either in parallel or at the same time. The resulting effective diffusion coefficient might be estimated by eq. 23. The comparison of the of $D_{P,eff}$ with D_{AB} and $D_{Kn,eff}$ provides the possibility to identify the dominant diffusion regime.

$$D_{P,eff} = \frac{\varepsilon}{\tau} * D_P = \frac{\varepsilon}{\tau} * \frac{1}{{}^{1}\!/_{D_{AB}} + {}^{1}\!/_{D_{Kn}}} \qquad \textbf{eq. 23}$$

Configurational diffusion:

The factors which govern intracrystalline diffusion are very important for the discussion of molecular sieve catalysts. Zeolites present a particular kind of diffusion, which deviates from the classical molecular and Knudsen diffusion regimes, precisely because of the similitude of sizes between the molecules and the pores of the catalysts [79]. This diffusion regime was named by Weisz as configurational diffusion [165]. One unique feature of this diffusion regime is the sensitivity of the diffusion coefficient towards changes of the ratio of the molecular size to pore size. Small variations in this ratio molecular size to pore size can lead to drastic changes in the diffusion coefficient. The typical configurational diffusion coefficients are between 10^{-9} and 10^{-13} cm^2*s^{-1} [163]. The following equation (eq. 24), proposed by Xiao and Wei [166], allows the estimation of the configurational diffusion coefficient D_{cd}.

$$D_{cd} = \frac{1}{z} * \left[\frac{8kT}{\pi M}\right]^{\frac{1}{2}} * \alpha * exp\left(\frac{-E_d}{RT}\right) \qquad \textbf{eq. 24}$$

Where z is the coordinate number and α is the distance between adjacent occupancy sites. In Configurational diffusion the movement of the molecules is restricted by the energy barrier E_d posed by the walls [167]. According to Xiao and Wei [166], the type of diffusion is dependent of the dynamic diameter of the molecule (d_m) and the diameter of the channel pore (d_p). They define the parameter λ as the ration of d_m to d_p. And give a transient region from Knudsen to configurational diffusion at $0.6 < \lambda < 0.8$ form MFI at 300 K.

5.1.3. Interaction of pore diffusion and chemical reaction

The apparent kinetic parameters might be influenced by transport phenomena as discussed before. Such problems occur, if the reaction is faster than the transport of the educt molecule towards the active site. Since the pore diameters of zeolitic pores are rather small, the diffusion process is quite slow and therefore the reaction might be limited by the transportation of the educts.

Quantification of the interactions between pore diffusion and chemical reaction

For a theoretical approach, a cylindrical single pore can be used. It is assumed that the catalyst is in steady state condition, which means, that there are no changes with respect to time in the concentration, temperature and no radial gradients. Therefore, the difference in the

concentration at the inlet and at the outlet can be ascribed to the catalytic reaction on the mantle area of the pore.

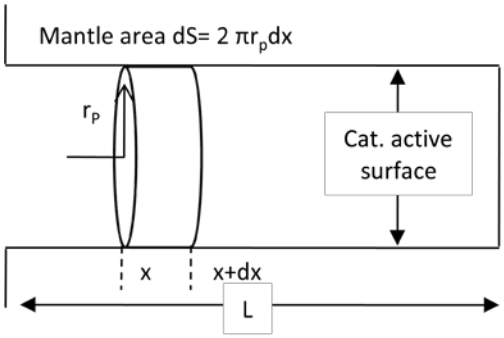

Figure 38: Quantification of the interactions between pore diffusion and chemical reaction (drawn in accordance to [163])

$$\frac{d_{n1}}{d_t} = 0 = -D_{eff}\pi r_p^2 \frac{dc_1}{dx} - \left[-D_{eff}\pi r_p^2 \left(\frac{dc_1}{dx} + \frac{d^2c_1}{dx^2}\right)\right] - r_s dS \qquad \textbf{eq. 25}$$

Where r_s is the reaction rate correlated to the surface of the pores, r_p is the pore radius and dS is the differential mantle area of the pore.

In case of a reaction, where $r_s = k_s * c_i$ and the introduction of the dimensionless values $c_1/c_{1,s}$ und x/L eq. 25 results in:

$$0 = \frac{d^2\left({}^{c_i}/_{c_{i,s}}\right)}{d\left({}^{x}/_{L}\right)^2} - L^2 * \frac{2k_s c_{1,s}}{r_p D_{eff} c_{1,s}} \left(\frac{c_i}{c_{i,s}}\right) \qquad \textbf{eq. 26}$$

Where

$$\Phi = L * \sqrt{\frac{2k_s c_{1,s}}{r_p D_{eff} c_{1,s}}} \qquad \textbf{eq. 27}$$

Φ is the so called Thiele modulus, which describes the ratio between the reaction rate and the pore diffusion. In case of a first order reaction the Thiele modulus can be simplified to:

$$\Phi = L * \sqrt{\frac{k}{D_{eff}}} \qquad \textbf{eq. 28}$$

To calculate the concentration profile along the entire length of the pore, the differential equation (eq. 27) has to be solved with the following boundary conditions:

For x/L = 0 → $c_1/c_{1,s} = 1$,

For x/L = 1→ $c_1/c_{1,s} = c_{1,L}/ c_{1,s}$ and $d(c_1/c_{1,s})/d(x/L) = 0$

The following result is obtained:

$$\frac{c_1}{c_{1,s}} = \frac{\cosh[\Phi(1 - x/L)]}{\cosh \Phi} \qquad \textbf{eq. 29}$$

for a first order reaction. To calculate the effective reaction rate $r_{s,eff}$ the local reaction rate $r_s(x)$ has to be averaged over the pore length and results in:

$$r_{s,eff} = k_s \frac{\tanh\Phi}{\Phi} c_{1,s} \qquad \textbf{eq. 30}$$

Since the Thiele modulus describes the correlation of the reaction rate and the pore diffusion it can be used to calculate the pore usage of the catalyst, which is defined as [163]:

$$\eta = \frac{k_s \frac{\tanh \Phi}{\Phi} c_{1,s}}{k_s c_{1,s}} = \frac{\tanh\Phi}{\Phi} \qquad \textbf{eq. 31}$$

Determination of the diffusion coefficient:

The diffusion coefficient can be experimentally determined by plotting the logarithm of the reaction constant versus the inverse temperature (Arrhenius plot). According to the classical theory, the activation energy is only half of the intrinsic value if the reaction is influenced by pore diffusion. The diffusion coefficients can be determined by plotting two lines (in the pore diffusion regime and the kinetic regime). At the intersection of these two lines, the Thiele modulus approaches unity. This fact can be used to determine the effective diffusivity of the reactant in the porous network of a zeolite [161] with eq. 27 and eq. 28.

5.2. Determination of the kinetic parameters

5.2.1. Catalysts and test procedure

In the previous chapter, the advantages of the incorporation of nanoscale precious metal clusters in the porous system of a zeolite was discussed and compared to "state-of the art" catalysts. Among these advantages are the improved thermal and hydrothermal stability as well as the increased resistance against sulphur poisoning, especially regarding the oxidation of NO to NO_2.

In this chapter, the kinetic parameters of the PtB(Ar) catalyst will be determined and compared to those of the reference catalysts. The PtB(Air) catalyst was not further investigated due to its poor catalytic performance, resulting in no industrial interest.

To determine the kinetic parameters of these catalysts, the concentrations of the different educt gases (propane, ethylene, CO) and oxygen as well the temperature were varied as listed in Table 16. To ensure, that the structure of the precious metal clusters and therefore its performance are not affected by the catalytic test, all catalysts were aged at 550 °C for 12 h prior the tests. For the PtEA catalyst the aging temperature was 450 °C and the catalyst was tested in a temperature range not exceeding this temperature to ensure, that the high platinum dispersion is not affected and the influence of the noble metal dispersion on the reaction can be determined.

Table 16: Test condition for the determination of the kinetic parameters

	Concentration [ppm]	Temperature [°C]
Propane	100→200 (20 ppm steps)	500→350
Ethylene	1000→600 (200 ppm steps)	160→100
CO	1000→600 (200 ppm steps)	160→100
Oxygen	20.5 vol%→ 5 vol% (5 % steps)	500→350

The GHSV was 150 000 h^{-1}.

5.2.2. Results

Propane:

To derive the catalytic parameters for the oxidation of propane, the conversion for different educt concentrations is plotted against the average temperature of the catalysts. The comparison of the three different catalysts is shown in Figure 39.

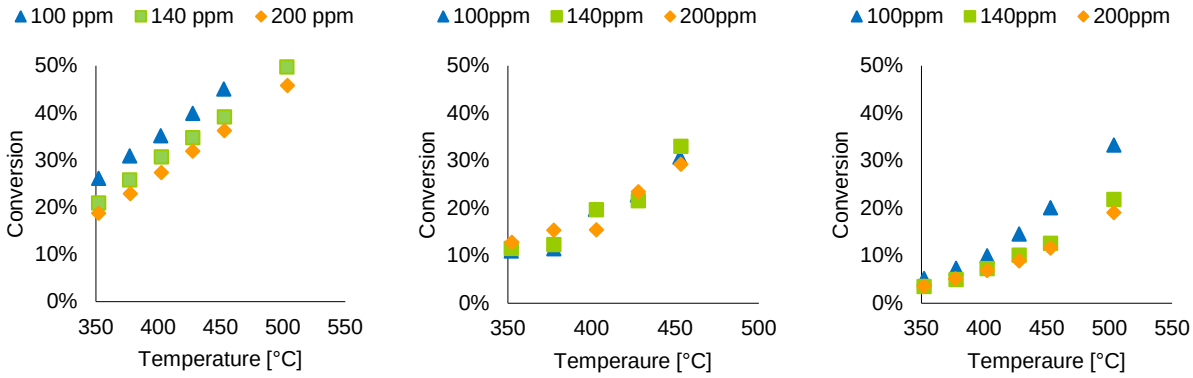

Figure 39: Conversion as a function of the temperature plots for the oxidation of propane over PtB(Ar) (left), PtEA (middle) and EnviCat2520 (right).

The propane conversion over the PtB/(Ar) catalyst is strongly dependant on the concentration and is decreased from 26 % to 18 % if the concentration of propane is increased from 100 ppm to 200 ppm at 350 °C and from 55 % to 46 % at 550 °C. In case of the PtEA catalyst, the conversion is only slightly affected by the increase of the propane concentration, whereas the catalytic activity of the EnviCat2520 increases with decreasing pollutant concentration. From these data, the rate of the reaction is calculated for each temperature. The order of the reaction is determined by plotting then the logarithm of the rate against the logarithm the average concentration. The slope of the straight line corresponds to the order of the reaction as described in 5.1.1. In Figure 40 the plots for the different catalysts at the different temperatures are shown.

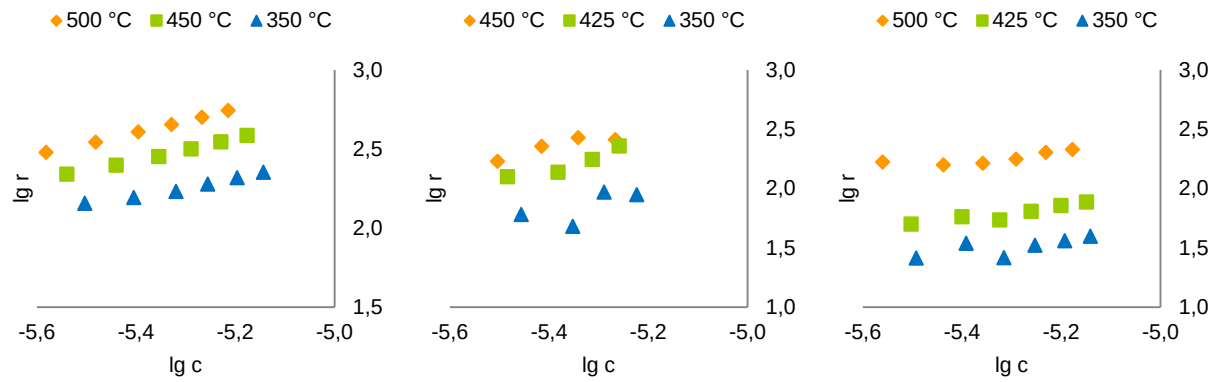

Figure 40: Determination of the reaction order for the oxidation of propane over PtB(Ar) (left), PtEA (middle) and EnviCat2520 (right).

For the PtB(Ar) catalyst, the order of the reaction increases from 0.56 to 0.72 with increasing temperature. In case of the EnviCat2520, the order of the reaction depends only slightly on the temperature and increases from 0.67 to 0.74. Contrary to this, the order of the reaction over the PtEA catalyst is independent of the temperature and is 0.92.

The rate constant $k_{(n)}$ of the reaction is calculated according to eq. 12. In Figure 41 the logarithm of $k_{(n)}$ is plotted against the inverse temperature to gain the activation energy and $k_{(0)}$ according to the Arrhenius equation. For simplification it was assumed that the reaction was independent of the oxygen concentration since oxygen was present in huge excess.

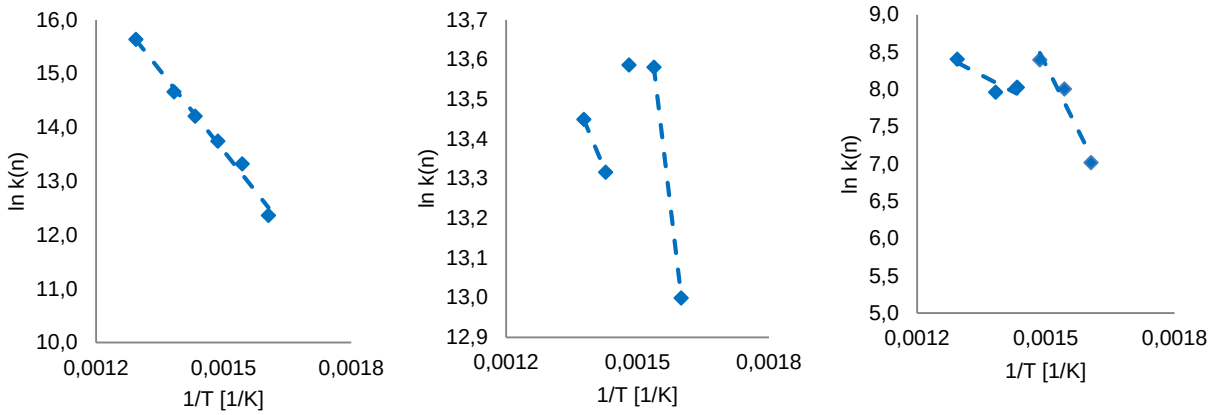

Figure 41: Arrhenius plots for the oxidation of propane over PtB(Ar) (left), PtEA (middle) and EnviCat2520 (right).

In Table 17 the activation energies, the rate constants and the turnover frequencies (TOF)[3] of the three different catalysts are listed. The turnover frequency is calculated for the conversion of 100 ppm propane at 450 °C.

Table 17: n- order kinetic parameters of the oxidation of propane (calculated according to eq. 13)

	E_A [kJ/mol]	$k_{(0)}$ [$(mol^{(n-1)}*(m^3)^n/s)$]	TOF [s^{-1}][4]
PtB(Ar)	83	$7.0*10^5$	$1.7*10^{-2}$
PtEA (425-450 °C)	22	$7.5*10^0$	$1.1*10^{-2}$
PtEA (350-400 °C)	77	$3.4*10^5$	
EnviCat (450-500 °C)	25	$3.4*10^5$	$8.8*10^{-3}$
EnviCat (350-450 °C)	96	$5.7*10^{-2}$	

Carbon monoxide and ethylene:

The kinetic parameters for the oxidation of carbon monoxide and ethylene were determined in the same manner as described for the oxidation of propane. The temperature versus conversion plots for the two educt gases over the different catalysts are shown in Figure 42.

[3] The turnover frequency is defined as the amount of educt gas molecules converted per amount of precious metal per second [s^{-1}]. If not mentioned otherwise the TOF is calculated from the maximum conversion obtained during the experiment for the individual catalyst.

[4] Determined at 450 °C and 100 ppm propane

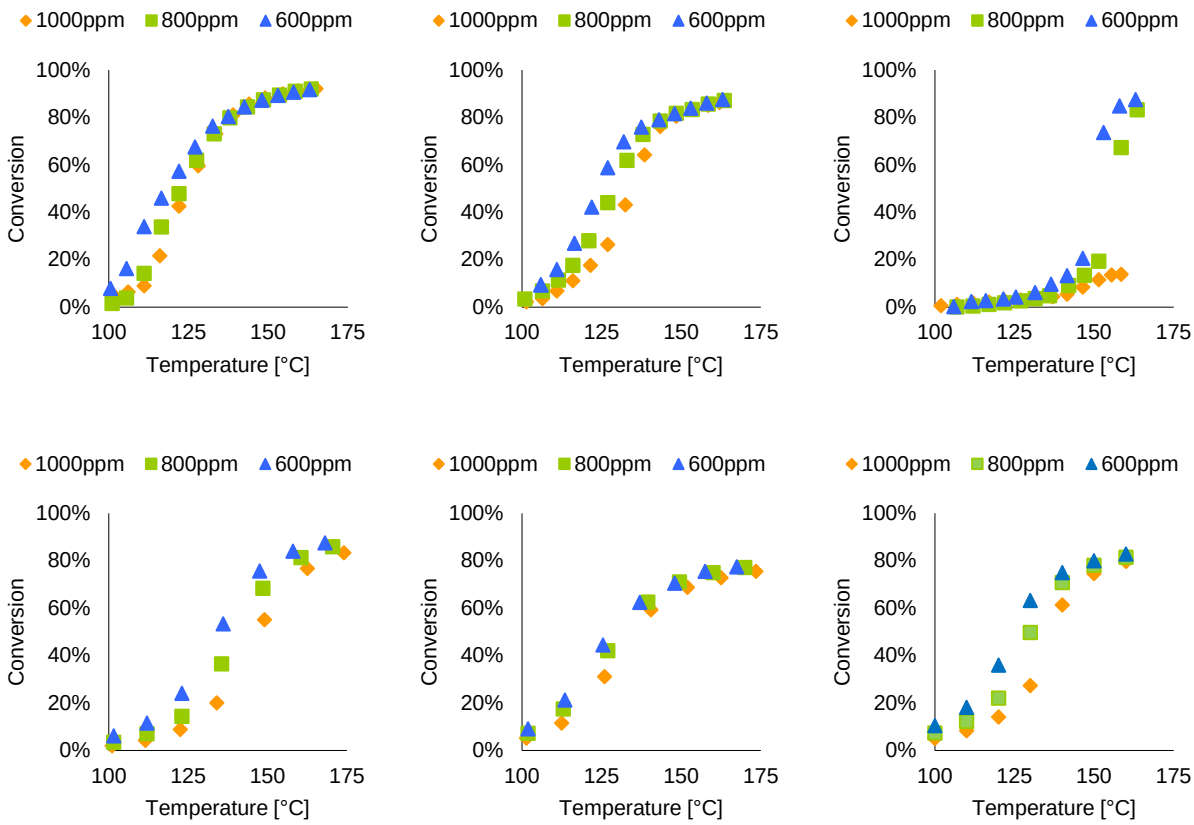

Figure 42: Conversion as a function of the temperature plots over PtB(Ar) (left), PtEA (middle) and EnviCat2520 (right). Upper row: oxidation of CO, lower row: oxidation of ethylene

All of the catalysts tested are sensitive to the educt gas concentration. The light-off temperatures (Table 18) are shifted to higher temperatures if the educt concentration is increased. The light-off temperatures show, that the PtB(Ar) catalyst is the most active catalyst for the oxidation of carbon monoxide for all concentration and is least influenced by the changes of the CO concentration since the light-off temperature has the smallest increase if the concentration is risen from 600 ppm to 1000 ppm. The PtEA catalyst has medium activity and the LOT is shifted by 12 K. The EnviCat2520 has the poorest oxidation activity concerning the oxidation of CO. The reaction is ignited at 150 °C, if 600 ppm CO is in the feed. If the concentration is raised to 1000 ppm a maximum conversion of 14 % is achieved at 160 °C.

Table 18: Light-off temperatures for the oxidation of CO and ethylene

	CO 600 ppm	CO 1000 ppm	C_2H_4 600 ppm	C_2H_4 1000 ppm
PtB(Ar)	118	125	145	160
PtEA	122	134	129	137
EnviCat2520	150	n.a.	125	136

For the oxidation of ethylene, the order of reactivity of the catalysts is inverse compared to the oxidation carbon monoxide. The EnviCat2520 has the lowest light-off temperatures of 125 °C and 136 °C for 600 ppm and 1000 ppm, respectively, whereas the most active CO oxidation catalyst has the highest light-off temperature in case of the ethylene oxidation. The oxidation of 600 ppm ethylene is ignited at 145 °C and shifted by 15 K if the concentration is increased to 1000 ppm.

For both of the oxidation reactions, the order of the reaction strongly depends on the temperature of the catalyst (Figure 43). Generally, the reaction order is negative at lower temperatures and turns to positive if the temperature is increased. In case of the oxidation of CO over the PtB(Ar) and PtEA catalyst the reaction orders are calculated to be -0.5 and -0.75 over PtB(Ar) and PtEA catalyst, respectively. For the oxidation over the PtB(Ar) catalyst the order of the reaction becomes positive at ~117 °C whereas ~125 °C are required over the PtEA catalyst. Over the PtB(Ar) catalyst, the order approaches one at 135 °C whereas 140 °C are needed over the PtEA catalyst. The situation for the EnviCat2520 is different compared to the two other catalysts. In case of the EnviCat2520, the reaction order is close to zero for temperatures between 100 °C and 125 °C. Above 125 °C, only the two lower CO concentrations are considered in the calculation of the reaction rate since the experiment with the highest concentration is not ignited. At 160 °C the reaction order is 0.7 for the oxidation of CO over the EnviCat2520.

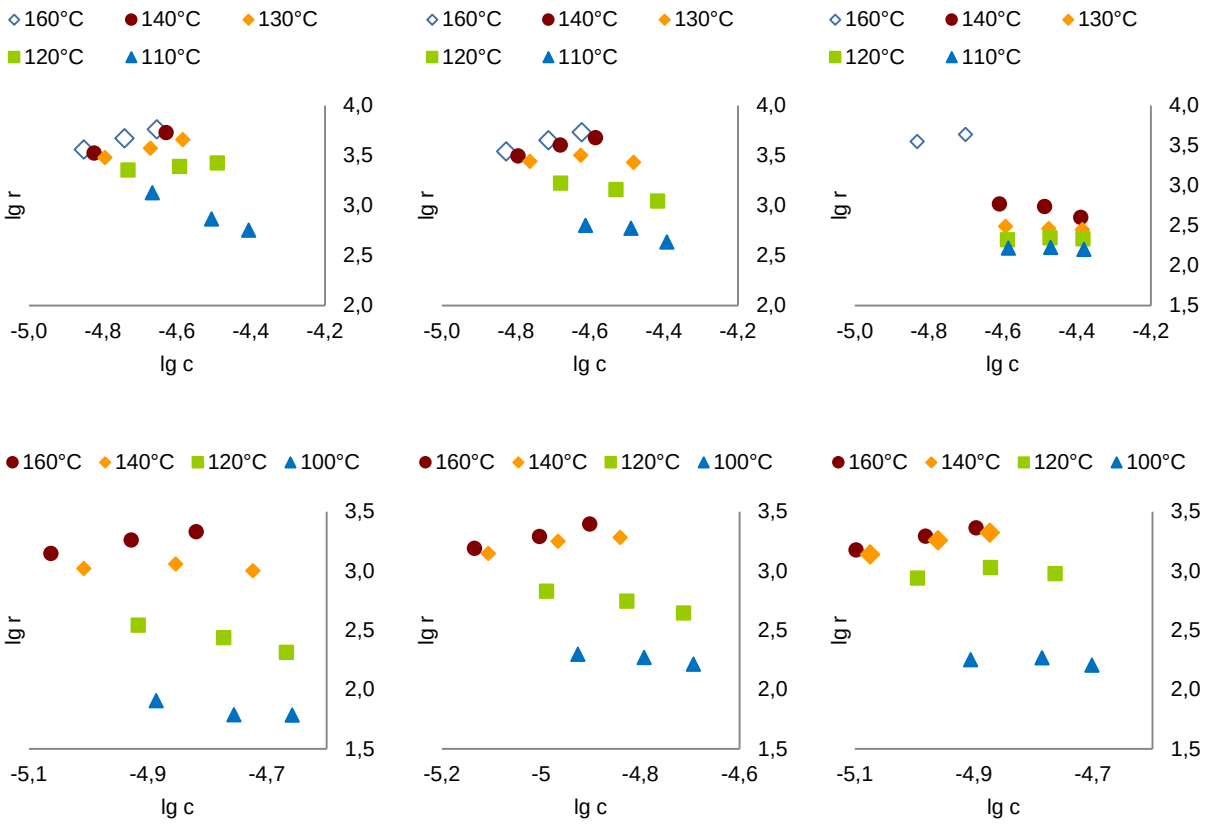

Figure 43: Determination of the reaction order for the oxidation of CO over PtB(Ar) (left), PtEA (middle) and EnviCat2520 (right). Upper row: oxidation of CO, lower row: oxidation of ethylene

The situation for the oxidation of ethylene is different compared to the oxidation CO. For the oxidation of ethylene, the reaction order is negative over the PtB(Ar) catalyst and the EnviCat2520 at lower temperatures for all concentration. In case of the platinum zeolite the order is -0.6 between 100 °C and 130 °C and approaches 0.75 at 160 °C. Over the EnviCat2520, the order is -0.5 at temperatures of 120 °C and below and becomes 0.9 at the final temperature.

The change of the reaction order over the PtEA catalyst is more sensitive compared to the two other catalysts. Considering all three concentrations, the order increases from 0.72 to 0.92 with increasing temperature. In the temperature range between 100 °C and 120 °C the rate changes with the ethylene concentration. The rate is positive, if calculated from the results of the two lower concentration (600 ppm and 800 ppm) and raises from 0.14 to 0.74. Contrary to this, the reaction order calculated from the experiments with the higher concentration (800 ppm and 1000 ppm) is -0.3.

The negative orders of the reactions indicate that at low temperature, the kinetics of the oxidation is influenced by adsorption processes of either oxygen or ethylene. Additionally, the results are also influenced by uncertainties of the test unit. Especially the results at low

conversion and small temperature changes are uncertain. Therefore, the activation energy is calculated at higher temperatures, at which reasonable amounts of the educt molecule are oxidised. The determination of the activation energy at elevated temperatures, where reaction rate increases rapidly within a very narrow temperature range results in doubtful results, what have to be considered in the interpretation. However, the Arrhenius plots, assuming first order, for the two oxidation reactions over the different catalysts are shown in Figure 44.

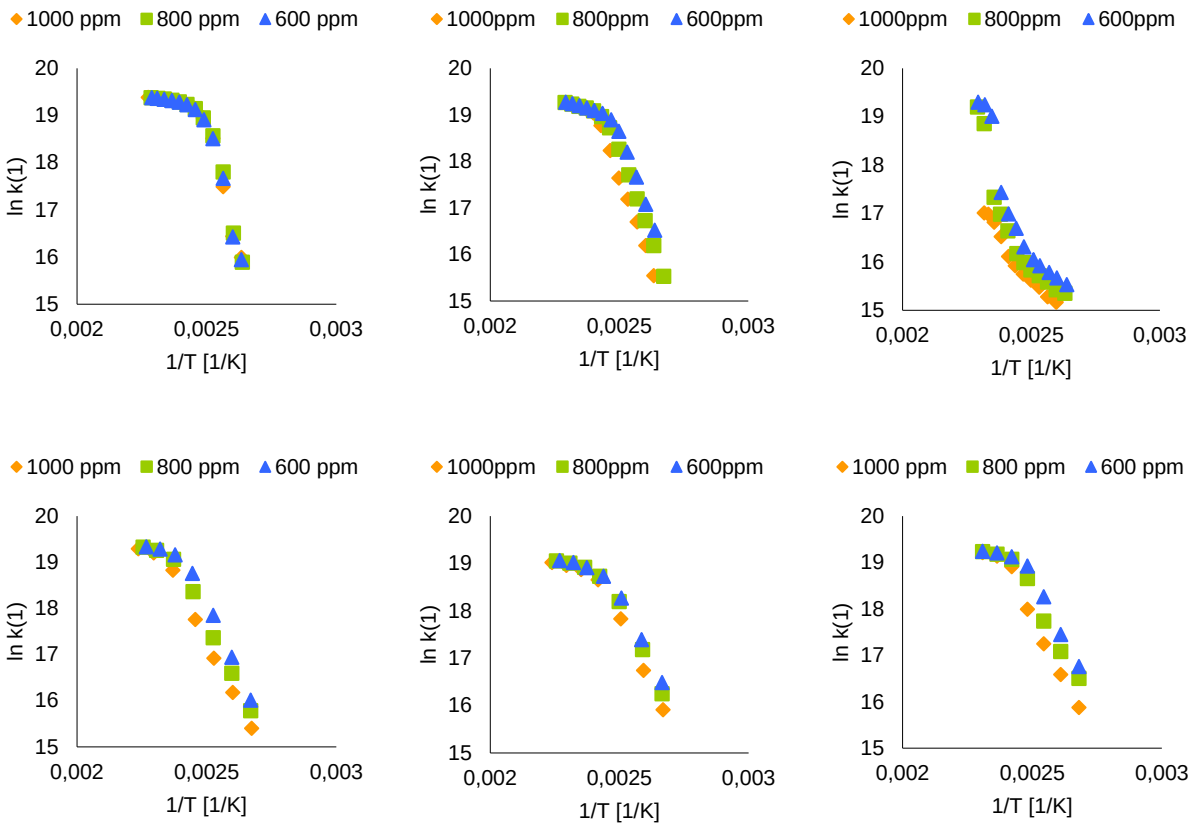

Figure 44: Arrhenius plots for the oxidation of CO over PtB(Ar) (left), PtEA (middle) and EnviCat2520 (right). Upper row: oxidation of CO, lower row: oxidation of ethylene

For the determination of the kinetic parameters, a compromise between the adsorption phenomena at low temperatures and the sudden increase of the conversion has to be found. A temperature range between 125 °C and 135 °C for PtB(Ar), 110 °C and 120 °C for PtEA and between 105 °C and 115 °C in case of the EnviCat2520 were used for the calculation of the kinetic parameters of the CO oxidation.

For the ethylene oxidation, a temperature range from 120 °C to 140 °C was chosen for the EnviCat2520 and the PtB(Ar) catalyst. For the calculation of the data for the PtEA the temperature range could be lowered to 110 °C to 130 °C, since the adsorption effect seems to be less pronounced compared to the other catalyst.

The first order reaction constant $k_{(1)}$ (eq. 14), including the adsorption as well as the kinetics of the reaction is calculated. These results are summarized in Table 19 for the CO oxidation and Table 20 for the oxidation of ethylene. The obtained values for the CO oxidation are in line with the data reported in literature e.g. by Yao [29] for the CO oxidation over platinum based catalysts. For the EnviCat2520 fairly low activation energies and values of k are determined.

Table 19: First order kinetic data for the CO oxidation (calculated according to eq. 14)

CO [ppm]	PtB(Ar)			PtEA			EnviCat2520		
	E_A [kJ/mol]	$k_{(0)}$ [m³/s]	TOF [s^{-1}]	E_A [kJ/mol]	$k_{(0)}$ [m³/s]	TOF [s^{-1}]	E_A [kJ/mol]	$k_{(0)}$ [m³/s]	TOF [s^{-1}]
1000	123	$4.8*10^{17}$	$3.0*10^{-1}$	120	$6.5*10^{16}$	$2.9*10^{-1}$	40	$2.8*10^{8}$	$5.1*10^{-2}$
800	102	$1.0*10^{15}$	$2.7*10^{-1}$	131	$3.0*10^{18}$	$2.4*10^{-1}$	35	$3.0*10^{8}$	$2.4*10^{-1}$
600	112	$1.8*10^{16}$	$2.7*10^{-1}$	129	$2.4*10^{18}$	$1.9*10^{-1}$	34	$1.8*10^{8}$	$1.9*10^{-1}$

The calculated activation energies for the oxidation of ethylene, are in the rage reported in other studies, ranging from ~30 kJ/mol to ~110 kJ/mol as summarized by Ackelid and Peterson [158]. They concluded that the apparent activation energy and the rate constant strongly depend on the ethylene concentration, which is also indicated by the results obtained in this work, where the most active catalyst has the highest apparent activation energy.

Table 20: First order kinetic data for the ethylene oxidation (calculated according to eq. 14)

C_2H_4 [ppm]	PtB(Ar)			PtEA			EnviCat2520		
	E_A [kJ/mol]	$k_{(0)}$ [m³/s]	TOF [s^{-1}]	E_A [kJ/mol]	$k_{(0)}$ [m³/s]	TOF [s^{-1}]	E_A [kJ/mol]	$k_{(0)}$ [m³/s]	TOF [s^{-1}]
1000	84	$8.3*10^{11}$	$1.5*10^{-1}$	91	$1.1*10^{13}$	$1.1*10^{-1}$	112	$7.1*10^{15}$	$1.4*10^{-1}$
800	73	$5.3*10^{10}$	$1.2*10^{-1}$	78	$3.1*10^{11}$	$1.1*10^{-1}$	90	$1.3*10^{13}$	$1.2*10^{-1}$
600	59	$1.0*10^{9}$	$9.1*10^{-2}$	75	$1.5*10^{11}$	$8.2*10^{-2}$	59	$1.5*10^{9}$	$8.8*10^{-2}$

Influence of the oxygen concentration on the oxidation of propane:

The reaction rate does not only depend on the hydrocarbon concentration but is also influenced by the oxygen concentration. For lean conditions the conversion of the VOC is limited by the amount of oxygen available for the oxidation. In excess of oxygen (rich conditions), the oxygen might strongly adsorb on the catalysts surface, resulting in a hindrance of the VOC adsorption. This poisoning effect of the oxygen is for example described by Arnby et al. [156, 168] and Carlson [169]. Both studied the influence of the oxygen concentration towards the reaction rate for the oxidation of propane at the transition region from lean to rich conditions and found that the highest conversion can be achieved under stoichiometric oxygen concentration. In this study the influence of higher oxygen concentrations, between 20 % and 5 %, is investigated. The oxygen concentrations were

chosen in the range, as they typically occur in the oxidation of VOCs. The oxygen concentration was varied from 20 % down to 5 % in 5 % steps. The influence of the oxygen concentration on the propane conversion is studied by the oxidation of 180 ppm propane in the feed. The oxygen to propane ratio is calculated with eq. 32, reaching from 55 to 222 under the reaction conditions chosen. The oxygen conversion is calculated by the oxidation of propane. In Figure 45, the oxygen conversion versus the average temperature in dependency of the oxygen concentration over the three catalysts is plotted.

$$S = \frac{[O_2]}{5[C_3H_5]} \qquad \textbf{eq. 32}$$

The catalysts tested show nearly the same behaviour towards the changes of the oxygen concentration. For high oxygen concentration (20 % and 15 %) the differences are marginal. The oxygen consumption is slightly increased by the reduction of the concentration from 15 % to 10 % and clearly increased if the concentration is decreased from 10 % to 5 %. The increase of the oxygen conversion is most pronounced over the PtB(Ar) catalyst and least pronounced over the EnviCat2520.

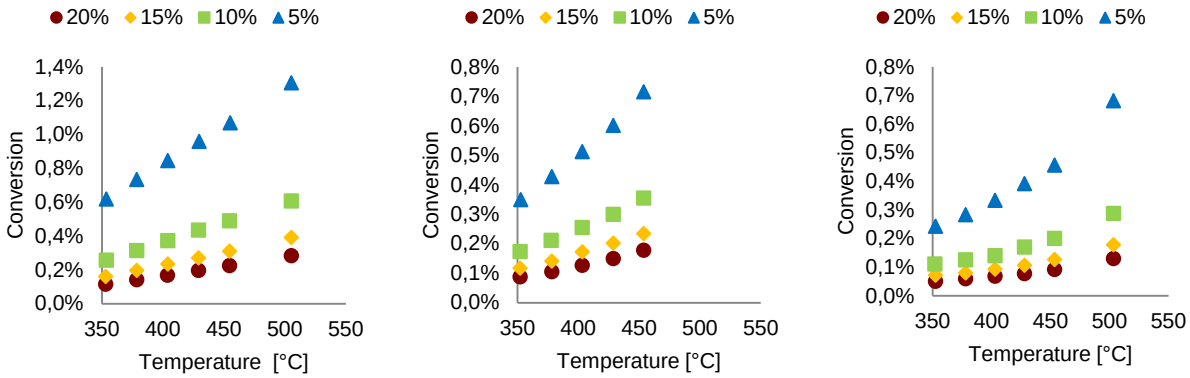

Figure 45: The conversion of oxygen[5] over PtB(Ar) (left), PtEA (middle) and EnviCat2520 (right)

The reaction orders are calculated as described above and they were found to be independent of the temperature but strongly dependent on the oxygen concentration. Considering the two highest concentrations the reaction order is 0 to -0.1 for all catalysts.

[5] Calculated based on the conversion of 180 ppm propane

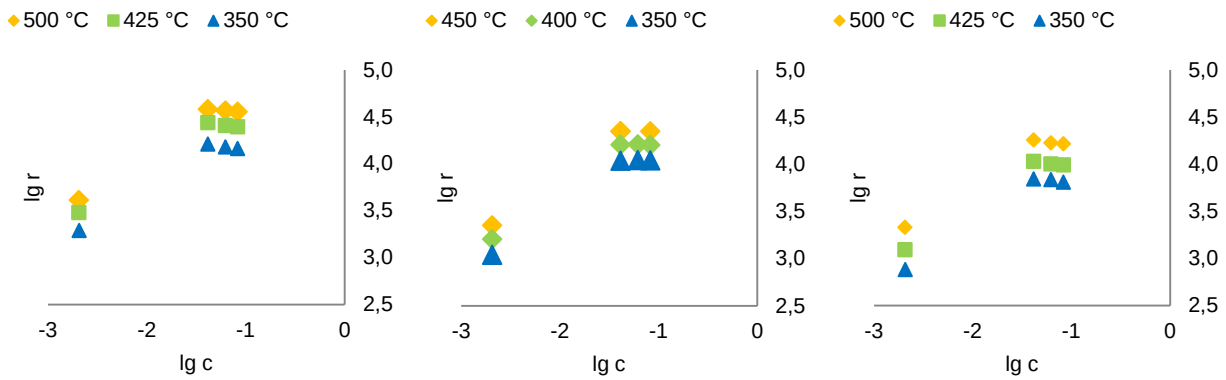

Figure 46: Determination of the reaction order for the conversion of oxygen over PtB(Ar) (left), PtEA (middle) and EnviCat2520 (right)

Contrary to the slightly negative order at higher concentration, the reaction order is positive at lower oxygen concentrations. The order over all catalysts is calculated to be ~0.75 for 5 and 10 % oxygen, respectively.

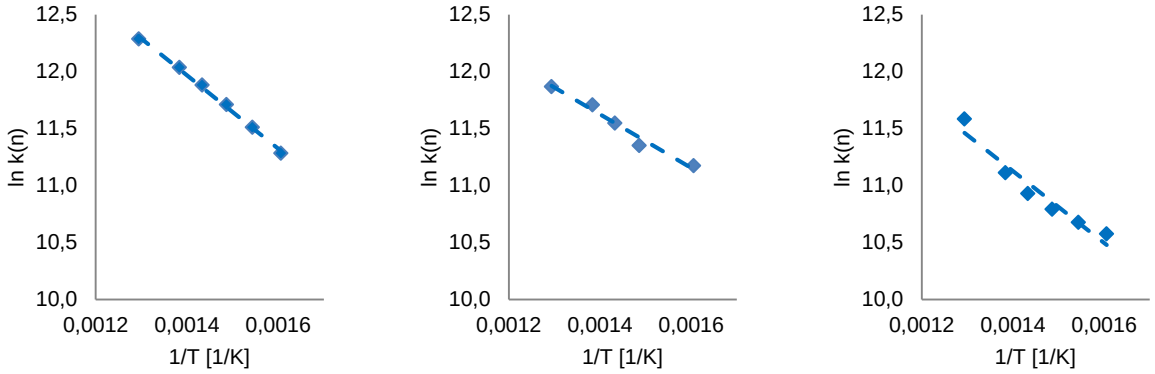

Figure 47: Arrhenius plot for the conversion of oxygen, PtB(Ar) (left), PtEA (middle) and EnviCat2520 (right)

The activation energies, the rate constants and the turnover frequencies for oxygen are calculated are summarized in Table 21.

Table 21: Kinetic parameters for the conversion of oxygen calculated by the oxidation of 180 ppm propane (calculated according to eq. 13)

	E_A [kJ/mol]	$k_{(0)}$ [$(mol^{(n-1)}*(m^3)^n/s)$]	TOF [s^{-1}]
PtB(Ar)	28	5.2	1.54
PtEA	23	1.5	1.22
EnviCat2520	19	$4.7*10^{-1}$	0.64

For the calculation of the kinetic parameters for the oxidation of propane, CO and ethylene it is assumed that these parameters are independent of the oxygen concentration. The variation of the oxygen concentration and the results obtained in this experiment show that this assumption is acceptable for high oxygen concentrations since the results obtained for 15 % and 20 % oxygen are nearly identically.

5.2.3. Discussion

The three different catalysts investigated, clearly differ in their reactivity towards the different educt gases. Among the factors influencing the performance are: the platinum particle size which influences the interactions between the catalyst, oxygen and the hydrocarbon. Moreover, the carrier influences the electronic structure of the platinum deposited, influencing the catalyst gas interactions and of course the hydrocarbon which was to be oxidized. These parameters will be discussed in the following chapter.

Propane oxidation:

The kinetic parameters for the oxidation of propane are summarised in Table 17. For the developed PtB(Ar) catalyst, the experimentally obtained data for the activation energy are in line with reported data. For the oxidation of propane activation energies between 72 [170-172] and 105 kJ/mol [173] over alumina based catalysts are reported. Garetto et al. [90, 91] reported activation energies between 88 and 121 kJ/mol over Pt-zeolite catalysts. For the PtEA catalyst and the EnviCat2520 the Arrhenius plot shows unusual characteristics. At low temperatures, the determined kinetic data for the oxidation of propane are in accordance with data reported in literature and comparable to the data obtained for the PtB(Ar) under identical pre-treatment and reaction conditions. At temperatures exceeding 425 °C, the slope in the Arrhenius plot suddenly drops to 20-25 kJ/mol. This is nearly one fourth of the original value and corresponds to the activation energy determined for oxygen. The drop of the activation energy is accompanied by a decrease of the rate constant by 6 orders of magnitude. Such a change in the Arrhenius plot might be interpreted by a change in the reaction mechanism. But the accuracy of the experimental set-up is not precise enough to analyze this phenomenon.

Pre-treatment and cluster size:

It is generally agreed in literature, that the oxidation of propane over platinum based catalysts follows the so called Langmuir-Hinshelwood mechanism, in which both educts are adsorbed on the catalyst. This reaction can be either competitive, if both reactants adsorb on the same active site or non-competitive. This is the case if the reactants absorb on different sites of the catalyst. Contrary to most catalysts studied in literature, the catalysts in this study are not reduced prior the catalytic test but treated in air at 550 °C (PtB(Ar) and EnviCat2520) and 450 °C (PtEA), respectively. Therefore, the platinum clusters are in a partially oxidized state and the degree of the oxidation depends on the cluster size and support of each catalyst. As discussed above, the PtB(Ar) catalyst is more stable towards oxidation as the EnviCat2520. The situation for the PtEA catalyst is different since this catalyst was pre-treated at 450 °C instead of 550 °C to maintain the dispersion. This explains the different initial activity in the oxidation of propane (see Figure 39). In case of the EnviCat2520, the surface is most probably oxidized to PtO whereas the surface of the PtB(Ar) catalyst is only partly oxidized.

As a result of the Langmuir-Hinshelwood mechanism proposed in literature for the oxidation of propane, oxygen can inhibit the oxidation of propane since both educts compete for the same sites on the platinum clusters [171] and the adsorption of oxygen is stronger than the adsorption of propane. This inhibition is even more pronounced if the catalyst is pre-oxidized as in this study. The influence of the cluster size towards the reactivity is an ongoing issue in the discussion [28, 90, 91, 159, 168, 173]. The overall activity of the catalyst depends on the interaction with reactants, oxygen and propane. As mentioned in literature, small platinum particles (< 2 nm) have a high number of unsaturated platinum atoms on the cluster surface, and thus have strong interaction with the oxygen atoms attached. The increase of the reactivity of platinum clusters exceeding a size of 2-3 nm is explained with a decrease of the Pt-O bond strength. An optimum platinum dispersion of 20 % for the oxidation for the oxidation of propane is proposed by Marecot et al. [174]. This is in line with the results obtained in this work, since the PtB(Ar) catalyst consisting of platinum particles of ~3 nm and the PtEA catalyst with a platinum particle size between 10 and 20 nm have comparable activation energies, pre-exponential factors and turnover frequencies which clearly differ from those of the EnviCat2520, that consists of platinum clusters with a cluster size of 250 nm and more. The reaction orders of the PtB(Ar) catalyst and the PtEA catalyst differ slightly and are 0.73 for the PtB(Ar) and 0.67 for the PtEA, respectively. The reaction order for the oxidation of propane over EnviCat2520 was found to be 0.24. This difference in the reaction order over

the catalysts investigated can be interpreted by different reaction mechanism over PtB(Ar) and PtEA on one hand and EnviCat2520 on the other hand.

It is proposed by Radic et al. [28] for the oxidation of hexane and toluene, that the reaction follows a Mars van Krevelen or and Eley-Rideal mechanism, in which the hydrocarbon reacts from the gas-phase or is only weakly adsorbed. The atomic oxygen is chemisorbed on the PM of the catalyst. Most studies conclude that the reactivity of a platinum based catalyst is independent of the dispersion if they exceed a certain size of approximately 2 to 3 nm.

The reaction rate is increased on clusters exceeding this size because the activation energy of the oxygen chemisorption rate is lowered and the Pt-O bond is weakened. This correlates with the results obtained in this work, since no remarkable differences between the PtB(Ar) and PtEA catalyst were found. The situation over the EnviCat2520 with extremely large clusters might be different, especially the reaction order is changed from ~0.7 to 0.2 but no literature studying clusters with this size was available and more detailed studies are necessary to understand the effect of an increase of the cluster size from 3 to 250 nm.

For deeper understanding of the mechanism, especially the nature of the oxygen species adsorbed on the different catalysts and the resulting influence on the reactivity and reaction mechanism more detailed studies are necessary.

Influence of the carrier:

In addition to the platinum distribution and dispersion, the nature of the support and the resulting influence on the activity is discussed in literature. Garetto et al. [90, 91] found a drastic increase of the reaction rate if zeolite supports were used instead of metal oxides. They concluded that, the effect is correlated with an increase of the hydrocarbon uptake which is the highest in case of a zeolite based catalysts due to the higher porosity and surface area compared to the metal oxides used in this study and that other effects such as dispersion and acidity of the support are minor compared to this effect. Increase in the reactivity is found for the PtB(Ar) catalyst at temperatures exceeding ~400 °C (Table 17), whereas the three catalysts have comparable activation energies, pre-exponential factors and turnover frequencies at lower temperatures.

Garetto et al. [90, 91] reported reaction orders of 1 for propane over all catalysts tested and of 0 for oxygen over metal oxide based catalyst, whereas the reaction order with respect to oxygen was found to be -1 in case of zeolite based catalyst. The activation energies reported are between 37 kJ/mol over Pt/MgO and 121 kJ/mol over Pt/BEA, the pre-exponential factors

are $2.93*10^5$ for Pt/MgO and $8.10*10^{17}$ $h^{-1}kPa^{-(1+\beta)}$[6]. The increased activation energy and pre-exponential factor are explained by the negative order with respect to oxygen over the zeolite based catalyst. The reaction order for oxygen for the catalysts investigated herein was found to be 0 to -0.1 (Figure 46) and ~0.7 for propane over PtB(Ar) and PtEA and ~0.2 over the EnviCat2520. The activation energy for the propane oxidation over the PtEA and EnviCat2520 catalyst drops to ~25 kJ/mol with increasing reaction temperature (see Table 17). The activation energy of ~25 kJ/mol corresponds to the activation energy calculated for O_2 (see Table 21), which might indicate that the reaction mechanism has changed over these two catalysts with the increase of the temperature and support the initial assumption of a change in the reaction mechanism from a Langmuir-Hinshelwood mechanism to an Eley-Rideal mechanism in which only the oxygen is dissociatively chemisorbed and the hydrocarbon reacts from the gas phase with the activated oxygen attached to the platinum surface. Since no change in the activation energy is observed in case of the PtB(Ar) catalyst, it might be assumed that in case of this catalyst the reaction mechanism is not affected by the increase of the temperature and that both reactants are adsorbed on the platinum particle. This could be explained by the electron deficiency of the clusters on which the C-H or C-C bond cleavage is more likely than on electron rich clusters.

Carbon monoxide and ethylene oxidation:

The catalytic oxidation of CO and ethylene clearly differ from the oxidation of propane. Contrary to propane, CO and ethylene are σ-donors and at the same time π-acceptors, whereas alkanes are σ-donors. Although CO and ethylene, both have empty π-orbitals, the back-bonding from the metal to the empty π-orbital plays a lesser role in case of ethylene than in case of in CO [175]. In addition to the σ-donation, ethylene can interact with a vacant orbital of the platinum cluster via its occupied bonding π-orbital [175]. The same is true for the oxygen molecule, resulting in strong competition for the same adsorption sites for either oxygen and ethylene and/or CO resulting in self-poisoning in the oxidation of alkenes and CO as reported in many publications [11, 156-158, 168, 176] The effect of competitive adsorption is also recognizable over the catalysts investigated in the present study and differs remarkably over the different catalysts, educts and concentration of educt gases.

[6] β is the reaction order in the mentioned publication.

CO oxidation:

The favoured mechanism in literature is the interaction between adsorbed CO and adsorbed O_2 (Langmuir-Hinshelwood mechanism) [29], in which CO strongly adsorbs on the surface, causing self-poisoning of the catalyst surface. The same is true for unsaturated hydrocarbons such as ethylene, since both molecules can exhibit strong interactions with the platinum surface through their π-bonds. Zafiris and Grote [177] have proven, that the reaction between CO and O_2 can be structure sensitive by comparing two Pt/Al_2O_3 catalysts with clusters sizes of 1.7 and 14 nm. This structure sensitivity is explained by the differences in the electronic structure of the small clusters, since in small clusters the average number of Pt-Pt bonds is smaller resulting in a high electron density in the cluster available for the back bonding to the $2\pi^*$-orbital of the CO molecule [178]. The influence of electron density and the oxidation state of platinum on oxidation of CO is discussed by Yung-Fang [29], who reported a large increase of the CO oxidation activity if the platinum based catalyst is reduced during the experiment. This explains the differences between the EnviCat2520 and the Pt(Ar). Contrary to this, electron deficient clusters are more likely surrounded by oxygen, either as ions or adsorbed oxygen species resulting in less competitive adsorption with CO and therefore an increased activity. Compared to the PtB(Ar) the PtEA consists of larger platinum clusters and most likely a higher electron density in the clusters since no electron withdrawal from the Siralox carrier is expected. As mentioned above, the influence of the dispersion should not be responsible if the cluster size is increased from 3 nm to ~20 nm. Therefore, the slightly increased low temperature activity of the PtB(Ar) catalyst has to be ascribed to the less competitive adsorption between CO and O_2 over electron deficient clusters. Contrary to the CO oxidation activity over PtB(Ar) which is independent of the CO concentration, the LOT over the PtEA catalyst is shifted to higher temperatures if the CO concentration is increased from 600 ppm to 1000 ppm (see Table 18).

Ethylene oxidation:

As already motioned above, the oxidation of ethylene is strongly self-inhibited. This is especially true for low temperatures and for the EnviCat2520 and the PtB(Ar) catalyst. In case of the PtEA catalyst, the reaction order for ethylene is ~-0.2 at 100 °C and below turning to positive exceeding 120 °C. The inhibiting effect over the EnviCat2520 and the PtB(Ar) catalyst is more pronounced. For both catalysts, a reaction order of ~-0.6 is found at 100 °C, which increases with increasing temperature. Both catalysts strongly interact with oxygen.

Oxygen:

The kinetic parameters calculated for the oxygen conversion are obtained indirectly by calculating the oxygen conversion by the oxidation of propane added, resulting in a low accuracy. Nevertheless the results will be discussed briefly.

For lean conditions the conversion of the VOC is limited by the amount of oxygen available for the oxidation. In excess of oxygen (rich conditions), the oxygen might strongly adsorb on the catalyst surface, resulting in a hindrance of the VOC adsorption. This poisoning effect of the oxygen is for example described by Arnby et al. [156, 168] and Carlson et al. [169]. Both studied the influence of the oxygen concentration on the oxidation of propane. Carlson [169] investigated an oxygen concentration range between 0 vol% to 1.12 vol% with a constant propane concentration of 0.15 vol%, resulting in a oxygen to propane ratio of 1.5. Arnby et al. [156, 168] studied the influence of oxygen concentrations between 0.05 vol% and 10 vol% with 1000 ppm propane (oxygen to propane ration 0.1 to 20). Both report a maximum activity at the transition region from lean to rich conditions and found that the highest conversion can be achieved at stoichiometric oxygen concentration. In this study, oxygen to propane ratios of 55 to 222 are investigated since the typical catalytic combustion of hydrocarbons is run in large excess of oxygen.

The oxygen conversion strongly depends on the cluster size and increases with a decrease in the clusters size in the order EnviCat2520 < PtEA < PtB(Ar). The rate constant and the TOF follow the same trend, whereas the activation energy increases from 19 kJ/mol (EnviCat2520) to 28 kJ/mol PtB(Ar). Furthermore, the results obtained here support the influence of the cluster size on the activation of oxygen in different states as already discussed above. This trend additionally supports the theory of the self-poisoning by oxygen as discussed by Arnby et al. [156, 168] and Carlson et al. [169].

Over all catalysts investigated here, the oxygen conversion for high oxygen to propane ratios is not affected by the changes in the oxygen concentration. Reducing the oxygen concentration to 5 vol% the conversion is remarkably increased and consequently the reaction order is increased from ~0 to 0.75 for all catalysts. Therefore, the results obtained here justify the assumption that the reaction order is independent of the oxygen concentration, on which the calculation of the kinetic parameters for the oxidation of propane, CO and ethylene were based on.

5.3. Transport limitations in the zeolite based catalysts

The encapsulation of catalytically active precious metal into the microporous of a zeolite might result in transport limitation of the reaction. To understand the influence of the encapsulation of the active sites, the transport limitations that might arise from such incorporation are investigated. To identify the influence of the zeolite structure on the pore diffusion, the washcoat-layer thickness is varied. In addition to the estimation of transport limitations in the washcoat layer, the bulk mass transport is calculated.

5.3.1. Catalyst and test procedure

Transport limitations are caused by the washcoat layer thickness. The developed synthesis provides the possibility to introduce a high concentration of platinum into the zeolite. Thus the amount of washcoat can be reduced compared to other zeolite base precious metal catalysts. This effect can be studied by the variation of the washcoat layer thickness. Therefore, the honeycombs were coated with 100 g/l, 66 g/l and 33 g/l, further denoted as PtB100, PtB66 and PtB33, respectively. The Pt loading on the honeycomb was kept constant at 1 g/l. To avoid changes in the platinum particle size and distribution of the clusters, which might change the reactivity of the Pt zeolite, all catalysts were prepared as described in chapter 3.1. The Pt concentration on the zeolite is 3 wt%. For the higher loaded honeycombs, the H-form of the zeolite was added to the platinum impregnated zeolite. In case of the 33 g/l catalyst, the pure Pt-zeolite was used. The washcoat was coated on a 200 cpsi 20 mm long cordierite honeycomb (2.5 mm diameter). The coated honeycombs were calcined at 350 °C for 5 h and aged at 550 °C for 12 h prior to the tests to avoid structural changes of the platinum dispersion and the washcoat structure during the test. The influence of the washcoat thickness on the diffusion was studied for propane, CO and ethylene, respectively.

The kinetic parameters for the oxidation of the mentioned VOCs are evaluated by the variation of the educt gas concentration as well as the temperature, which were varied from high temperatures/concentrations down to low temperatures/concentrations. After the conditions were changed, it was waited for 25 min to ensure stable condition for the next measurement. The test conditions are listed in Table 22.

Table 22: Test conditions

	Concentration [ppm]	Temperature [°C]
Propane	200→100 (20 ppm steps)	500→350
C_2H_4	1000→600 (100 ppm steps)	160→100
CO	1000→600 (100 ppm steps)	160→100

The GHSV was 150 000 h^{-1}.

5.3.2. Results

Film diffusion limitation:

To determine the influence of the film diffusion, the maximal theoretical conversion of propane (500 °C), ethylene and CO (160 °C) were determined with eq. 16. The maximum possible conversions according to radial diffusion inside the honeycomb channels for the reactants were calculated with eq. 15 to be 84 %, 92 % and 95 %, respectively[7].

Pore diffusion limitation:

The conversion versus temperature profiles, as well the derived Arrhenius plots, of the oxidation of the three different pollutants are presented in the following figures.

The oxidation of propane is strongly dependent on the washcoat layer thickness as shown in Figure 48. The conversion as a function of the temperature plot clearly shows that the propane conversion strongly depends upon the washcoat layer thickness and that the conversion is remarkably reduced if the loading is increased from 66 g/l to 100 g/l. Contrary to this decrease, the conversion in nearly unaffected by the doubling the coated amount from 33 g/l to 66 g/l.

[7] The calculation is based on a channel diameter of 2 mm and a length of 2 cm. The geometric surface area *a* is 18.98 cm^2/cm^3 and the open frontal area is 72.5 % (data provided from Corning). The gas velocity is 1.1 m/s. The gas density [air] is 0.82 kg/m^3 at 160 °C 0.45 kg/m^3 for 500 °C, the viscosity of air is $8.15*10^{-5}$ m^2/s at 500 °C and $2.96*10^{-5}$ m^2/s. The diffusion coefficients for the educt gases in air are calculated to be 0.59 cm^2/s, 0.39 cm^2/s and 0.31 cm^2/s for propane, CO and ethylene.

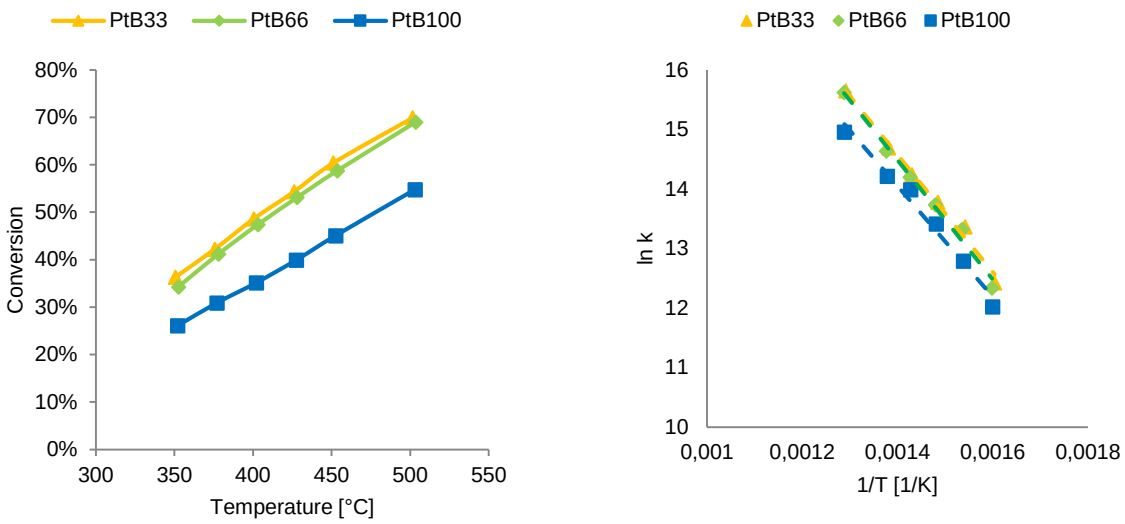

Figure 48: Conversion as a function of the temperature (left) and Arrhenius plot (right) for the propane oxidation

Opposite to the change in the conversion of propane with the change of the washcoat loading, the activation energy and the rate constant are not affected by the decrease of the washcoat loading as summarized Table 23 indicating a loss of "active sites" as discussed in 1.3.3.

Table 23: Kinetic parameters for the oxidation of propane for different washcoat loading

	E_A [kJ/mol]	$k_{(0)}$ [m³/s]
PtB100	77	$1.6*10^5$
PtB66	83	$5.7*10^5$
PtB33	82	$5.6*10^5$

In case of CO and ethylene oxidation, the temperature versus conversion profile shows the typical S-shaped curve (Figure 49 and Figure 50). It is obvious, that the activation energy becomes progressively smaller as the temperature is increased, which is a clear evidence for pore diffusion limitation. The kinetic parameters summarized in Table 24 are calculated in the intrinsic kinetic regime. For the calculation only the low temperature values (100–130 °C for ethylene and 115–135 °C for CO) with conversions not exceeding 80 % were considered.

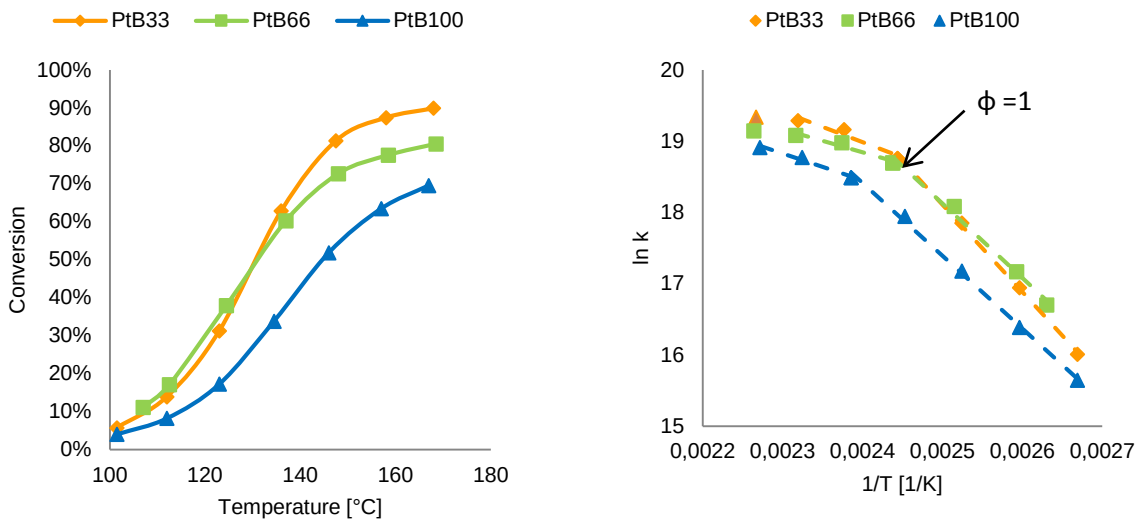

Figure 49: Conversion as a function of the temperature plot (left) and Arrhenius plot (right) for the ethylene oxidation (800 ppm)

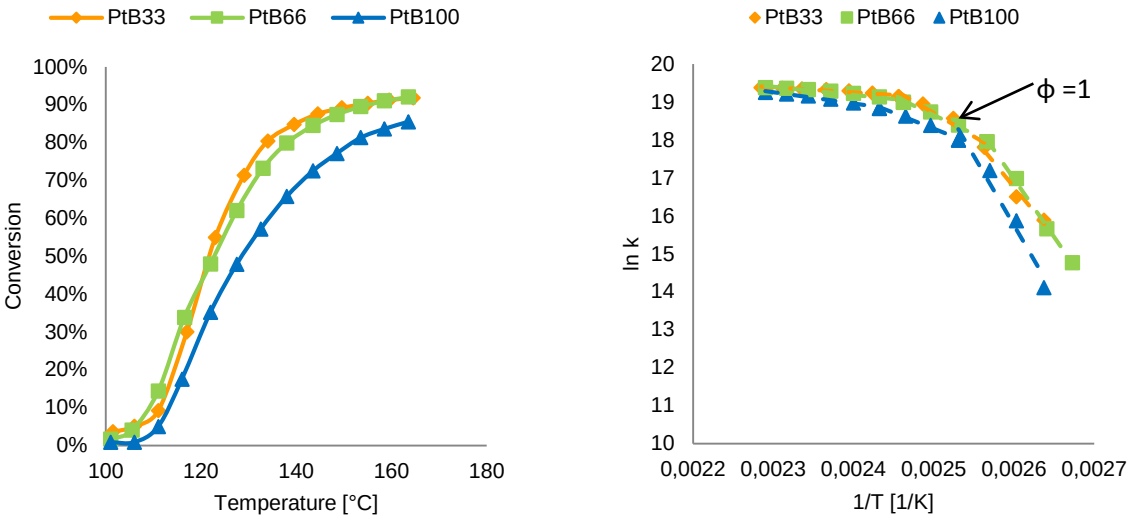

Figure 50: Conversion as a function of the temperature plot (left) and Arrhenius plot (right) for the CO oxidation (800 ppm)

Table 24: Kinetic parameters for the oxidation of ethylene (left) and CO[8] (right) for different washcoat loadings

	E_A [kJ/mol]	k_0 [m³/s]	E_A[kJ/mol]	k_0 [m³/s]
PtB33	99	$1.8*10^{14}$	102	$1.0*10^{15}$
PtB66	79	$2.1*10^{11}$	83	$2.7*10^{12}$
PtB100	82	$1.1*10^{12}$	69	$3.1*10^{10}$

[8] 600 ppm CO or ethylene, respectively

As discussed in chapter 5.2.1 the determination of the kinetic parameters for ethylene and CO are doubtful due to adsorption of the educt molecule and the erratic increase of the conversion. Therefore, first order reaction is assumed to derive the kinetic parameters.

Diffusion coefficients:

The effective diffusion coefficients are calculated from the Arrhenius plot. The line in the region with a significant influence of pore diffusion has a slope of one-half of the intrinsic value according to classical theory. At the intersection of the two straight lines, the Thiele modulus approaches unity. This fact can be used to determine the effective diffusivity of ethylene and carbon monoxide by using eq. 28.

Table 25: Kinetic parameter for the oxidation of ethylene (left) and CO (right) derived at the interception of the kinetic and pore diffusion regime

	$k_{(0)}$ [m³/s]	T [K]	$k_{(0)}$ [m³/s]	T [K]
PtB33	$1.3*10^8$	406	$2.1*10^8$	406
PtB66	$1.2*10^8$	404	$1.5*10^8$	410
PtB100	$1.0*10^8$	415	$1.0*10^8$	406

To quantify the influence of the pore diffusion upon the reaction the effective diffusion coefficients at 130 °C (temperature of the intersection of the two straight lines) are calculated. To estimate the influence of the different diffusion regimes the binary diffusion coefficient, the effective Knudsen diffusion coefficient and the effective pore diffusion coefficient were calculated. For the washcoat pores a diameter of 60 nm and a tortuosity of 5 is assumed. The diffusion coefficients for the zeolite pores are calculated with the pore diameter of the zeolite of 6.5 Å and tortuosity of 1.43. The porosity ε is 0.41 for the zeolite pores and 0.45 for the transport pores[9].

The results are summarized in Table 26 and Table 27. The effective Knudsen diffusion coefficients were calculated by using the eq. 20 to eq. 22. Since D_{Kn} depends on the molecular mass, which is identically for ethylene and CO, only one value is given.

[9] Calculated with the measured density (0.85 kg/l), the calculated density of the zeolite (1.45 kg/l) and the density of quartz (2.65 kg/l), porosity = 1-0.85/1.45 and 1-1.45/2.65, respectively.

Table 26: Diffusion coefficients of CO

	D_{AB} [m²/s]	$D_{Kn,\,eff,\,WC}$ [m²/s]	$D_{P,\,eff,\,WC}$ [m²/s]	$D_{Kn,\,eff,\,zeo}$ [m²/s]	$D_{P,\,eff,\,zeo}$ [m²/s]	D_{eff} [m²/s]
PtB33	$1.07*10^{-4}$	$3.20*10^{-6}$	$3.11*10^{-6}$	$3.31*10^{-8}$	$1.06*10^{-7}$	$1.25*10^{-8}$
PtB66						$5.98*10^{-9}$
PtB100						$1.53*10^{-9}$

Table 27: Diffusion coefficients of ethylene

	D_{AB} [m²/s]	$D_{Kn,\,eff,\,WC}$ [m²/s]	$D_{P,\,eff,\,WC}$ [m²/s]	$D_{Kn,\,eff,\,zeo}$ [m²/s]	$D_{P,\,eff,\,zeo}$ [m²/s]	D_{eff} [m²/s]
PtB33	$8.19*10^{-5}$	$3.20*10^{-6}$	$3.11*10^{-6}$	$3.31*10^{-8}$	$3.31*10^{-8}$	$1.21*10^{-8}$
PtB66						$6.01*10^{-9}$
PtB100						$1.51*10^{-9}$

The comparison of the effective diffusion coefficient and the Knudsen diffusion coefficient clearly show that the reaction is mainly limited by the zeolite pores and to a lesser extent by the transport pores. The calculated value and the measured value for the low load honeycomb are in good correlation. The determined diffusion coefficients for the higher loaded catalysts (with 66 g/l and 100 g/l) are due to the increased diffusion length and the resulting increased hindrance in the diffusion of the educt molecule to the active centre. The calculated diffusion coefficients for propane are listed in Table 28.

Table 28: Diffusion coefficient for propane at 500 °C

D_{AB} [m²/s]	$D_{Kn,\,eff,\,WC}$ [m²/s]	$D_{P,\,eff,\,WC}$ [m²/s]	$D_{Kn,\,eff,\,zeo}$ [m²/s]	$D_{P,\,eff,\,zeo}$ [m²/s]	D_{eff} [m²/s]
$1.93*10^{-4}$	$3.53*10^{-6}$	$3.43*10^{-6}$	$3.66*10^{-8}$	$3.66*10^{-8}$	n.a.

5.3.3. Pore diffusion limitations and reaction rate

Thiele modulus and pore usage:

The Thiele modulus φ describes the correlation between the diffusion and the reaction rate as shown in eq. 27 and eq. 28. If the Thiele modulus is > 3 the reaction is limited by pore diffusion, whereas a value < 0.3 indicates that the reaction is kinetically limited. The Thiele modulus is calculated for the three different washcoat loadings and with the diffusion coefficients based on the dimensions of the transport pores and the zeolite pores, to indentify the contribution of the two pore types on the transport limitations. The pore usage is derived from the Thiele modulus by eq. 31.

For the oxidation of propane the Thiele modulus and the derived degree of the pore usage are listed in Table 29. It is obvious, that the Thiele modulus and the degree of pore usage strongly depend on the washcoat loading on the honeycomb and the influence of the pore diffusion limitation can be reduced if the layer thickness is decreased. This can be seen by the

increasing pore usage with raises from 32 % in case of PtB100 to 58 % for PtB33 at 350 °C. Additionally, both parameters depend on the mean temperature since the rate of the reaction increases with increasing temperature. The values calculated for the Thiele modulus are in the transient region between the kinetic and pore diffusion regime, therefore the overall reaction is affected by both, the kinetic of the reaction as well as the transport of the educt molecule.

Table 29: Thiele modulus and efficiency in percent for the oxidation of propane[10] (200 ppm)

$D_{eff,\ P\ Zeo}$	PtB33		PtB66		PtB100	
	φ	η	φ	η	φ	η
500 °C	1.58	58.2	2.23	43.9	3.15	31.6
450 °C	1.40	63.3	2.00	48.2	3.23	30.9
400 °C	1.21	69.3	1.74	54.0	2.79	35.6
350 °C	0.98	76.9	1.43	62.4	2.26	43.2

$D_{eff.\ P\ WC}$	PtB33		PtB66		PtB100	
	φ	η	φ	η	φ	η
500 °C	0.16	99.1	0.23	98.3	0.22	98.4
450 °C	0.14	99.3	0.23	98.2	0.19	98.8
400 °C	0.12	99.5	0.20	98.7	0.17	99.1
350 °C	0.10	99.7	0.16	99.1	0.14	99.4

The same is true for the oxidation of ethylene and CO. The diffusion coefficients of the smaller molecules is lower than the calculated diffusion coefficients of propane but on the other hand the rate of these reactions is much faster, since the oxidation of unsaturated molecules and CO is easier than the oxidation of saturated hydrocarbons such as propane. So the lower diffusion coefficients are overcompensated by the fast reaction and therefore, the reaction is limited by pore diffusion at temperatures exceeding ~130 °C for all three washcoat loadings.

Table 30: Thiele modulus and efficiency in percent for the oxidation of CO (1000 ppm)

$D_{eff,\ P\ Zeo}$	PtB33		PtB66		PtB100	
	φ	η	φ	η	φ	η
160 °C	1.26	67.7	1.85	51.5	2.10	46.1
150 °C	1.24	68.1	1.78	53.0	2.07	46.8
140 °C	1.21	69.0	1.59	58.0	1.99	48.5
130 °C	1.13	71.7	1.05	74.5	1.75	53.9
120 °C	0.82	82.3	0.41	94.7	1.19	69.9
110 °C	0.30	97.2	0.31	97.0	0.47	93.1

$D_{eff,\ P\ WC}$	PtB33		PtB66		PtB100	
	φ	η	φ	η	φ	η
160 °C	0.23	98.3	0.34	96.3	0.39	95.3
150 °C	0.23	98.3	0.33	96.5	0.38	95.4
140 °C	0.22	98.4	0.29	97.2	0.37	95.7
130 °C	0.21	98.6	0.19	98.8	0.32	96.7
120 °C	0.15	99.2	0.08	99.8	0.22	98.4
110 °C	0.05	99.9	0.06	99.9	0.09	99.7

Table 31: Thiele modulus and efficiency in percent for the oxidation of ethylene (1000 ppm)

[10] The washcoat thickness are $2.8*10^{-5}$, $1.4*10^{-5}$ and $9.8*10^{-6}$ m for the PtB(100), PtB(66) and PtB(33), respectively.

$D_{eff,\ P\ Zeo}$	PtB33		PtB66		PtB100	
	φ	η	φ	η	φ	η
160 °C	1.23	68.6	1.63	56.7	1.72	54.5
150 °C	1.18	70.2	1.42	62.6	1.65	56.2
140 °C	0.98	76.7	1.04	74.8	1.52	59.8
130 °C	0.58	90.1	0.68	86.9	1.15	71.3
120 °C	0.38	95.4	0.48	93.1	0.66	87.8
110 °C	0.27	97.7	0.35	96.1	0.42	94.5

$D_{eff,\ P\ WC}$	PtB33		PtB66		PtB100	
	φ	η	φ	η	φ	η
160 °C	0.23	98.3	0.32	96.8	0.30	97.1
150 °C	0.22	98.5	0.30	97.0	0.26	97.8
140 °C	0.18	98.9	0.28	97.5	0.19	98.8
130 °C	0.11	99.6	0.21	98.5	0.13	99.5
120 °C	0.07	99.8	0.12	99.5	0.09	99.7
110 °C	0.05	99.9	0.08	99.8	0.06	99.9

5.3.4. Discussion

To complete the kinetic consideration and to determine the influence arising from the incorporation of the catalytically active component into the porous structure of a zeolite, the influence of the washcoat layer thickness was studied. For the estimation of the diffusion coefficients, the diffusion coefficients for the molecular diffusion (D_{AB}), the effective Knudsen diffusion ($D_{Kn,\ eff}$) and the effective pore diffusion ($D_{P,\ eff}$) are calculated and compared with the experimentally obtained data. The influence of the different diffusion in the zeolite and washcoat as well as the influence of the washcoat layer thickness will be discussed here.

Diffusion in transport pores:

The influence of the transport pores in the washcoat is estimated by the calculation of the molecular diffusion coefficients, the effective Knudsen coefficients and the effective pore diffusion coefficients as summarized in the Table 26, Table 27 and Table 28. The comparison of the coefficients calculated for the molecular diffusion and Knudsen diffusion for the three reactant gas molecules with the pore diffusion coefficient show that the values for the Knudsen diffusion and the pore diffusion are very similar but clearly differ from those obtained for the molecular diffusion. This comparison clearly indicates a strong influence of the washcoat pore structure on the diffusion of all three reactant gases.

Diffusion in zeolite pores:

In addition to the transport limitation by the washcoat, it can be expected that the diffusion is further influenced by the zeolite pores. The comparison of the effective diffusion coefficients, Knudsen and pore diffusion, calculated for the transport pores and zeolite pores show that the coefficients are decreased by approximately two orders of magnitude if the dimensions of the zeolite are considered in the calculation. The comparison of the calculated values with the

experimentally obtained data for the different washcoat loadings show that the results obtained for the low washcoat loaded catalysts (PtB33) are in fairly good correlation with the calculated Knudsen and pore diffusion coefficients based on the zeolite pores. The diffusion coefficients for the higher loaded catalyst (PtB66 and PtB100) are further decreased and indicate an increased transport limitation caused by the addition of H-form zeolite. For the oxidation of propane no experimental data are available but the same effect has to be expected and diffusion coefficients in the same range or even lower have to be expected due to larger size of the molecule. The addition of zeolite increases both, the amount of the washcoat pores as well as the amount of the zeolite pores. The increased amount of pores can be interpreted as an increase of the diffusion length in the pores, resulting in further diffusion limitation. For a better understanding of the origin of the diffusion limitation an additional experiment in which the size of the zeolite crystallite is varied at constant washcoat loading is necessary. This experiment could not be realized within this thesis and the results obtained here have to be interpreted carefully due to the experimental uncertainties of the test unit applied. Nevertheless, it can be concluded that the decrease of the experimentally obtained diffusion coefficient are mainly caused by the zeolite pores, which are responsible for the increase of the transport limitation.

Influence of the washcoat layer thickness (Thiele modulus):

The correlation between the reaction rates, the diffusion and the length of the diffusion is given by the Thiele modulus which is calculated with eq. 28 and the results are summarized in Table 29 to Table 31.

The trend of the Thiele modulus as well as the conversion versus temperature profile for the oxidation of CO and ethylene clearly show that at higher temperature the reaction is limited by transport processes whereas at lower temperatures the reaction is kinetically hindered.

The Thiele modulus increases with the temperature from 0.3 to 1.3 for the oxidation of CO and from 0.3 to 1.2 in case of the ethylene oxidation. At low temperature the kinetic regime is dominant, whereas at higher temperatures and at higher washcoat thickness, the Thiele modulus indicates a pronounced influence of transport limitation. In the first case the change can be explained with a faster reaction rate at higher temperatures. In the latter case the increased transport limitation is responsible for the change in the Thiele modulus. To indentify the influence of the different diffusion regimes the Thiele modulus for the transport pores is additionally calculated. The values obtained for the transport pores are only slightly dependent on the washcoat layer thickness and are all around 0.3. That would mean that the reaction is always kinetically controlled and not influenced by an increase of the washcoat

thickness what is contrary to what was discussed before and experimentally obtained. The calculation of the Thiele modulus together with the interpretation of the diffusion coefficients as discussed above lead to the conclusion, that the increase of the transport limitation with increasing washcoat loading is mainly influenced by the increased amount of the zeolites pores, which is interpreted as increased diffusion length in these pores as discussed above and not by the transport pores in the washcoat. This assumption has to be experimentally proven as mentioned above.

5.3.5. Conclusion

The developed synthesis opens up the possibility to impregnate the zeolite with a high concentration of precious metals such as platinum or rhodium which is highly dispersed through the zeolite and therefore its pore structure. Due to the high concentration of the active components, the washcoat layer thickness can be reduced compared to state of the art catalyst. The reduction of the washcoat material reduces the transport limitations as shown in the Figure 48 to Figure 50. To estimate the influence of the pore diffusion, two regimes were considered. First the diffusion in the zeolite pores and second the diffusion in the washcoat pores. The comparison of the calculated pore diffusion coefficients, the Thiele modulus and the experimentally obtained diffusion coefficients for the oxidation of CO and ethylene lead to the conclusion that the limitation of the transport is mainly due to the zeolite pores. The amount of these pores could by reduced due to the improved synthesis resulting in a higher precious metal concentration. Nevertheless at high reaction rates, the reaction is hindered by pore diffusion, since the Thiele modulus is in the transient region (see Table 30 and Table 31). The situation is different for the oxidation of propane, where the oxidation is limited by pore diffusion in the whole temperature range investigated (see Table 29). In addition to the pore diffusion limitation the film diffusion has to be considered for the overall transport limitations. The maximum theoretical conversion based on the geometry of the honeycomb and the reaction conditions is calculated in Chapter 5.3.2. In case of CO an ethylene oxidation the experimentally obtained is almost identical to the theoretically maximum conversion, resulting in a film diffusion limitation at the highest temperatures. Again for propane oxidation the situation is different since the reaction is more controlled by pore diffusion limitations and as a result limitation by film diffusion is much less pronounced. The film diffusion limitation can be reduced by an increase of the cell density of the honeycomb applied as substrate for the washcoat. The increase the cell density might be on the cost of the catalyst self-life since these substrates suffer from easier blocking by solid particles in the

exhaust gas. Therefore a compromise has to be found for each individual application of the catalyst.

6. Conclusions

The incorporation of precious metal clusters in zeolites has been a hot topic in catalysis for a long time. Nevertheless, it was not possible to synthesize those clusters in a high concentration. It is discussed, that those nanoclusters have unique properties, such as a high catalytic activity and a high thermal and hydrothermal stability.

In this work a new class of precious metal containing zeolite was synthesised, differing from existing PM-zeolites in the increased amount of PM nanoclusters incorporated in the pore structure of the zeolite. It was demonstrated, that the success of the synthesis crucially depends on the choice of the precursors and the calcination conditions. Sulphite precursors were successfully applied for the synthesis for Pt, Pd and Rh zeolites. It was also demonstrated that the same platinum cluster size and distribution can be achieved by the utilisation of $Pt(NO_3)_2$. These results favour the conclusion that strong electron withdrawal ligands leading to strong interactions between the PM and the zeolite are required for a successful synthesis. The calcination atmosphere which is required depends on the precious metal used. For the platinum and palladium containing zeolites, inert gas calcination favours the formation of the desired clusters whereas air has to be applied for rhodium zeolites. This shows that the atmosphere depends on the precious metal and not on the ligand. For the interactions of Rh with the support a structure was postulated consisting of "Zeo-Al_2O_3-$RhAlO_4$-Rh_2O_3".

Catalytic tests as well as the investigation on the (hydro)thermal stability clearly show improved properties towards existing precious metal catalyst.

Although a lot of promising results could been shown here not all open questions have been answered. Especially the processes occurring during the calcination and the role of the ligand for example sulphite and nitrate or similar ligands may influence the structure of the nanoclusters and their interaction with the support and therefore the catalytic performance of the final product. Additionally, the influences of the zeolite composition (especially the Si/Al ratio and the degree of dealumination) and framework structure and their influence on the interactions with the nanoclusters and the resulting electronic structure need to be further investigated and therefore should be the topic for ongoing advanced studies.

7. Summary

The synthesis and the characterization of platinum based zeolites with increased temperature stability and improved catalytic activity at low temperatures was the aim of this thesis. These goals could be achieved by the incorporation of the platinum clusters into the pore system of zeolites. The mobility as well as the size of the clusters is reduced by the incorporation. Platinum sulphite acid was found to be the most promising precursor for the synthesis of the desired nanoclusters homogenously distributed in the zeolite structure in a high concentration. The high concentration makes the difference between the developed synthesis and existing procedures in which the precious metal is introduced into the zeolite e.g. by ion-exchange. The developed synthesis could also be successfully applied for rhodium and palladium sulphite. Although sulphur containing precursors are used in the synthesis, the sulphur is successfully eliminated by the calcination process resulting in sulphur free precious metal zeolites.

An IR method was developed to characterize the precious metal distribution on the zeolite. This method is based on the selective poisoning of the metal clusters located on the outer surface of the zeolite with adamantane-carbonitrile. Adamantane-carbonitrile was chosen for the selective poisoning since this molecule is too bulky to enter into the pores and channels of zeolites. The distribution of the clusters can be estimated by the amount of carbon monoxide adsorbed on the metal clusters before and after the selective poisoning. An additional characteristic of the developed zeolites is that no reflexes of platinum are detected in the XRD pattern despite of the high concentration of the introduced precious metal.

The improved thermal stability and reactivity of the synthesised Pt-zeolite was proven by XRD and IR measurements of the fresh and thermally aged zeolite as well as by catalytic tests and comparison with different reference catalysts. In addition to the desired improvements of the temperature stability and low temperature activity, the resistance against catalyst poisons such as sulphur is significantly enhanced. In addition to the platinum zeolite it is possible to synthesis rhodium based catalysts with improved thermal stability, which is of special interest in the three-way catalysis.

For a better understanding, kinetic measurements were carried out for the developed PtB catalyst and the reference catalyst and the diffusion in the zeolite was studied. The comparison of the reaction orders for the propane oxidation over the three catalysts studied here show that only in case of the developed PtB catalyst the reaction rate depends on the temperature. The comparison of the rate constant and the turnover frequencies clearly show

that the developed catalyst is more active than the two state of the art catalysts. The same is true for the oxidation of CO. But in this case the reaction order was found that the rate is strongly dependent on the temperature, which is negative at low temperatures and approaches 1 with increasing temperature for the PtB and PtEA catalyst, whereas a maximum reaction rate of 0.7 is reached in case of the EnviCat2520. The oxidation of ethylene differs to the two other reactants and the EnviCat2520 was found to have the highest rate constant and turnover frequency. From the results obtained for the kinetics of the three catalysts and educt gases as well as from literature, a correlation between the cluster size and the catalytic activity could be demonstrated. It could be verified that the oxidation of NO, CO and alkanes is favoured over small clusters in the pores, whereas the oxidation of alkenes is favoured on larger clusters located on the outer surface of the zeolite crystallites. This is explained by the different electronic structures of the platinum clusters and therefore different interactions with the educt molecules and oxygen and resulting in the different performance mentioned. Additionally, the developed synthesis provides the impregnation with a high concentration of platinum into the zeolite. As a benefit, the amount of zeolite can be reduced. The influence of the washcoat thickness on the transport limitation was studied. For all educt gases the catalytic performance was significantly improved by the reduction an in case of CO and ethylene concentration the theoretical maximum conversion was nearly reached which leads to the conclusion that at high temperatures the reaction is limited by film diffusion. To estimate the influence of the different pores in the washcoat and in the zeolite the diffusion coefficients for both regimes are calculated and compared with the experimentally obtained data, leading to the conclusion that the pore diffusion limitation is mainly caused by the zeolite pores and not by the much larger washcoat pores.

8. Zusammenfassung

Ziel der Arbeit war die Entwicklung und Charakterisierung von thermisch stabileren, platinhaltigen Zeolith-Katalysatoren mit verbesserter Tieftemperaturaktivität. Ansatz hierfür war der Einschluss von Pt-Clustern in dem Porensystem des Zeolithen. Durch den Einschluss der Cluster sollte deren Beweglichkeit verringert und dadurch die thermische Stabilität verbessert werden. Platin-Sulfit erwies sich dabei als die bevorzugte Ausgangsverbindung, die die Synthese der erwünschten Cluster in hoher Konzentration ermöglicht. Durch die hohe Konzentration unterscheidet sich die entwickelte Synthese deutlich von den bekannten Herstellungsverfahren von edelmetallhaltigen Zeolithen, bei denen das Edelmetall zum Beispiel mittels Ionenaustausch eingebracht wird. Diese Synthese lässt sich auch auf andere sulfithaltige Edelmetall Precursoren (z.B. Palladium-Sulfit oder Rhodium-Sulfit) übertragen. Das entwickelte Verfahren ermöglicht auch die Synthese von legierten Clustern. Durch die Wahl der richtigen Kalzinierungsbedingungen können schwefelfreie Katalysatoren hergestellt werden.

Zur Bestimmung der Edelmetallverteilung auf dem Zeolithen wurde eine IR Methode entwickelt, die auf der selektiven Vergiftung von Pt-Clustern auf der äußeren Oberfläche der Zeolithen beruht. Als Referenz dient hierbei die Menge an CO die vor beziehungsweise nach der Vergiftung mit Adamantancarbonitril auf dem Platin absorbiert werden kann. Da Adamantancarbonitril zu groß ist, um in das Porensystem einzudringen, bindet es selektive an das Platin auf der äußeren Oberfläche. Ein weiteres Merkmal der nach der entwickelten Methode hergestellten Katalysatoren ist, dass die XRD Diffraktogramme trotz der hohen Edelmetall-Konzentration frei von Reflexen des jeweiligen Metalls sind. Durch beide Methoden als auch durch TEM Aufnahmen konnte bestätigt werden, dass sich die Platincluster nahezu ausschließlich in den inneren Poren des Zeolithen befinden. Die verbesserte thermische Stabilität und Reaktivität der Platin-Zeolith-Katalysatoren konnte durch Alterungsexperimente und den Vergleich mit Referenzkatalysatoren nachgewiesen werden. Neben der erwünschten Verbesserung der thermischen Stabilität und der Tieftemperaturaktivität konnte Widerstandsfähigkeit gegenüber Katalysatorgiften wie zum Beispiel Schwefel deutlich verbessert werden. Die Synthese konnte auch auf Rhodium-Zeolithe übertragen werden und führte auch hier zu einer deutlich verbesserten thermischen Stabilität führt, was insbesondere für die Drei-Wege-Katalysatoren von Bedeutung ist.

Um die Eigenschaften des Platin Zeolith-Katalysators besser zu verstehen wurden kinetische Messungen durchgeführt und mit den Daten der Referenzkatalysatoren verglichen. Außerdem wurde der Einfluss des Stofftransportes in dem Zeolithen untersucht. Der Verglich der

Reaktionsordnung der drei Katalysatoren für die Oxidation von Propan zeigt, dass nur der neu entwickelte PtB Katalysator eine Abhängigkeit der Reaktionsordnung von der Temperatur zeigt. Die verbesserte Aktivität zeigt sich deutlich bei dem Vergleich der Reaktionsgeschwindigkeiten und der Umsetzungszahlen. Das Gleiche gilt für die Oxidation von CO. Allerdings zeigt sich bei der Betrachtung der Reaktionsordnung eine starke Abhängigkeit von der Temperatur, die bei tiefen Temperaturen negativ ist und sich im Falle des PtB und PtEA Katalysators bei hohen Temperauren 1 annähert, wohingegen im Falle des EnviCAt2520 eine maximale Reaktionsordnung von 0.7 erreicht wird. Die Oxidation von Ethene unterscheidet sich deutlich von den beiden anderen Eduktgasen. Für die Umsetzung des Alkenes besitzt der EnviCat2520 die höchste Aktivität, was sich bei dem Vergleich der Reaktionsgeschwindigkeit und der Umsetzungsfrequenz zeigt. Durch die in dieser Arbeit verglichenen Katalysatoren und Eduktgase als auch durch den Vergleich mit der Literatur konnte ein Zusammenhang zwischen der Clustergröße und der Reaktivität nachgewiesen werden. Es konnte bestätigt werden, dass die Oxidation von NO, CO und Alkanen bevorzugt an kleinen Clustern im Inneren der Zeolith-Struktur ablaufen. Im Gegensatz werden Alkene deutlich schneller an größeren Clustern an den äußeren Oberflachen umgesetzt. Die unterschiedliche Reaktivität wird mit der veränderten Elektronendichte der Platincluster erklärt, die sowohl von der Clustergröße als auch von den Eigenschaften des Trägers beeinflusst wird. Die Unterschiede in der Elektronendichte des Clusters beeinflussen die Wechselwirkung mit den Eduktgasen als auch mit dem Sauerstoff. Sie sind deshalb für die unterschiedlichen Reaktivitäten verantwortlich.

Wie eingangs erwähnt, ermöglicht die entwickelte Syntheseroute die Einbringung sehr hoher Edelmetallmengen in den Zeolithen und dadurch eine deutliche Verringerung der Washcoat-Menge, die auf eine Wabe aufgebracht werden muss um die gewünschte Menge an Edelmetall zu erzielen. Dadurch kann die Washcoat-Dicke reduziert werden was zu einer Verringerung der Transportwiderstände führt. Deshalb wurde zusätzlich der Einfluss der Schichtdicke auf den Stofftransport untersucht. Die Verringerung der Schichtdicke führte für alle drei Gase zu einer deutlich verbesserten Umsetzung. Im Falle von CO und Ethenen wurden nahezu die maximalen theoretischen Umsätze erreicht und es wurde gezeigt dass die Reaktion bei hohen Temperaturen durch den Stofftransport in den Wabenkanälen limitiert ist. Zur Abschätzung des Einflusses der Porendiffusion wurden die Diffusionskoeffizienten sowohl für die Zeolith-Poren als auch die Washcoat-Poren berechnet und mit den experimentell erhaltenen Werten verglichen, wodurch gezeigt werden konnte das die Diffusion hautsächlich durch die Zeolith-Poren beeinflusst ist und die Poren in dem Washcoat eine untergeordnete Rolle spielen.

9. Appendix

9.1. Figures

9.2. Tables

9.3. Abbreviations

Acronyms:

AAS	atom adsorption spectroscopy
AdaCNA	adamantane-carbonitrile
AO	atomic orbital
B.A.	Brønsted acid site
BEA	zeolite Beta
BET	Brunauer Emmett Teller
CAFE	Clean air for Europe
DOC	diesel oxidation catalyst
DPF	diesel particulate filter
EGR	exhaust gas recirculation
E-PRTR	European Pollutant Release and Transfer Register
FAU	faujasite
FCC	fluidic catalytic cracking
FTIR	Fourier transformed infrared spectroscopy
FWHM	full width at half maximum
GHSV	gas hourly space velocity (h^{-1})
HC	hydrocarbon
HSAB	hard soft acid base
IPPC	Integrated Pollution Prevention and Control
IR	infrared
IUPAC	International Union of Pure and Applied Chemistry
L.A.	Lewis acid site
LOT	light-off temperature (50 % conversion)
LTL	Linde Type L
MFI	Mobile five
MOR	mordenite
NMHC	non-methane hydrocarbon
Off	offretite
PM	particulate matter
PM	precious metal
PSA	platinum sulphite acid
PtB(Air)	air calcined PSA impregnated BEA

PtB(Ar)	argon calcined PSA impregnated BEA	
PtEA	platinum ethanol amine impregnated Siralox	
PV	pore volume	
RhB(Air)	air calcined RSA impregnated BEA	
RhB(Ar)	argon calcined RSA impregnated BEA	
RSA	rhodium sulphite acid	
SCR	selective catalytic reduction	
TA	technische Anleitung	
TEM	transmission electron microscopy	
TGA	thermogravimetric analysis	
TOF	turnover frequency	s^{-1}
TPD	temperature programmed desorption	
TWC	three-way catalyst	
VHF	very high frequency	
VOC	volatile organic compound	
XRD	x-ray powder diffraction	
ZMS-5	Zeolite Socony Mobil-five	

Constants:

R	ideal gas constant = 8.3145 J mol^{-1} K^{-1}
c	speed of light = 2.998 * 10^8 m s^{-1}
N_A	Avogadro constant = 6.022 10^{23} mol^{-1}

Dimensionless numbers:

Re	Reynolds number
Sc	Schmidt number
Sh	Sherwood number

Greek Letters

β	line broadening at FWHM	
ε	porosity	dimensionless
ε	void fraction of honeycomb, dimensionless	dimensionless
η	effectiveness factor	dimensionless
Θ	Thiele modulus	dimensionless
Λ	mean free path	m
λ	air to fuel ratio	dimensionless
λ	wavelength	nm
μ	dynamic viscosity	kg/m*s
ν	stoichiometric number of the reaction	dimensionless
ρ	gas density at operation condition	g/cm^3
τ	cluster size	nm
τ	tortuosity	dimensionless

Latin Letter:

A	frontal area of the honeycomb	cm^2
a	geometric surface area per unit volume	cm^2/cm^3
A	mass of air consumed by the engine	kg
c	reactant gas phase concentration	$kmol/m^3$
cpsi	cells per square inch	dimensionless
d	diameter	cm
D	diffusion coefficient	m^2/s
E_a	activation energy	J/mol
F	mass of fuel consumed by the engine	kg
k	rate constant	$m^3/kg*s$
K	shape factor	dimensionless
k_g	mass transfer coefficient	cm/s
L	length	m
m	mass	g
M	molecular mass	g/mol
n	amount of substance	mol
p	pressure	bar
r	reaction rate	different

T	temperature	K
U	mean gas velocity	m/s
W	total mass flow rate	g/s

Subscripts:

cd	configurational diffusion
ch	diameter of honeycomb channel
eff	effective
Kn	Knudsen
m	molecule
p	pore
s	surface
WC	washcoat
Zeo	zeolite
0	first order
n	rate depending

9.4. References

1. Ertl G., Knötzinger H., Schüth F. and Weitkamp J., *Handbook of Heterogeneous Catalysis*. 2nd Edition ed. Vol. 5. 2008, Weinheim: Wiley-VCH.
2. *Clean Air For Europe*, European Union, 2001, 2001/81/EC.
3. Bundesministerium für Umwelt N.u.R., *Erste Allgemeine Verwaltungsvorschrift zum Bundes–Immissionsschutzgesetz*. 2002, Carl Heymanns Verlag KG: Köln.
4. *Integrated Pollution Prevention and Control*, European Commision, 2008, 2008/1/EC.
5. *The European Pollutant Release and Transfer Register*. 2010, European Environment Agency.
6. Holleman A.F., Wieberg, N., *Lehrbuch der anorganischen Chemie*. 101 ed. 1995, Berlin; New York: de Gruyter.
7. Warnatz J., Maas U. and Dibble R.W., *Verbrennung*. 3 ed. 2001, Berlin: Springer.
8. Buekens A., *Encyclopedia of Life Support Systems*, Bhaskar N. and Cholakov G.S., Editors. 2005, Eolss Publishers: Oxford.
9. Heneghan C.S., Hutchings G.J. and Taylor S.H., Catalysis, 2004. **17**: p. 105-151.
10. Spivey J.J., Industrial and Engineering Chemistry Research, 1987. **26**(11): p. 2156.
11. Cant N.W. and Hall W.K., Journal of Catalysis, 1970. **16**(2): p. 220.
12. Sinfelt J.H. and Yates D.J.C., Journal of Catalysis, 1967. **8**(1): p. 82.
13. Pauling L., Proceedings of the Royal Society, 1949. **196**: p. 343.
14. Muto K., Katada N. and Niwa M., Applied Catalysis A: General, 1996. **134**(2): p. 203.
15. Burch R. and Loader P.K., Applied Catalysis B: Environmental, 1994. **5**(1-2): p. 149.
16. McCarty J.G., Catalysis Today, 1995. **26**: p. 283.
17. Oh S.H., Mitchell P.J. and Siewert R.M., Journal of Catalysis, 1991. **132**(2): p. 287.
18. Burch R., Crittle D.J. and Hayes M.J., Catalysis Today, 1999. **47**(1-4): p. 229.
19. Choudhary V.R. and Rane V.H., Journal of Catalysis, 1991. **130**(2): p. 411.
20. Gelin P. and Primet M., Applied Catalysis B: Environmental, 2002. **39**: p. 1-37.
21. Hwang C. and Yeh C., Journal of Molecular Catalysis A: Chemical, 1996. **112**(2): p. 295.
22. Hwang C. and Yeh C., Journal of Catalysis, 1999. **182**: p. 48.
23. Burch R. and Hayes M.J., Journal of Molecular Catalysis A: Chemical, 1995. **100**(1-3): p. 13.
24. Hicks R.F., Qi H., Young M.L. and Lee R.G., Journal of Catalysis, 1990. **122**: p. 280.
25. Hicks R.F., Qi H., Young M.L. and Lee R.G., Journal of Catalysis, 1990. **122**(2): p. 295.
26. Lieske H., Lietz G., Spindler H. and Völter J., Journal of Catalysis, 1983. **81**(1): p. 8.
27. Nandi R.K., Molinaro F., Tang C., Cohen J.B., Butt J.B. and Burwell R.L., Journal of Catalysis, 1982. **78**(2): p. 289.
28. Radic N., Grbic B. and Terlecki-Baricevic A., Applied Catalysis B: Environmental, 2004. **50**(3): p. 153.
29. Yao Y.-F.Y., Journal of Catalysis, 1984. **87**(1): p. 152.
30. Jayat F., Lembacher C., Schubert U. and Martens J.A., Applied Catalysis B: Environmental, 1999. **21**(3): p. 221.
31. Niwa M., Awano K. and Murakami Y., Applied Catalysis, 1983: p. 317.
32. Ishikawa A., Komai S., Satsuma A., Hattori T. and Murakami Y., Applied Catalysis A: General, 1994. **110**(1): p. 61.
33. Yazawa Y., Yoshida H. and Hattori T., Applied Catalysis A: General, 2002. **237**(1-2): p. 139.
34. Yazawa Y., Takagi N., Yoshida H., Komai S., Satsuma A., Tanaka T., Yoshida S. and Hattori T., Applied Catalysis A: General, 2002. **233**(1-2): p. 103.

35. Pliangos C., Yentekakis I.V., Papadakis V.G., Vayenas C.G. and Verykios X.E., Applied Catalysis B: Environmental, 1997. **14**(3-4): p. 161.
36. Blyholder G., Journal of Molecular Catalysis A., 1997(119): p. 11.
37. Blyholder G., Journal of Physical Chemistry, 1964. **68**: p. 2772.
38. Yazawa Y., Yoshida H., Takagi N., Komai S., Satsuma A. and Hattori T., Journal of Catalysis, 1999. **187**(1): p. 15.
39. Yoshida H., Yazawa Y. and Hattori T., Catalysis Today, 2003. **87**(1-4): p. 19.
40. Yao H.C., Stepien H.K. and Gandhi H.S., Journal of Catalysis, 1981. **67**(1): p. 231.
41. Lee A.F., Wilson K., Lambert R.M., Hubbard C.P., Hurley R.G., McCabe R.W. and Gandhi H.S., Journal of Catalysis, 1999. **184**(2): p. 491.
42. Hubbard C.P., Otto K., Gandhi H.S. and Ng K.Y.S., Journal of Catalysis, 1993. **144**(2): p. 484.
43. Burch R., Halpin E., Hayes M., Ruth K. and Sullivan J.A., Applied Catalysis B: Environmental, 1998. **19**(3-4): p. 199.
44. Hinz A., Skoglundh M., Fridell E. and Andersson B., Journal of Catalysis, 2001. **201**: p. 247.
45. Corro G., Fierro J.L.G. and Odilon V.C., Catalysis Communications, 2003. **4**: p. 371.
46. Heck R.M. and Farrauto R.J., *Catalytic Air Pollution Control*. 2nd ed. 2002: Wiley Interscience.
47. Weitkamp J. and Gläser R., *Chemische Technik: Prozesse und Produkte.*, ed. Dittmeyer R., Keim W., Kreysa G., and Oberholz A. Vol. 1. 2004, Weinheim: WILEY-VCH Verlag GmbH & Co. KGaA.
48. Bartholomew C.H., Applied Catalysis A: General, 2001. **212**(1-2): p. 17.
49. Forzatti P. and Lietti L., Catalysis Today, 1999. **52**(2-3): p. 165.
50. Völter J., Lietz G., Spindler H. and Lieske H.J., Journal of Catalysis, 1987. **104**: p. 375.
51. Jamieson J. C. and Olinger B., The American Mineralogist, 1969. **52**: p. 1477.
52. Heck R.M. and Farrauto R.J., Applied Catalysis A: General, 2001. **221**(1-2): p. 443.
53. Miyazaki A., Balint I. and Nakano Y., Journal of Nanoparticle Research, 2003. **5**(1): p. 69.
54. Maxted E.B., Adv. Catal., 1951. **3**: p. 129.
55. Cullis C.F. and Willatt B.M., Journal of Catalysis, 1984: p. 187.
56. Simone D.O., Kennely T., Brungard N.L. and Farrauto R.J., Applied Catalysis, 1991. **70**: p. 87.
57. Roth D., Gélin P., Primet M. and Tena E., Applied Catalysis A: General, 2000. **203**(1): p. 37.
58. Marceau E., Lauron-Pernot H. and Che M., Journal of Catalysis, 2001. **197**(2): p. 394.
59. Meeyoo V., Trimm D.L. and Cant N.W., Applied Catalysis B: Environmental, 1998. **16**(2): p. L101.
60. Padeste C., Cant N.W. and Trimm D.L., Catalysis Letters, 1994. **28**(2): p. 301.
61. Hoyos L.J, Praliaud H. and Primet M., Applied Catalysis A: General, 1993. **98**.
62. Maesen T. and Marcus B., Studies in Surface Science and Catalysis. **137**: p. 1.
63. de Jong K.P., Mesters C.M., Peferoen D.G., van Brugge P.T. and de Groot C., Chemical Engineering Science, 1996. **51**: p. 2053.
64. Bellusi G., Pazzunconi G., Pereg C., Girotti G. and Terzoni G., Journal of Catalysis, 1995. **157**: p. 227.
65. Smith K., Zhenhua Z. and Hodgson P.K., Journal of Molecular Catalysis, 1998. **134**: p. 121.
66. Ochs T. and Turek T., Chemical Engineering Science, 1999. **54**(20): p. 4513.
67. Turek T., Journal of Catalysis, 1998. **174**(1): p. 98.
68. Turek T., Catalysis Today, 2005. **105**(2): p. 275.

69. Brandenberger S., Kröcher O., Tissler A. and Althoff R., Catalysis Reviews, 2008. **50**: p. 492.
70. Kögel M., Mönnig R., Schwieger W., Tissler A. and Turek T., Journal of Catalysis, 1999. **182**(2): p. 470.
71. Rauscher M., Kesore K., Mönnig R., Schwieger W., Tißler A. and Turek T., Applied Catalysis A: General, 1999. **184**(2): p. 249.
72. Löwenstein W., American Mineralogist, 1954. **39**: p. 92-96.
73. Busco C.A., Barbaglia M., Bolis V., Foddanu G.M. and Ugliengo P., Thermochimica Acta, 2004. **418**: p. 3.
74. Barthomeuf D., Materials Chemistry and Physics, 1987. **17**: p. 49.
75. Ribeiro F.R., Alvarez F., Henriques C., Lemos F., Lopes J.M. and Ribeiro M.F., Journal of Molecular Catalysis A: Chemical, 1995. **96**(3): p. 245.
76. Vaudry F., Renzo F.D., Fajula F. and Schulz P., Journal of the Chemical Society, Faraday Transactions, 1998. **94**(4): p. 617 - 621.
77. Kumar R., Cheng W.C., Rajagopalan K., Peters A.W. and Basu P., Journal of Catalysis, 1993. **143**(2): p. 594.
78. Barthomeuf D., Catalysis Reviews, 1996. **38**(4): p. 521.
79. Ribeiro F.R., Alvarez F., Henriques C., Lemos F., Lopes J.M. and Ribeiro M.F., Journal of Molecular Catalysis A: Chemical, 1995. **95**: p. 245-270.
80. Higgins J.B., LaPierre R.B., Schlenker J.L., Rohrman A.C., Wood J.D., Kerr G.T. and Rohrbaugh W.J., Zeolites, 1988. **8**: p. 446.
81. Marques J.P., Gener I., Ayrault P., Bordado J.C., Lopes J.M., Ribeiro F.R. and Guisnet M., C.R. Chimie, 2005. **8**: p. 399.
82. Meier W.M., Oison D.H. and Bärlocher C.H., *Atlas of Zeolite Structure Types*. 5 ed. 2001, London: Elsevier.
83. Creyghton E.J., van Duin A.C.T., Jansen J.C., Kooyman P.J., Zandbergen H.W. and van Bekkum H., Journal of the Chemical Society, Faraday Transactions, 1996. **92**(22): p. 4637.
84. Sachtler W.M.H. and Zhang Z.C., Advances in Catalysis, 1993. **39**: p. 129.
85. Gates B.C., Chemical Reviews, 1995. **95**(3): p. 511.
86. Stakheev A.Y. and Kustov L.M., Applied Catalysis A: General, 1999. **188**(1-2): p. 3.
87. Mojet B.L., Miller J.T., Ramaker D.E. and Koningsberger D.C., Journal of Catalysis, 1999. **186**(2): p. 373.
88. Ji Y., van der Eerden A.M.J., Koot V., Kooyman P.J., Meeldijk J.D., Weckhuysen B.M. and Koningsberger D.C., Journal of Catalysis, 2005. **234**(2): p. 376.
89. Sullivan J.A. and Cunningham J., Applied Catalysis B: Environmental, 1998. **15**(3-4): p. 275.
90. Garetto T.F., Rincón E. and Apesteguía C.R., Applied Catalysis B: Environmental, 2007. **73**(1-2): p. 65.
91. Garetto T.F., Rincón E. and Apesteguía C.R., Applied Catalysis B: Environmental, 2004. **48**(3): p. 167.
92. Guczi L. and Kiricsi I., Applied Catalysis A: General, 1999. **186**(1-2): p. 375.
93. Kühl G.H., *Catalysis and Zeolites- Fundamentals and Applications*, ed. Weitkamp J. and Puppe L. 1999, Heidelberg: Springer. 564.
94. Stakheev A.Y., Khodakov A.Y., Kustov L.M., Kazansky V.B. and Minachev K.M., Zeolites. **12**(7): p. 866.
95. Wrabetz S., Guntow U. and Schlögl R., Studies in Surface Science and Catalysis, 1997. **105**: p. 583.
96. Sachtler W.M.H., Tzou M.S. and Jiang H.J., Solid State Ionics. **26**(2): p. 71.
97. Chmelka B.F., Went G.T., Csencsits R., Bell A.T., Petersen E.E. and Radke C.J., Journal of Catalysis, 1993. **144**(2): p. 506.

98. Sachtler W.M.H., Tzou M.S. and Jiang H.J., Solid State Ionics, 1987. **26**(2): p. 71.
99. Tzou M.S., Teo B.K. and Sachtler W.M.H., Journal of Catalysis, 1988. **113**(1): p. 220.
100. Gallezot P., Catalysis Reviews-Science and Engineering, 1979. **20**: p. 121.
101. Jacobs P.A. and Bayer H.K., Journal of Physical Chemistry, 1979. **83**: p. 1174.
102. Verdonck J., Jacobs P.A., Genet M. and Poncelet. G., JCS Faraday, 1980. **74**: p. 403.
103. Kubanek P., Schmidt H.W., Spliethoff B. and Schüth F., Microporous and Mesoporous Materials, 2005. **77**(1): p. 89.
104. Sachtler W.M.H., Accounts of Chemical Research, 1993. **26**(7): p. 383.
105. Villegas J.I., Kubicka D., Karhu H., Österholm H., Kumar N., Salmi T. and Murzin D.Y., Journal of Molecular Catalysis A: Chemical, 2007. **264**(1-2): p. 192.
106. Treesukol P., Srisuk K., Limtrakul J. and Truong T.N., Journal of Physical Chemistry B, 2005. **109**(24): p. 11940.
107. Hutt M., Tißler A. and Schwarzer H.C., Stabilisierte Hochtemperaturkatalysatoren, Süd-Chemie AG, PCT/EP2009/003333, 2007, Germany
108. Hutt M., Tißler A., Wanninger K. and Manoylova O., Katalysator zur Oxidation von NO, Süd-Chemie AG, DE10200915592, 2008, Germany
109. Hutt M., Tißler A. and Klose F., Alterungsstabiler Rh-Zeolith-Katalysator, Süd-Chemie AG, DE102009053951, 2009, Germany
110. Hutt M., Tißler A. and Klose F., Alterungsstabiler Pd- und Pd/Pt- Zeolith- Oxidations-Katalysator mit Platin und Palladium homogen in den Poren eines Zeolithen, Süd-Chemie AG, DE102009053944, 2009, Germany
111. Reisinger M., Hausmann R., Chen B., Tacke T., Stochniol G. and Panster P., Catalyst for destruction of CO, VOC and halogenated organic emissions, Degussa, WO2001EP10374 20010908, 2000,
112. Maletz G., Kurth V., Bentele A., Wanninger K. and Tissler A., Coating composition for diesel oxidation catalyst, Süd-Chemie AG, 10 2007 057 305.9, 2007, DE
113. Zecchina A., Bordiga S., Spoto G., Marchese L., Petrini G., Leofanti G. and Padovan M., Journal of Physical Chemistry, 1992. **96**: p. 4991.
114. Pazè C., Zecchina A., Spera S., Cosma A., Merlo E., Spano G. and Girotti G., Physical Chemistry Chemical Physics, 1999. **1**: p. 2627.
115. Zecchina A. and Arean C.O., Chemical Society Reviews, 1996. **25**: p. 187.
116. Lohse U., Loffler E., Hunger M., Stockner J. and Patzelova V., Zeolites, 1987. **7**: p. 11.
117. Zholobenko V.L., Kustov L.M., Kazansky V.B., Loeffler E., Lohser U., Peuker C. and Oehlmann G., Zeolites, 1990. **10**: p. 304.
118. Bourgeat-Lami E., Massiani P., Renzo F.D., Espiau P. and Fajula F., Applied Catalysis, 1991. **72**: p. 139.
119. Miller J.T., Hopkins P.D., Meyers B.L., Ray G.J., Roginski R.T., Zajac G.W. and Rosenbaum N.H., Journal of Catalysis, 1992. **138**: p. 115.
120. Kiricsi I., Flego C., Pazzuconi G., Parker W.O., Millini R. and Perego C., Journal of Physical Chemistry, 1994. **98**: p. 4627.
121. Pearson R.G., Journal of the American Chemical Society, 1963. **85**: p. 3533.
122. Pearson R.G., *Chemical Hardness*. 1997, Weinheim: Wiley-VCH. 198.
123. Paukshtis E.A. and Yurchenko E.N., Russian Chemical Reviews, 1983. **52**: p. 42.
124. Knötzinger H., *Elementary Reaction steps in Heterogeneous Catalysis*, ed. Joyner R.W. and van Santen R.A. 1993: Kluwer, Dordrecht. 267.
125. Lercher J.A., Gründling C. and Eder-Mirth G., Catalysis Today, 1996. **27**: p. 353.
126. Knözinger H., *Acid-Base Catalysis*, ed. Tanabe K., Hattori T., Yamaguchi T., and Tanaka T. 1989, Weinheim: Verlag Chemie.
127. Knözinger H., *Elementary Reaction steps in Heterogeneous Catalysis*, ed. Joyner R.W. and van Santen R.A. 1993: Kluwer, Dordrecht. 267.

128. Peri E.A., *Catalysis - Science and Technology*, ed. Anderson J.R., Boudart, M. Vol. 5. 1984, Berlin: Springer Verlag. 171.
129. Zaki M.I. and Knötzinger H., Journal of Catalysis, 1989. **199**(2): p. 311.
130. Datka J., Gila B., Kawałeka M. and Staudteb B., Journal of Molecular Structure, 1999. **511**: p. 133.
131. Nesterenko N.S., Avdey A.V. and Ermilov A.Y., International Journal of Quantum Chemistry, 2006. **106**(10): p. 2281-2289.
132. Scarano D., Spoto G., Bordiga S., Zecchina A. and Lamberti C., Surface Science, 1992. **276**(1-3): p. 281.
133. Tsyganenko A.A., Denisenko L.A., Zverev S.M. and Filimonov V.N., Journal of Catalysis, 1985. **94**(1): p. 10.
134. Benesi H.A., Journal of Catalysis, 1973. **28**: p. 176.
135. Jacobs P.A. and Heylen C.F., Journal of Catalysis, 1974. **34**: p. 267.
136. Knötzinger H. and Stolz H., Berichte der Bunsengesellschaft für Physikalische Chemie, 1971. **75**: p. 1055.
137. Montanari T., Bevilacqua M. and Busca G., Applied Catalysis A: General, 2006. **307**(1): p. 21.
138. Areán O.C., Escalona Platero E., Peñarroya Mentruit M., Rodríguez Delgado M., Llabrés i Xamena F.X., García-Raso A. and Morterra C., Microporous and Mesoporous Materials, 2000. **34**(1): p. 55.
139. Nowaki W., Helvetica Chimica Acta, 1945. **28**: p. 1233.
140. Montanari T., Marie O., Daturi M. and Busca G., Applied Catalysis B: Environmental, 2007. **71**: p. 216.
141. García-Cortés J.M., Pérez-Ramírez J., Rouzaud J.N., Vaccaro A.R., Illán-Gómez M.J. and Salinas-Martínez de Lecea C., Journal of Catalysis, 2003. **218**(1): p. 111.
142. Nakatsuji T., Yamaguchi T., Li J., Sato N. and Matsuzono Y., Catalysis Communications, 2009. **10**(6): p. 763.
143. Wang Q.L., Giannetto G. and Guisnet M., Journal of Catalysis, 1991. **130**(2): p. 471.
144. Zholobenko V.L., Lei G.D., Carvill B.T., Lerner B.A. and Sachtler W.M.H., Journal of the Chemical Society, Faraday Transactions, 1994. **90**(1): p. 233.
145. Stakheev A.Y., Shpiro E.S., Tkachenko O.P., Jaeger N.I. and Schulz-Ekloff G., Journal of Catalysis, 1997. **169**(1): p. 382.
146. Chakarova K., Hadjiivanov K., Atanasova G. and Tenchev K., Journal of Molecular Catalysis A: Chemical, 2007. **264**(1-2): p. 270.
147. Datka J., Gila B., Kawałeka M. and B. S., Journal of Molecular Structure, 1999. **511**: p. 133.
148. Weber W.A. and Gates B.C., Journal of Catalysis, 1998. **180**(2): p. 207.
149. Primet M., Vedrine J.C. and Naccache C., Journal of Molecular Catalysis, 1978. **4**(6): p. 411.
150. Shannon R.D., Vedrine J.C., Naccache C. and Lefebvre F., Journal of Catalysis, 1984. **88**(2): p. 431.
151. Bergeret G., Gallezot P., Gelin P., Ben Taarit Y., Lefebvre F., Naccache C. and Shannon R.D., Journal of Catalysis, 1987. **104**(2): p. 279.
152. Regalbutoa J.R., Ansela O. and Millerb J.T., Topics in Catalysis, 2006. **39**: p. 237.
153. Jiménez C., Romero F.J., Roldán R., Marinas J.M. and Gómez J.P., Applied Catalysis A: General, 2003. **249**(1): p. 175.
154. 5. Internationales Forum Abgas- und Partikelemissionen, 2008: p. 126-144.
155. Gupta A., Gaur V. and Verma N., Chemical Engineering and Processing, 2004. **43**(1): p. 9.
156. Arnby K., Törncrona A., Andersson B. and Skoglundh M., Journal of Catalysis, 2004. **221**(1): p. 252.

157. Ackelid U., Wallenberg L.R. and Petersson L.G., Catalysis Letters, 1996. **39**(1): p. 129.
158. Ackelid U., Olsson L. and Petersson L.G., Journal of Catalysis, 1996. **161**(1): p. 143.
159. Vaccaro A.R., Mul G., Pérez-Ramírez J. and Moulijn J.A., Applied Catalysis B: Environmental, 2003. **46**(4): p. 687.
160. Wang H., Tobin R.G., Lambert D.K., DiMaggio C.L. and Fisher G.B., Surface Science, 1997. **372**: p. 267.
161. Turek T., Applied Catalysis B: Environmental, 1996. **9**(1-4): p. 201.
162. Wanninger K., Hutt M., Maletz G., Bentele A. and Schneider M., Dieseloxidationskatalysator mit Platin und Palladium homogen in den Poren eines Zeolithen, Süd-Chemie AG, DE102009053919, 2009, Germany
163. Baerns M., Hofmann H. and Renken A., *Chemische Reaktionstechnik. Lehrbuch der Technischen Chemie*. 1987, Stuttgart: Thieme Verlag.
164. Fuller E.N., Schettler P.D. and Giddings J.C., Industrial and Engineering Chemistry, 1966. **85**: p. 18-27.
165. Weisz P.B., Chemical Technology, 1973. **3**: p. 498.
166. Xiao J. and Wei J., Chemical Engineering Science, 1992. **47**(5): p. 1123.
167. *Zeolites in Industrial Seperation and Catalysis*. 1 ed, ed. Kulprathipanja S. 2010, Weinheim: Wiley-VCH. 618.
168. Arnby K., Assiks J., Carlsson P.-A., Palmqvist A. and Skoglundh M., Journal of Catalysis, 2005. **233**(1): p. 176.
169. Carlsson P.-A., Mollner S., Arnby K. and Skoglundh M., Chemical Engineering Science, 2004. **59**(20): p. 4313.
170. Hiam L., Wise H. and Chaikin S., Journal of Catalysis, 1968. **10**: p. 272.
171. Morooka Y., Morikawa Y. and Ozaki A., Journal of Catalysis, 1967. **7**: p. 23.
172. Schwartz A., Holbrook L. and Wise H., Journal of Catalysis, 1971. **21**: p. 199.
173. Otto K., Andino J.M. and Parks C.L., Journal of Catalysis, 1991. **131**(1): p. 243.
174. Marécot P., Fakche A., Kellali B., Mabilon G., Prigent P. and Barbier J., Applied Catalysis B: Environmental, 1994. **3**(4): p. 283.
175. Elschenbroich C., *Organometallics*. 2006, Weinheim: Wiley-VCH.
176. Bourane A., Derrouiche S. and Bianchi D., Journal of Catalysis, 2004. **228**(2): p. 288.
177. Zafiris G.S. and Gorte R.J., Journal of Catalysis, 1993. **140**(2): p. 418.
178. Fanson P.T., Delgass J. and Lauterbach J., Journal of Catalysis, 2001. **204**: p. 35.